

CAPITAL UNIVERSITY OF SCIENCE AND
TECHNOLOGY, ISLAMABAD



A Reliable Protection Scheme for Fast DC Fault Clearance in a VSC-Based Meshed MTDC Grid

by

Rifat Ara

A thesis submitted in partial fulfillment for the
degree of Doctor of Philosophy

in the

Faculty of Engineering

Department of Electrical Engineering

2021

A Reliable Protection Scheme for Fast DC Fault Clearance in a VSC-Based Meshed MTDC Grid

By

Rifat Ara

(PE131002)

Dr. Mohamad Kamarol Mohd Jamil, Associate Professor

Universiti Sains Malaysia, Pulau Pinang, Malaysia

(Foreign Evaluator 1)

Dr. Saad Mekhilef, Professor

University of Malaya, Kuala Lumpur, Malaysia

(Foreign Evaluator 2)

Dr. Umer Amir Khan

(Thesis Supervisor)

Dr. Noor Muhammad Khan

(Head, Department of Electrical Engineering)

Dr. Imtiaz Ahmed Taj

(Dean, Faculty of Engineering)

DEPARTMENT OF ELECTRICAL ENGINEERING
CAPITAL UNIVERSITY OF SCIENCE AND TECHNOLOGY
ISLAMABAD

2021

Copyright © 2021 by Rifat Ara

All rights reserved. No part of this thesis may be reproduced, distributed, or transmitted in any form or by any means, including photocopying, recording, or other electronic or mechanical methods, by any information storage and retrieval system without the prior written permission of the author.

Dedicated To my beloved parents father **Mr. G.M Mattoo** and my late mother
Rafiq Bano who taught me every aspect of life.

Dedicated to my respected supervisor **Dr. Umer Amir Khan**, without his
sincere help and support this work could not have been done.



CAPITAL UNIVERSITY OF SCIENCE & TECHNOLOGY ISLAMABAD

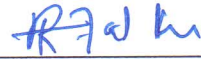
Expressway, Kahuta Road, Zone-V, Islamabad
Phone: +92-51-111-555-666 Fax: +92-51-4486705
Email: info@cust.edu.pk Website: <https://www.cust.edu.pk>

CERTIFICATE OF APPROVAL

This is to certify that the research work presented in the thesis, entitled “**A Reliable Protection Scheme for Fast DC Fault Clearance in a VSC-Based Meshed MTDC Grid**” was conducted under the supervision of **Dr. Umer Amir Khan**. No part of this thesis has been submitted anywhere else for any other degree. This thesis is submitted to the **Department of Electrical Engineering, Capital University of Science and Technology** in partial fulfillment of the requirements for the degree of Doctor in Philosophy in the field of **Electrical Engineering**. The open defence of the thesis was conducted on **August 06, 2021**.

Student Name :

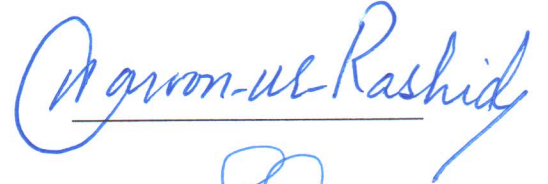
Rifat Ara (PE-131002)



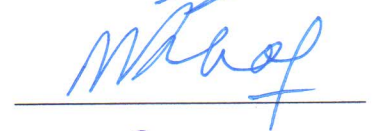
The Examination Committee unanimously agrees to award PhD degree in the mentioned field.

Examination Committee :

- (a) External Examiner 1: Dr. Haroon ur Rashid
Professor
PIEAS, Islamabad
- (b) External Examiner 2: Dr. Shaikh Saaqib Haroon
Associate Professor
UET, Taxila
- (c) Internal Examiner : Dr. Muhammad Ashraf
Professor
CUST, Islamabad








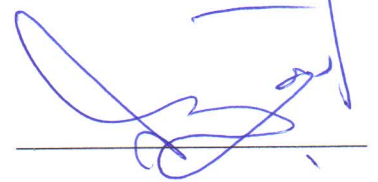
Supervisor Name :

Dr. Umer Amir Khan
Assistant Professor
CUST, Islamabad



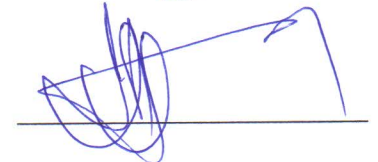
Name of HoD :

Dr. Noor Muhammad Khan
Professor
CUST, Islamabad



Name of Dean :

Dr. Imtiaz Ahmad Taj
Professor
CUST, Islamabad



AUTHOR'S DECLARATION

I, **Rifat Ara (Registration No. PE-131002)**, hereby state that my PhD thesis titled, **“A Reliable Protection Scheme for Fast DC Fault Clearance in a VSC-Based Meshed MTDC Grid”** is my own work and has not been submitted previously by me for taking any degree from Capital University of Science and Technology, Islamabad or anywhere else in the country/ world.

At any time, if my statement is found to be incorrect even after my graduation, the University has the right to withdraw my PhD Degree.



(Rifat Ara)

Dated: *06/* August, 2021

Registration No : PE-131002

PLAGIARISM UNDERTAKING

I solemnly declare that research work presented in the thesis titled “**A Reliable Protection Scheme for Fast DC Fault Clearance in a VSC-Based Meshed MTDC Grid**” is solely my research work with no significant contribution from any other person. Small contribution/ help wherever taken has been duly acknowledged and that complete thesis has been written by me.

I understand the zero tolerance policy of the HEC and Capital University of Science and Technology towards plagiarism. Therefore, I as an author of the above titled thesis declare that no portion of my thesis has been plagiarized and any material used as reference is properly referred/ cited.

I undertake that if I am found guilty of any formal plagiarism in the above titled thesis even after award of PhD Degree, the University reserves the right to withdraw/ revoke my PhD degree and that HEC and the University have the right to publish my name on the HEC/ University Website on which names of students are placed who submitted plagiarized thesis.



(Rifat Ara)

Dated: 06/ August, 2021

Registration No : PE-131002

List of Publications

It is certified that following publication(s) have been made out of the research work that has been carried out for this thesis:-

1. Ara, Rifat, et al., "A Reliable Protection Scheme for Fast DC Fault Clearance in a VSC-Based Meshed MTDC Grid." *IEEE Access*, vol. 8, pp. 88188-88199, year 2020.
2. Ara, Rifat, and Umer Amir Khan. "An Alternate Grid-splitting Scheme and Efficient Algorithm for Voltage Source Converter Based Multiterminal DC Grid Protection and Restoration Control." 2018 International Conference on Power Generation Systems and Renewable Energy Technologies (PGSRET). IEEE, 2018.

Rifat Ara
(PE131002)

Acknowledgement

First and foremost, praises and thanks to Almighty Allah for His showers of blessings, and courage in every aspect of my life and throughout my research work to complete it successfully.

I would like to express my deep and sincere gratitude to my research supervisor, **Dr. Umer Amir Khan**, (Assistant Professor, Electrical Engineering Department), for giving me the opportunity to do research on this important topic. His dynamism, sincere guidance, vision, rigorous knowledge, and motivation have deeply inspired me. He has taught me the methodology to carry out the research and to present the research works as clearly as possible. It was a great privilege and honor to work and study under his guidance. I am extremely grateful for what he has offered me.

I would like to express my deep gratitude to **Dr. Aamir Iqbal Bhatti** (Professor and Dean ORIC), for his constant encouragement, necessary background knowledge, and control research lab for my work. The completion of this research thesis could not have been accomplished without his immense support and timely assistance. It has been a great honor for me to work under his guidance, and I am extremely grateful to him.

The appreciation also goes to **Dr. Bang Wook Lee**, (Member HVDC Research Committee of KNIFE, Power Cable Experts Committee of the Korean Agency CIGRE). His research work is a key support to this thesis.

I would like to express my special thanks of gratitude to **Dr. Imtiaz Taj** (Dean Faculty of Engineering), for his kindness and genuine support throughout this research work, despite of his busy schedules.

I am highly thankful to **Dr. Noor Mohammad Khan**, (Professor and Head of the Department of Electrical Engineering) for his support and encouragement during my research.

I would like to thank **Dr. Fazal-Ur-Rehman**, (Professor, Department of Electrical Engineering) for his support and constant encouragement.

I would like to thank **Engr. Khalid**, (Assistant Professor and Director Graduate Studies), for his timely support to complete this thesis successfully.

Finally, I am extending my thanks to the management of Capital University of Science and Technology, for their support to do this work.

Abstract

A multi-terminal high voltage DC (MTDC) Grid is the optimal solution to minimize the global energy crisis to a great extent. It is a cost-effective transmission system to transmit a bulk amount of sustainable electrical power over long distances with overall lower transmission losses and investments saving land and money. A VSC-based Modular-Multilevel-Converter HVDC/MTDC (VSC-MMC-HVDC/MTDC) technology with a key benefit of constant voltage polarity offers considerable benefits and various attractive features to fulfill the basic requirements of the future Super-Grid. However, the protection of a DC system is more challenging and difficult than its counterpart AC system's protection. In a DC system the fault current reaches to a huge value within a few milliseconds. Major hurdles which prevent the integration and development of the HVDC systems include absence of naturally zero-current points (absence of frequency), minimum impedance, and the lack of high rating DC circuit breakers (DCCBs). Hence, extreme vulnerability of a VSC-HVDC/MTDC system to the DC faults, particularly a solid DC line/cable short circuit fault is a major threat to its operation and development (scalability). Indeed, the core design demand for a feasible MTDC protection scheme capable of clearing the DC fault within a few milliseconds (5 msec. or less) of the critical time limit, has remained a key technical gap in both research and practice so far and needs to be addressed. The proposed scheme utilizes the joint performance of communication-based optical sensing schemes, independent sub-schemes, fast isolation tools, and simple backup into one scheme. In this work, firstly the 3-level, bi-polar half-bridge VSC-MMC-MTDC meshed grids of 3 and 4 terminals are validated in the MATLAB using Sims-Cape Power Systems. Afterwards DC cable P2P and P2G faults are analysed with appropriate simulation results and data. Particularly the DC cable P2P faults are analysed using varied fault distances, fault impedances, and fault locations within the grid. Finally, a comprehensive protection scheme is proposed for a meshed VSC-MTDC system. The scheme utilizes the joint performance of current differential and TW methods based on distributed current measuring units (assumed optical sensor

networks), discrete-wavelet-transform (DWT), current derivative data, overcurrent relays, active and passive FCLs, bidirectional Hybrid DCCBs (HDCCBs), half-bridge VSC-MMCs, ACCBs, and other simple backup plans. All the important aspects of the total DC fault clearance time are explored both theoretically and with appropriate simulation results. These important aspects include accurate faulty line/segment determination, quick real-time fault detection, relatively accurate fault location, significant fault current limiting, and fully selective isolation of only the faulty line from the system without shutting down the entire grid. Through this effective fault coordination, the DC fault current is significantly reduced to much below 1.7 kA and the fault clearance time achieved is up to 5.2 ms. The scheme is capable to fulfil all the general requirements of a feasible MTDC protection scheme such as comprehensive, robust, novel, fully selective, cost-effective, reliable, and scalable. Technical feasibility of the proposed concepts can be verified experimentally using the extensive set of simulation results obtained. Further, the scheme is not only applicable to the target meshed VSC-MTDC grid, but its general methodology can be implemented to any meshed MTDC grid with any number of terminals.

Contents

Author's Declaration	v
Plagiarism Undertaking	vi
List of Publications	vii
Acknowledgement	viii
Abstract	x
List of Figures	xv
List of Tables	xx
Abbreviations	xxi
Symbols	xxiii
1 Introduction	1
1.1 Background and Motivation	1
1.2 Various Benefits Offered by an MTDC Transmission Grid	4
1.3 Potential of Pakistan to Eliminate its Energy Crisis	7
1.4 An Overview of Modern HVDC Converter Technologies	10
1.5 Why a VSC-based HVDC Technology for the Future Super-grid	13
1.5.1 AC-side transformer	16
1.5.2 AC-side filters	16
1.5.3 Phase Reactor	16
1.5.4 DC-side Capacitor	17
1.5.5 DC-lines	17
1.5.6 AC/DC Converter	18
1.6 Research Objective	23
1.7 Main Fault Isolating Unit (Fault Clearing Unit) Used in the System Model	26
1.8 Thesis Structure	27

2	Literature Survey	28
2.1	Introduction	28
2.2	Device Based Protection Strategies	28
2.2.1	AC Circuit Breakers	28
2.2.2	Converter Configurations	29
2.2.3	Proposed DC Circuit Breakers (Prototypes)	31
2.2.3.1	Mechanical DC Circuit Breaker	32
2.2.3.2	Solid State Circuit Breaker or Semiconductor Circuit Breaker	33
2.2.4	Various Types of Fault Current Limiters	35
2.3	Various Methods of Faulty Line Determination and Fault Detection	38
2.3.1	Overcurrent Protection	39
2.3.2	Current and Voltage Derivative Methods	39
2.3.3	Conventional Differential Protection and TW Principles	40
2.3.3.1	Optical Sensor Schemes	42
2.4	Research Gap	51
2.5	Problem Statement	51
2.6	Research Contribution	53
2.7	Summary	62
3	Critical DC Faults in an MTDC Grid	63
3.1	Grid Modelling	63
3.2	MTDC Faults	66
3.2.1	DC Line to Ground or Pole to Ground (L2G/P2G) Fault	67
3.2.2	Simulation Results of P2G Faults	68
3.2.3	DC Line to Line or Pole to Pole (L2L/P2P) Fault	69
3.2.4	Simulation Results of P2P Faults	75
3.2.5	Important Findings	81
3.2.6	Summary and Discussions	81
4	Proposed Scheme	84
4.1	Fast Fault Detection	86
4.1.1	Why the Wavelet Transform	88
4.1.1.1	The Discrete Wavelet Transform (DWT)	94
4.1.1.2	Simulation Results of the Fault Detection with the DWT	96
4.1.1.3	Important Findings about the DWT	102
4.2	Proposed Effective Fault Current Limiting	103
4.2.1	Effective DC Fault Current Suppression Results	104
4.3	Determination of a Faulty Line	109
4.3.1	Determination of a Faulted Line Between a Source and a Load Terminal in an MTDC Grid	111
4.3.2	Determination of a Faulty Segment	112
4.3.3	Results of Accurate Faulty Line and Faulty Segment Determination	114

4.4	DC Fault Current Interruption and Isolation of the Faulty Line . . .	116
4.4.1	DC Fault Current Interruption and Isolation Results	121
4.5	Fault Location in an MTDC Grid	123
4.6	Auxiliary Protection Methods (Simple Back up Plans)	125
4.6.1	Simple backup Plans with DCCBs Failure and Bus-bar Faults	127
4.6.2	Instantaneous Overcurrent Protection	128
4.6.3	Current Derivative Direction Principles	129
4.7	Summary	129
4.7.1	Faulty line Determination/Discrimination:	130
4.7.2	Real time Detection of the Fault with DWT (Sensitive and Robust Scheme)	133
4.7.3	Effective limiting of the DC fault current and Fault Coordination	134
4.7.4	Fully Selective Isolation of only the Faulty Line (Fast, Novel and Seamless scheme)	137
4.7.5	Relatively Accurate Fault Location	140
5	Conclusion and Future Work	146
5.1	Limitation and Future Work	147
	Bibliography	149
	A Appendix	161

List of Figures

1.1	A conceptual network of the European future Super-grid linking energy projects like DESERTEC and Med-grid across North Africa, the Middle East and Europe [3]	3
1.2	Cost against transmission distance for an HVDC and HVAC system [19].	8
1.3	Conventional HVDC system with the current source converters (LCC-HVDC system) [23].	12
1.4	HVDC Station with Voltage Source Converters (VSC-HVDC System) [24]	12
1.5	Pi-model of a single pole for a DC transmission link [98]	17
1.6	2-terminal VSC-HVDC transmission link. The controlled power is the power entering the phase reactor with a positive direction towards the VSC station [98]	19
1.7	Block Diagram of a 3-terminal meshed MTDC grid with positive P2G and P2P faults	19
1.8	(a) Huge DC fault current for a solid P2P fault at 60 msec. and at 10 km to the source Station node B1. (b) DC link voltage for a solid P2P fault at 5 km to the source node B1 (MMC1) without protection	22
1.9	Bewley Lattice diagram incorporating OHL, UGC and distributed optical current sensors for the fault current development [76]	23
1.10	DC Fault Clearing unit (Fault Isolation Unit)	26
2.1	Mechanical DCCB (a) Air-blast MDCCB Basic Topology [93] (b) Passive type. (c) Active Type	33
2.2	Semiconductor (Solid State) DCCB with IGBT Breaker Topology [39]	34
2.3	Proactive HDCCB Prototype from ABB (Hybrid 1 type) [96]	35
2.4	Optical FBG sensor construction [55]	44
2.5	Fiber Grating Sensor Experimental Implementation taken from [55]	44
3.1	A four-terminal meshed MTDC grid with optical sensor networks, fault locators and protection devices.	64

3.2	(a) DC fault current profile for an internal P2G fault incepted at 0.3 s in the positive pole of link L_{13} . (b) DC voltage profile at the positive poles. (c) DC voltage profile at the negative poles. (d) DC voltage profile at the positive pole for an internal P2G fault at 0.5 s with no converter blocking after the fault for a three terminal meshed grid.	68
3.3	Total contributions to the fault current for a P2G fault in L_{13} at 1 km to B_1 without protection. Faulty cable L_{13} current (solid red curve), MMC_1 DC current (blue short dash) and healthy cable currents (wine and royal) for a four terminal meshed grid.	69
3.4	DC Cable Short Circuit Fault Equivalent Circuits of MMC DC side (a) the converter model (b) DC Capacitor discharge stage. (c) Diode freewheeling stage. (d) Grid current feeding stage.	72
3.5	Internal and external faults using series of the differential current measurements with the current direction principle based on optical sensors.	73
3.6	A clear TW effect seen in the development of DC fault current at a distance of 1 to 10 km to a VSC converter station.	74
3.7	(a) HVDC link voltage without protection for a solid P2P fault at a distance of 5 km to the source node B_1 (MMC_1). (b) Current reversal b/w S_1 and S_2 oriented for the positive current flow from the sending MMC_1 to the receiving MMC_2 terminal due to an internal mid-line P2P fault in the cable L_{12} without protection.	75
3.8	a) Huge P2P fault current at a distance of 1 km to the source node B_1 for strong AC source (800 kV). (b) DC fault current with multiple peaks without protection.	75
3.9	Influence of different distances to a solid P2P fault on the DC fault current transients showing the damped transient (blue dash).	76
3.10	Delayed fault current profile for a solid P2P fault at 1 ms in L_{12} with B_1 at 10 km and B_2 at 190 km to the fault without protection.	76
3.11	Influence of varied distances to a solid P2P fault on the HVDC link voltage transients without protection.	79
3.12	Influence of varied distances to a solid P2P fault on the HVDC link voltage transients. Damped oscillations due to TWs without protection in the faulty line.	79
4.1	Flowchart for rapid fault detection using DWT (DSP).	87
4.2	Various types of the mother wavelets in WT.	89
4.3	Compressed and stretched wavelets to detect high and low frequencies in a non-stationary continuous time signal.	93
4.4	DWT with wavelet tree (MSD) decomposition for the three levels of detail showing Filter Bank.	95
4.5	Suddenly a high WC 'd6' registered for a solid P2P fault b/w S_1 at 10 km and S_2 at 20 km to the fault in the cable L_{12} . The fault is shortly detected at 270^{12} sample value with Haar-6 as the MW without protection. WCs are almost zero before & after the fault.	97

4.6	A P2P fault in the cable L_{12} at 1 km from B1 and 179 km from B2 ($R_f = 0.01 \Omega$) registered high wavelet coefficients for I_{12} and I_{21} . Maximum value is 1.3896e-05 with the index of 9000 using db-3 level-3 as the MW. The Fault inception time of 0.08s was translated to 9000 th sample value (highest coefficient magnitude).	97
4.7	With protection after installing FCU's and using $R_f = 500 \Omega$ WC on the faulty cable reduced greatly but its value still stayed well above the WC's of the healthy cable currents and the threshold levels.	98
4.8	Variation of Differential current profile with the increasing fault resistances showing corresponding <i>haar-2</i> coefficient magnitudes (right) and damping effect for P2P fault in the cable L_{12} (180 km long) for a four-terminal grid with B_1 (MMC_1) at 1 km to the fault location.	98
4.9	WCs of the differential current profile in the faulty cable L_{12} for a solid P2P fault with ' <i>Haar-2</i> ' as the MW after installing the FCUs (with protection)	99
4.10	(a) WCs of the differential current profile for a solid P2P fault in the cable L_{12} , on the healthy cables having consistently low magnitudes without FCUs (without protection). (b) Consistently low WCs of the differential current profiles on the healthy cables further reduced after installing FCUs (with protection).	99
4.11	A Solid P2P fault at 10 km to B_1 in the cable L_{12} (600km long) generates a high WC 'd6' (red-solid curve). WCs are almost zero before and after the fault. WC's of a damped transient are shown by green-solid curve.	100
4.12	(a) Consistently high WCs of the faulty line current (purple and red). Consistently low WCs of the healthy line currents (green, yellow etc.). (b) Huge P2P fault current with the fault start at 60 ms (red-curve left) and corresponding WCs (green right).	100
4.13	Consistently high WCs of the faulty line (dark-pink-left) and faulty segment (red-right). Consistently low WCs of the healthy lines (green, orange, left) and healthy segments (blue, green, light green, etc., right).	101
4.14	DC fault current limited to 3.387 kA with extra inductors of 200 mH 4/each cable and 2/each converter in a meshed MTDC grid. . .	105
4.15	Fault current reduced to 5 kA with 30 mH inductors at the DC outputs of only AC/DC converters with protection in the scheme. .	105
4.16	Fault current reduced to 1.7 kA with 50 mH inductors at the DC outputs of only AC/DC converters with protection in the scheme. .	105
4.17	Huge differential current derived from the faulted pair S_1 and S_2 is reduced to 12.6 kA with protection in the scheme.	106
4.18	Faulty line or faulty segment discrimination flow chart.	109
4.19	Discriminating a faulted line from the healthy ones at the fault related node B_1 taking both MMC_j & MMC_k as sources in an MTDC Grid.	111

4.20	A Faulty line L_{12} (red-solid curve) 300km long discriminated for a solid P2P fault at 1ms b/w S_1 at 10 km and S_2 at 40 km at B_1 by measuring the differential current sums without protection.	113
4.21	Differential current sums on the healthy cables for a solid P2P fault at 1ms b/w S_1 at 10km and S_2 at 40 km in the cable L_{12}	113
4.22	A Faulty segment (red-solid curve showing a clear TW effect in zoomed DC fault current like a staircase W/F) of L_{12} discriminated for a solid P2P fault at 1 km to S_1 (B_1) by measuring a series of differential currents on it without protection.	115
4.23	Damped profile of series differential currents for $R_f = 500 \Omega$ without protection.	115
4.24	Fully selective methodology to isolate only the faulted line with backup plans in an MTDC grid.	116
4.25	Huge DC fault current with multiple peaks without protection.	118
4.26	DC Fault current effectively limited to 4.8 kA, interrupted and isolated within a short time with protection.	119
4.27	Huge P2P fault current with strong AC sources (800 kV).	119
4.28	Fault is isolated at around 5.2 ms with protection.	120
4.29	Influence of different distances to a solid P2P fault on DC fault current transients showing the damped transient (blue dash).	120
4.30	DC fault currents with protection.	120
4.31	Flowchart for the fault location in a Transmission line.	123
A.1	Results for an internal P2P fault in the cable L_{12} (180 km long) at 1ms. (a) Series differential current profile on L_{12} for a solid P2P fault in it at 1 km to the sending node B_1 and 179 km from the receiving node B_2 discriminating the faulty segment of the cable L_{12} (red solid curve) with highest differential current of 41.92 kA derived from the faulted sensor pair. (b) Series differential current profile for a solid P2P fault at 20 km to B_1 and 160 km from B_2 discriminating the faulty segment of L_{12} (red solid curve) with highest differential current of 39.09 kA at 8.378 ms). (c) Damped series differential current profile for a high impedance P2P fault in the cable L_{12} with $R_f = 500 \Omega$ and at 1 km to B_1 . (d) DC fault currents I_{12} and I_{21} for a solid P2P fault in the cable L_{12} at 1 ms and at a distance of 105 km from B_1 (red solid curve) and 75 km from B_2 (blue dash curve) without delay between the two currents and without protection.	161
A.2	Internal P2P fault in DC line L12 shows zoomed area of initial 2ms that clearly distinguishes the faulted segment between S_1 & S_2 from non-faulted segments.	162

A.3	Solid internal P2P fault at 1 ms in the cable L_{12} (L_1) between S_1 and S_2 . Differential current sums measured at B_1 with selective discrimination of the faulty line L_{12} or its segment (red solid curve). (b) and (c) Differential current sums on both (+/-) poles of the healthy cables. (d) Delayed DC fault currents I_{12} and I_{21} for a solid P2P fault in the cable L_{12} at 1 ms and at a distance of 10 km from B_1 and 190 km from B_2 without protection.	162
A.4	Solid internal P2P fault at 1 ms in the cable L_{12} (180km) with equidistant sensor pairs. (a) Selective discrimination of the faulty segment of L_{12} between S_1 and S_2 (black solid curve). (b) Selective discrimination of the faulty segment between S_2 and S_3 (black sold curve) by measuring series of differential currents on the cable L_{12} . (c) and (d) Series differential current profiles on the healthy cables without protection.	163
A.5	Influence of different distances to a solid P2P fault.	163
A.6	Influence of different distances to a solid P2P fault at 1s in the cable L_{12} on DC fault current transients without protection.	164
A.7	(a) Influence of different distances to a solid P2P fault in the cable L_{12} at 2s on DC fault current transients and DC Voltage. DC voltage and DC fault current for the P2P fault at 3 km to source (red solid curves). (b) Influence of different distances to a solid P2P fault in the cable L_{12} at 1s with terminal 2 replaced by a load resistance of 200 M Ω	164
A.8	P2P fault in the cable L_{12} at 60 ms and at 10km to the source. (a) HVDC link voltage. (b) HVDC link fault current without protection.	165
A.9	P2P fault in the cable L_{12} at 60 ms and at 10 km to the source. (a) HVDC link voltage. (b) HVDC link fault current with protection. .	165
A.10	Solid P2P fault at 1ms. (a) Huge sum of the two fault currents without FCLs. (b) Effective suppression of the sum of fault currents with active and passive FCLs.	165
A.11	Effective active and passive fault current limitation with protection for a P2P fault at 1 ms both (a) and (b).	166
A.12	Influence of different distances to a P2P fault on HVDC link voltage transients for a solid P2P fault at 3s.	166
A.13	Solid P2P fault at 60 ms in the cable L_{12} . (a) Fault currents without protection. (b) Fault currents significantly reduced to much lower value with active/passive FCLs with protection.	166

List of Tables

2.1	Comparison Table with Specific Parameters and Authors	58
3.1	Simulation Parameters	65
4.1	Detailed Wavelet-Coefficient magnitudes using <i>Haar-3</i> as the mother-wavelet (MW)	102
4.2	Maximum current sums at DC buses with different distances to a P2P fault	116
4.3	Type-A and Type-D fault location methods for a solid P2P fault . .	125
4.4	A Detailed Comparison with Previous Research Work	141

Abbreviations

AC	Alternating Current
ACCB	AC Circuit Breaker
CB	Circuit Breaker
CSC	Current source Converter
CWT	Continuous Wavelet Transform
DC	Direct Current
DCCB	DC Circuit Breaker
DWT	Discrete Wavelet Transform
EM	Electromagnet
FCL	Fault Current Limiter
FCU	Fault Clearing Unit
HDCCB	Hybrid DCCB
HSS	High Speed Switch
HVAC	High Voltage AC
HVDC	High Voltage DC
MMC	Modular Multilevel Converter
MTDC	Multiterminal High Voltage DC
MW	Mother Wavelet
P2P	Pole-to-Pole
P2G	Pole-to-ground
RCB	Residual Circuit Breaker
RSFCL	Resistive Superconducting Fault Current Limiter
SWT	Stationary Wavelet Transform
STFT	Short Time Fourier Transform

TW	Travelling Wave
VSC	Voltage Source Converter
WC	Wavelet Coefficient
WT	Wavelet Transform

Symbols

D_f	Fault distance or distance to the fault
R_f	Fault Resistance
I_{diff}	Differential current
S_m	m^{th} optical sensor
V_{dc}	DC voltage
V_{ac}	AC voltage (source voltage)
ε_r	Relative Permittivity
τ	Optical compensation delay
I_{dc}	DC current
I_{nom}	Nominal DC current
I_{TH}	Threshold Current value
I_{cable}	Rated cable current
I_{quench}	RSFCL quenching current
I_{limit}	Limiting current

Chapter 1

Introduction

1.1 Background and Motivation

Our modern life depends on a constant supply of electrical power. Demand for a bulk integration of renewable energy in the power networks is rapidly increasing to withstand the increasing global energy crisis. Even, a temporary power outage can lead to relative chaos, financial setbacks, and the loss of lives. By 2050 the world population is expected to reach 9.8 or 10 billion. This will create very serious problems for our environment. Therefore, in order to meet the fast-growing energy demands, tackle economic, technical, and environmental concerns of conventional AC networks, deplete costly and vanishing fossil fuels, and prevent the effects of global warming, the outmoded infrastructure of the existing grid requires certain modifications.

Back to the history of electric power, Thomas Alva Edison (The Father of Electricity), a 32 year old young-man on Oct 27, 1879, announced the invention of an incandescent electric lamp in New York. Soon he operated the first DC power system in 1882 and started lighting in a small area of New York (up to 2 km) with the DC power using steam generation. However, he could not go beyond 2 km due to the lack of technology at that time. Nikola Tesla introduced the AC system to cover longer distances using transformers. Hence, the AC system

became more attractive for transporting the electric power over long distances [1]. Thus the “War of the Currents” between Edison and Tesla was won by Tesla, and only the AC power generation and transmission began in the 1890s.

There was no significant role played by the DC transmission system for the first 60 years of power transmission, until in the early 1950s when mercury valves were developed. The high voltage DC (HVDC) transmission system became economical in certain situations. However, it took another 20 years for the first HVDC rectifier based on semiconductor switches to go into the operation. The DC for long distance power transmission was revised when the island of Gotland to the mainland of Sweden in the Baltic Sea got linked by ASEA in the spring of 1970. This was the first Current Source Converter (CSC)-based HVDC or Classical HVDC link with a power rating of 20 MW and 100 kV transmission voltage [2]. In the mid-80s, there was a big milestone when a 6300 MW HVDC link between Sao Paulo and Itapua power plant was put into the operation using a CSC-based HVDC link.

Soon, with the development of the insulated gate bipolar transistors (IGBTs), ABB in 1996 developed the first Voltage Source Converter-based HVDC (VSC-HVDC) link on the Island of Gotland and started a new era for the HVDC transmission.

It is assumed that the existing outmoded grid is going to be replaced by the future modernized bidirectional digital grid, the evergreen Smart Grid, also known as the “Electricity Internet”. Several benefits offered by this grid include intelligent signal processing software’s, automatic operation, robustness, phase measuring units (health monitoring sensors), reduced carbon footprint, and visualization techniques. E-mobility, Plug-in Hybrid Electric vehicles, miro-CHP units/heat pumps, integration of diverse energy sources, smart meters and smart homes, overall reduced electricity cost, smart jobs, and zero-net energy buildings are the other benefits. However, the smart grid is not a single step and can’t happen at once. It is a long journey and is a tangential step-wise revolution brought to the Electrical Power Networks, which requires several years.

Additionally, the storage of electrical energy in large amounts and for longer periods is difficult and expensive in comparison to other energy carriers.

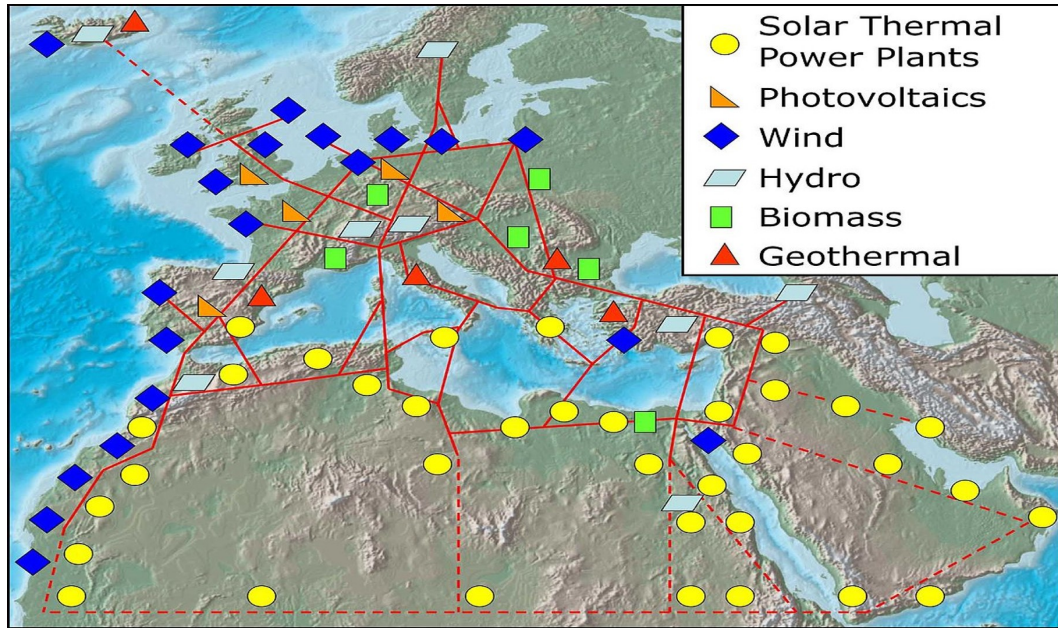


FIGURE 1.1: A conceptual network of the European future Super-grid linking energy projects like DESERTEC and Med-grid across North Africa, the Middle East and Europe [3]

Currently massive availability of the power electronic devices, wideband fiber optic telecommunication links, and the use of micro-computerized control units, have made the HVDC transmission technology a powerful technology. This has facilitated the operation of the Super-Grid called the multi-terminal high voltage DC MTDC or MTHVDC Grid [4–9].

Figure 1.1 shows the conceptual plan of the European future Super-grid that interconnects various European countries with North Africa, Middle East, turkey, and common wealth of independent states CIS (Russia). This serves as the backbone for the Super-Smart-Grid (SSG). The SSG aims at reconciling the two approaches of Super grid (wide area electricity network with the centralized control) and the concept of small-scale, local, and decentralized smart grids. The Super-grid interconnecting producers and consumers of electricity across vast distances would deliver inexpensive, low transmission loss, and high-capacity power. Smart grid capabilities use the local grids transmission and distribution network to coordinate distributed generation, grid storage, and consumption into a cluster that appears to the super grid as a virtual power plant.

Therefore, at present the MTDC transmission system is an optimal solution and cost-effective network to minimize the energy crisis worldwide largely. This Global

Grid acts as the backbone for a bulk integration of remotely distributed renewable (sustainable) energy resources, such as Offshore Wind Farms (OWFs), Solar, Hydro, Geothermal, Biomass, Tidal, and Offshore oil and gas rigs, etc.

MTDC is an easily expandable mesh, radial, ring or star type transmission network with multiple-interconnected sending and receiving terminals (more than two converter stations) for rectification and inversion purposes. This Super-grid incorporates the potential benefits of both the high voltage DC (HVDC) and high voltage AC (HVAC) systems. This grid is a cost-effective electric power transmission network, basically built to transmit a bulk amount of sustainable power to long and extra-long distances with lower transmission losses (less heat generation) and overall lower investments saving land and money.

ABBs Hydro-Quebec New England link project was the first large power scale MTDC transmission system in the world and initially five terminals were in operation [10]. Other notable VSC- based MTDC projects include the Tres-Amigas Superstation and the Atlantic Wind Connection [11, 12]. The Atlantic-Wind Connection, a proposed undersea transmission cable running from New Jersey to Virginia and delivering up to 6000 megawatts of offshore wind energy (EPRI) has been commissioned [13]. The two VSC-based MTDC systems in China are three-terminal 160 kV Nan'ao grid of wind farm integration commissioned in 2013 and Zhou-Shan Islands interconnection of five-terminal network commissioned in 2014 [14–16]. Another four-terminal HVDC grid pilot project interconnecting Beijing and Zhangjiakou has been commissioned in 2018 [15, 17]. ABBs 800 kV project with a distance coverage of 2500 km from North-East India to Agra, known as the North-East-Agra project is under construction [18]. Approximately another 20 projects have been commissioned and multiple manufacturers have entered the market including SIEMENS, ALSTOM, and RXPE etc.

1.2 Various Benefits Offered by an MTDC Transmission Grid

There are diverse reasons for choosing the DC transmission over its predecessor the AC transmission, because in many selective situations a DC system has more

capability and benefits than the AC system. A key advantage of the HVDC transmission system is that a DC link is not distance limited and there is no stability limit related to the amount of power to be transmitted. This leads to infinite extensions of these networks.

By making some modifications in the transmission system, the DC systems can coexist with the AC systems like integrating non-conventional sources of energy with conventional sources. Hence, the overall performance of the power system is effectively improved.

The HVDC/MTDC transmission system is superior to conventional HVAC systems in economic, technical, and environmental aspects. Various benefits offered by the MTDC/HVDC networks are as follows:

1. DC transmission is more reliable, risk resistant, and more efficient as there are no effects of proximity and skin, no varying electromagnetic fields, and hence, least blackouts/brownouts. DC has a superior power quality as the conductor cross-section is fully utilized and there are no induced body currents. The magnetic field produced by a DC line is stationary while in the AC line it is alternating, which can cause inducing body currents.
2. Transmission capacity (maximum length) of a DC OHL/DC cable is not limited by the inductive and capacitive parameters and there is no phase shift between the current and voltage.
3. Long/extra-long-distance bulk power transmission using fewer lines is a key benefit of the HVDC transmission technology. These extra-long transmission lines (ELTLs) are also called as non-homogeneous transmission lines or hybrid transmission lines (HTLs). They consist of the segments of underground cables (UGCs) and Overhead TLs (OHLs) respectively.
4. The overall transmission losses and investments are lower in the HVDC transmission systems, therefore, saving land and money. The effects of both the line inductance and capacitance have to be compensated along the AC line and this adds costs for the long distances. However, the inductance is irrelevant in a DC system, because of the zero frequency. Subsequently, an overhead DC line with its towers is less costly per km than an equivalent AC

line, if both the investment and capitalization of the total energy losses are considered. Additionally, typical bipolar HVDC lines use only two insulated sets of conductors rather than three. These have two independent poles, one at a positive voltage and the other at a negative voltage with respect to the ground. They are comparable to a double circuit AC line since, they can operate at the half power with one pole out of service. Hence, they require only one-third the number of insulated sets of conductors as for double circuit AC line. Thus, the HVDC transmission requires narrower rights-of-way and smaller transmission towers than the HVAC lines of comparable capacity. Furthermore, long-distance AC lines usually require intermediate switching stations, repeaters/regenerators, and reactive power compensation which increases the overall cost of the AC transmission.

5. Interconnection of weak and asynchronous AC systems and a possibility of connecting mainland networks to the islands. Asynchronous HVDC links often use back-to-back converters with no transmission line. They act as an effective “fire-wall” against the cascading outages of the asynchronous interconnections. The north-east blackout of North America in August 2003, is an example of this fire-wall. As the outage propagated around the lower Great Lakes and through Ontario and New York, it stopped at the asynchronous interface with the Quebec that was unaffected. The weak AC interconnections between New York and New England tripped, however, HVDC links from Quebec continued to deliver power to New England.
6. In DC there is no steady -state displacement current, therefore, the electric field is less severe in the DC lines compared to the AC lines. The transmission capacity or the maximum length of a DC OHL/DC cable is not limited by the inductive and capacitive parameters and there is no phase shift between the current and voltage.
7. Secure electricity and high-risk resistance.
8. The MTDC/HVDC transmission system provides secure electricity (high risk resistance). It provides flexible, decoupled control of the active power, and increased stability of the connected AC grid.

9. The MTDC transmission system can satisfy the ever-growing demand for renewable energy and reduce the congestion of existing AC transmission systems.
10. An MTDC/HVDC transmission system is environment-friendly with more efficient utilization of the existing power plants. A bulk integration of mostly green (clean) renewable energy resources particularly, the offshore wind farms is used to generate an abundant amount of smoother electricity with less environmental impact. Fewer public objections, pollution free environment, less interference of noise and other disturbances are the other factors that assist to capture a stronger and steadier wind in the OWF's.
11. As a replacement of costly and vanishing fossil fuels to reduce the emissions of hazardous elements like CO₂, methane, water vapors, SiO₂, etc., into the air. Clean air and reserved natural resources to prevent the effects of global warming and serious climate changes.
12. Underground HVDC cables have a better environmental profile than the overhead HVAC lines. An underground DC cable naturally has no audible noise emission. The material used in a DC cable has only 17.6% of the environmental impact of the AC overhead line, while the material weight of the AC overhead line is higher than that of a DC cable.
13. Global Power grid with international electricity trading, which can build strong international relationships.
14. Access to mega power markets.
15. Business and job opportunities.
16. More affordability and reduced electricity bills as the energy is mostly green (renewable).
17. More reliable due to least blackouts/brownouts hence, less investment in the infrastructure of the MTDC/HVDC networks.

1.3 Potential of Pakistan to Eliminate its Energy Crisis

The availability of abundant wind power of Southern coast of Sindh and Baluchistan with a potential of 122.6 gigawatts per year providing about 212 terawatts of

Electricity. Biomass (50,000 tons of solid waste, 225000 tons of crop residue, 1 million tons of animal manure produced 3 daily). In our country biogas potential of livestock (buffaloes, goats, and sheep) residue is about 20 billion cubic meters of gas per year. Pakistan has a potential of 2.334 million megawatt of electricity through solar system per year due to the sunny 8 to 10 hrs. per day. Nuclear power in Pakistan is provided by five commercial nuclear power plants (Pakistan is among 30 countries on top in the world). Pakistan is the first Muslim country in the world to operate civil nuclear power plants. It is assured that by the year 2030, there will be 8800 megawatts of the nuclear power expansion in Pakistan. Pakistan is world's 4th largest coal reserve, but the coal electricity generation is only 0.8% . Hydropower potential of Pakistan is 60,000 Mw, however only 7320 Mw has been developed.

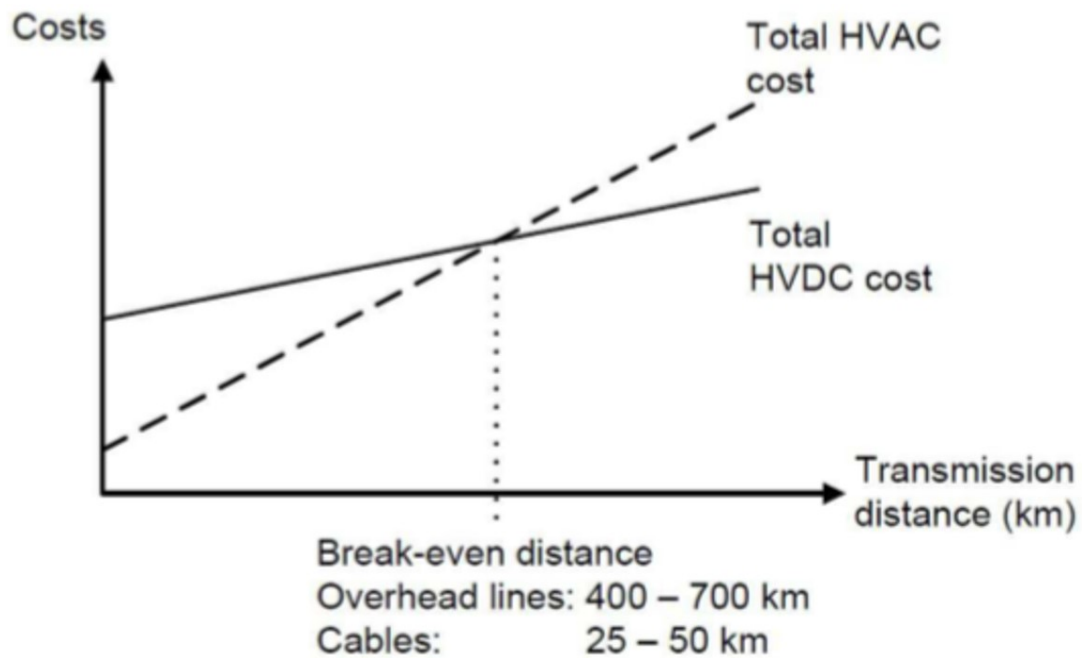


FIGURE 1.2: Cost against transmission distance for an HVDC and HVAC system [19].

AC is very useful for domestic and commercial uses, as the induction motors work only with AC. However, for long distance power transmission (greater than 400 miles), mega power projects and markets, DC transmission is the only optimal solution because of its superiority over AC transmission in economical, technical, and environmental aspects. Various benefits of the HVDC/MTDC transmission system over its counterpart HVAC transmission system are as follows:

-
- No intermediate taps for long distances, no L and C losses, no frequency (no reactance) and stability problems, therefore infinite extensions (no distance limitation).
 - No doubt the converters are expensive, however narrower Right-of way and towers, fewer, thinner, and cheaper DC transmission lines, lead to overall lower investments saving land and money.
 - Overall lower transmission losses (Least corona loss, less radio interference, no proximity and skin effects, no varying EM fields, and least voltage regulation).
 - No charging current and no stationary magnetic field due to the induced body currents
 - Unity power factor (no need of reactive compensation).
 - No frequency limitations, full conductor cross-section utilization, only R, hence no phase shift b/w I and V
 - For long HVAC overhead lines one serious problem is the reactive power consumption and production due to L and C effects leading to much wear and tear and more complicated line control.
 - Optimal, flexible, and decoupled control of the active power (easy control of power)
 - Due to lower losses and higher voltages (less heat generation), HVDC transmission is more reliable for long distances as there are least blackout/brownouts.
 - With least black outs, DC transmission is cost-effective for long distances and hence reduced electricity bills (no wastage of money in frequent repairing of the damaged infrastructure like that of AC systems)
 - Connection of mainland networks to the Islands
 - Asynchronous network ties facilitating access to the mega power markets/projects and International Electricity Trading.

- Business, job opportunities, more affordability, and energy savings/ storage.
- No environmental impact (environment friendly) almost green energy.

Figure 1.2 shows a comparative evaluation of HVDC and HVAC transmission systems. It is seen that the cost per unit length of an HVDC line is lower than that of an HVAC line of the same power capability/capacity. Indeed, maximum transmission capacity, efficiency, and cost-effectiveness increase beyond (600-800) km called the break-even distance.

1.4 An Overview of Modern HVDC Converter Technologies

In order to convert the electric power from AC to DC (rectifier) or DC to AC (inverter), a power electronic converter is required at each terminal of an MTDC grid. Two types of the HVDC converter technologies currently in practice are the classical Line Commutated Converter technology (LCC) or conventional Current Source Converter Technology (CSC) and the self-commutated Voltage Source Converter technology (VSC) [7, 15, 20–22]. The development of power electronic semiconductors in the late 1960s led to Thyristor-based valve CSC technology. It was first tested in Gotland transmission in 1967 and later introduced on a larger scale in Canada in 1972 with a rating of 320 MW. One of the largest HVDC system's is the Three Gorges-Shanghai link with a rating of 3000 MW and ± 500 kV. Conventional HVDC system with the Current Source Converters (LCC-HVDC) requiring a synchronous voltage source to operate is shown in Fig. 1.3.

Despite merits such as a high power transmission capacity of more than 10000 MW with a DC voltage of about ± 1100 kV, a bulk power transmission distance of more than 3000 km, lower station/switching losses, and low cost, conventional LCC technology is unable to meet the important requirements of the future Super-grid. The LCC-based HVDC system is considered inefficient due to its several drawbacks as follows:

1. In the CSC-based HVDC technology, the converters are built with semi-controllable switches called the Thyristors. A Thyristor can only control

the instant (firing angle) at which the current starts to conduct by a gate signal. The thyristor cannot be turned off with a gate signal directly [21, 22]. Thus, any distortion of the AC voltage leads to commutation failures and an interruption of the power flow. Hence, in a CSC-based HVDC link, both the rectifier and the inverter should have sufficiently strong AC grids for valve commutation. LCCs can only operate with the AC current lagging the voltage, so the conversion process requires reactive power.

2. In this converter technology, the direction of the power flow through the converter is determined by the DC voltage polarity. In other words, a DC voltage reversal is associated with the power reversal. The DC current has the same polarity (constant). Therefore, it has only active power control and reactive power absorption. Continuous operation of the active power below 5% may not be possible, which complicates the operation at low wind speeds.
3. The reactive power must be supplied externally which is usually done in steps with the switched filters and the other capacitive elements.
4. The DC side of a CSC uses series-connected large smoothing reactors to maintain the current continuity. There is a higher generation of voltage and current harmonics on the AC side of a CSC. Thus, large AC filters are required to take care of these harmonics which leads to a large size of the converter station.
5. A minimum short-circuit ratio greater than 2, slower controllability, and no inherent black start capability are other drawbacks. It cannot deliver power to a network without other generation sources.
6. The complexity of this converter technology is increased in a meshed MTDC grid as the reversal of active power flow is only done through the DC voltage reversal. Hence, a high-speed communication between all the terminals is mandatory for control purposes.
7. The CSC-HVDC converter stations cannot be used for offshore because they need a voltage source to commutate and because of their large footprint.

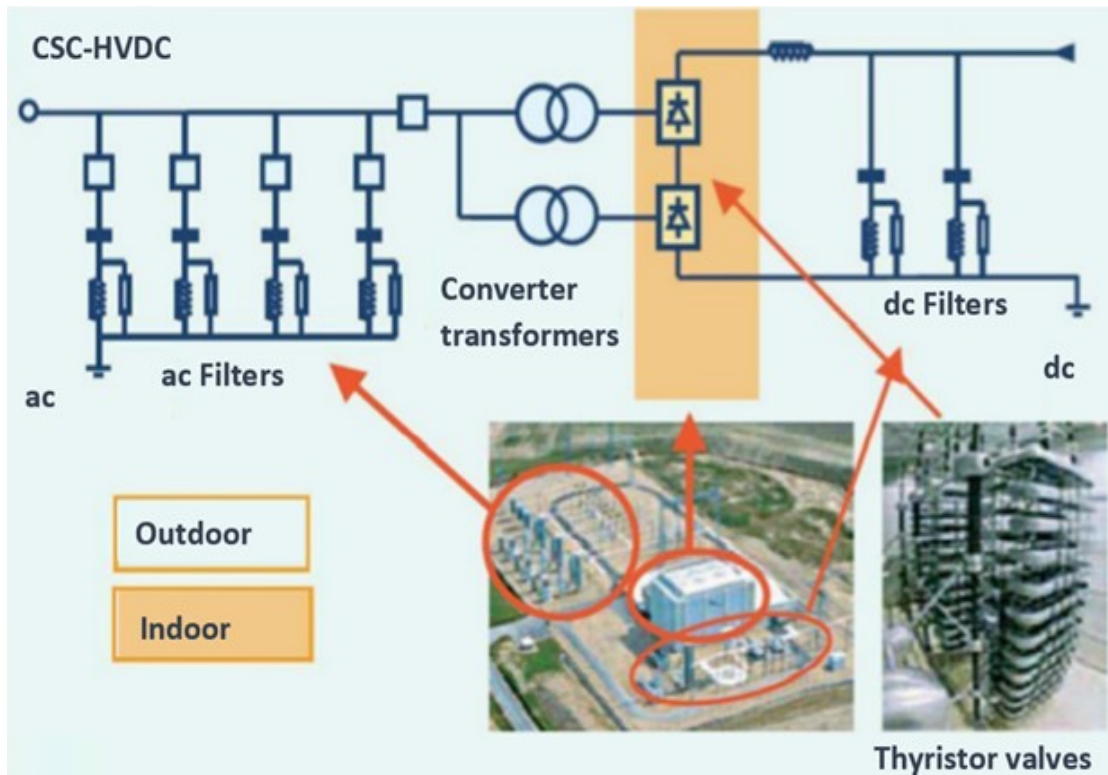


FIGURE 1.3: Conventional HVDC system with the current source converters (LCC-HVDC system) [23].

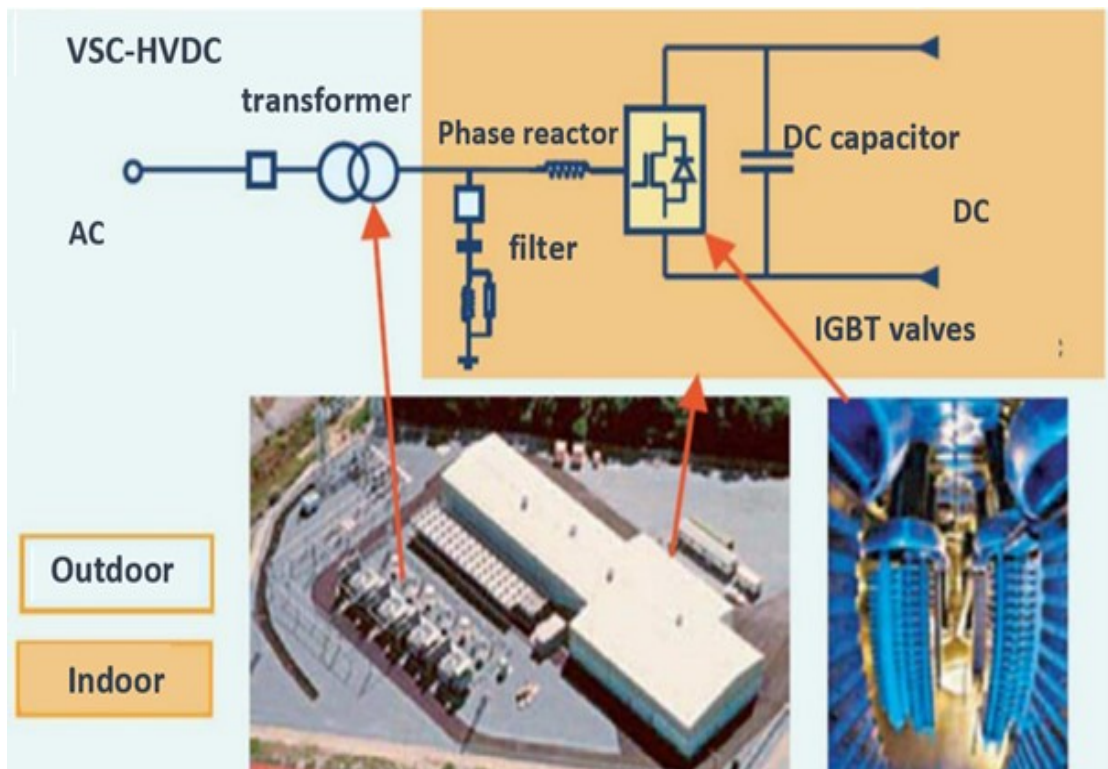


FIGURE 1.4: HVDC Station with Voltage Source Converters (VSC-HVDC System) [24]

1.5 Why a VSC-based HVDC Technology for the Future Super-grid

The first commercial VSC-based HVDC transmission using Pulse Width Modulation (PWM), was commissioned in 1999 on Gotland island with an underground cable (UGC) of 50 MW. ABB refers to the VSC-HVDC technology as HVDCTM. The VSC-based HVDC transmission system commercialized by Siemens is known as the HVDC PlusTM. A VSC-HVDC converter station shown in Fig. 1.4 mainly consists of high voltage valves having series-connected IGBTs, compact and dry high-voltage DC capacitors, high capacity control system, and solid dielectric DC cable. The size (volume and weight) of both the HVDC Light and HVDC Plus is very small (compact). The HVDC Light has a lower weight and the converters are based on PWM. In this topology of the multi-level approach, the individual module capacitors are uniformly distributed throughout the topology and each level is individually controlled to generate a small voltage step. Thus, each module within the multi-level converter is a discrete voltage source in itself, with a local capacitor to define its voltage step without creating the voltage ripple distortion across the converter's other phases. Hence, almost a sinusoidal voltage is generated by incrementally controlling each step at the AC outputs of the multi-valves. The VSC-MMC-HVDC/MTDC system with a key benefit of constant voltage polarity, explicitly offers considerable benefits and attractive features to fulfill the basic requirements of the future meshed Super-grid as follows:

1. Compared to a CSC-based MTDC network, various benefits of a VSC-based MTDC system include better controllability, flexible reactive power support for the AC grids/stability of the AC network, black-start capability, improved security, smaller filter sizes, little maintenance of the stations, no need for short circuit ratio, self-commutation, uninterrupted power flow control, and less environmental impact.
2. Functions like back-to-back link, dynamic voltage and frequency control, invisible power lines, operation in extremely weak AC systems, addition of the energy storage sourcing elements, no restriction on multiple in-feeds, oil-free cables, remote operation of the converter stations, no polarity reversal,

and simpler interface with the AC systems have made the VSC-based HVDC network a powerful technology for the MTDC projects. Some projects of building the hybrid grids are also going on. In a hybrid grid, positions with only in-feed like wind parks are connected with the CSC stations and the rest of the grid is then constructed from the VSC stations.

3. The VSC technology deploys many selective fault management strategies such as the fault blocking capability of the full-bridge MMC (FBMMC) technology. A VSC-HVDC link can be used for real-time power oscillation damping, voltage stability control, and power system stabilizer by modulating its active and reactive powers.
4. A VSC-based HVDC transmission technology has attractive technical and economic advantages over conventional CSC-based HVDC systems to enable the operation of the future Global-Grid. This technology is economically feasible to connect the small-scale renewable power generation plants to the main AC grid. Self-commutation, dynamic voltage and frequency control, and black-start capability allow this transmission technology to serve the isolated loads on the islands or offshore production platforms over long-distance submarine cables. This technology efficiently uses either long-distance land or submarine cables as the converters can operate at a variable frequency to efficiently drive large compressor (pumping loads) with high voltage motors. This capability can eliminate the need for running expensive local generation.
5. A VSC-based MTDC grid requires less or no communication between its interconnected converter stations during normal operation. Although the controllers at the VSC stations are identical in design, however, they work independently (independently control both the active and reactive powers). Thus, several VSC converters are interconnected to infinitely expand the MTDC networks. Both communication dependent and independent protection schemes can jointly perform well in these networks. A VSC-based HVDC link can be used as an AC link as the power flow reversal is done through the current reversal with the DC voltage polarity remaining constant. Thus, there is no need for polarity reversal to reverse the power flow.

6. Using the VSC technology, remote islands, mining districts, and drilling platforms can be supplied with the power from the main grid. This technology offers infinite extensions to the MTDC networks due to the implementation of extra-long hybrid transmission lines/mediums HTLs/HTMs [7, 27, 28]. This converter technology is an optimum approach to satisfy the ever-growing demand for renewable energy by constructing more Offshore Wind Farms (OWFs). Wind (stronger and steadier) captured in OWFs is used to generate a bulk amount of smoother electricity. This technology also relies on a new type of underground cable (UGC) which can replace the OHL at no cost penalty.
7. The VSCs consist of IGBT valves with pulse width modulation (PWM) to create any desired smooth voltage waveform (staircase) and any phase. An IGBT with fast commutation consists of a PNP Bipolar Junction Transistor and a MOSFET. Small-sized IGBT cells are connected in parallel in the IGBT chips and then in modules capable of handling current up to 2.4 kA with a blocking voltage of up to 6.5 kV. Advantages of the IGBTs like high short circuit current withstanding capability and fast interruption time (an IGBT is able to switch the fault current with a proper gate signal and turn-off time of about 3 μ s) [26], make them suitable switches for the VSCs. These switches are able to interrupt the fault current at any instant by a gating command.
8. A VSC-HVDC system can fully cope with the grid code and the wind farm can be separated from the AC network. Thus, the AC grid faults will not cause disturbances on the wind turbine or the faults in the wind farm will not affect the AC network.
9. A VSC-HVDC system can fully cope with the grid code and the wind farm can be separated from the AC network. Thus, the AC grid faults will not cause disturbances on the wind turbine or faults in the wind farm will not affect the AC network.
10. Optical sensing technology can facilitate high flexibility in the operation of a VSC-based MTDC/HVDC network. Because this converter technology implements the damage-resistant DC cables of extruded Polymer insulation

(DC voltage resistant cables)/cross-linked polyethylene (XLPE) cables of high mechanical strength, not possible with the CSC technology due to the voltage polarity. These cables are mostly buried except in the case of deep oceans. Therefore, in these cables, the reason for the fault is mostly due to the mechanical damages. Hence frequent faults on overhead TLs are the major causes of the MTDC/HVDC outages.

Figure 1.4 shows the key electrical components of a VSC-based HVDC system as follows:

1.5.1 AC-side transformer

This transformer connects a VSC station usually to the AC grid. Combination of AC grid and the transformer is called the AC Source Unit. Main functions of this transformer are to facilitate the connection of the converter to an AC system with a different rated voltage value, block homopolar harmonics to the main AC system and provide galvanic isolation between them.

1.5.2 AC-side filters

Switching action of the VSC-valves and use of Pulse Width Modulation (PWM) generate high frequency harmonics in the output of the converter. Thus, the voltage output of a VSC is not purely sinusoidal and contains a certain amount/number of harmonics. In order to remove or reduce the harmonic content of the VSC output voltage, a range of passive AC filters (2^{nd} order, 3^{rd} order or notch filters) connected in shunt between the phase reactor and the transformer are used. An RLC filter is used such that the tuned resonant frequency, quality factor, and the shunt reactive power are injected at the power frequency.

1.5.3 Phase Reactor

Another key component is the phase reactor which facilitates the active and reactive power transfer between the station and rest of the AC system. It attenuates the current ripples hence the peak-to-peak current ripple magnitude depends on its size. The larger the phase reactor, the lesser peak-to-peak ripple.

In other words, it filters the higher harmonic components from the converter's output current and limits short circuit currents through the valves. Since a larger

phase reactor also slows down the dynamic response of the converter, Therefore, there is a tradeoff in the phase reactor sizing.

1.5.4 DC-side Capacitor

DC-side capacitor is another key component which mainly performs three functions as: 1) filters the voltage ripples on the DC-side and maintains a stable DC voltage for VSC operation from which AC voltage is generated on the AC-side of the converter. 2) sinks undesired high frequency current components generated by the switching action of the converter valves and are injected to the DC-side. 3) acts as a temporary energy storage, keeping the power balance during transients. The time constant of the capacitor ranges from 2 ms to 4 ms. In practice, the size A DC capacitor is mainly determined by the desired transient behavior characterized by time constant.

Time constant is the time needed to fully charge the capacitor at nominal power and rated voltage levels. Also, the connection of the DC capacitors is in accordance with the adopted converter topology. In a symmetrical monopole topology, the DC capacitor unit is divided into two capacitors connected to the ground-clamped neutral point of the converter in the model.

1.5.5 DC-lines

DC transmission lines (cables and overhead lines) are used to transmit the power between the VSC-HVDC stations. As shown in Fig. 1.5, each DC pole is modeled as a Π -model, with resistance R_{pole} , inductance L_{pole} and two identical capacitors with capacitance $C_{pole}/2$ each.

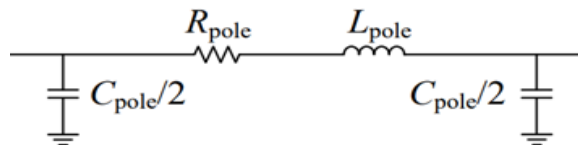


FIGURE 1.5: Pi-model of a single pole for a DC transmission link [98]

A hybrid transmission line HTL is a combination of cables (UGCs) and the overhead lines (OHLs). Cable poles (normally laid very close to each other) have a relatively high C and low L per km. On the contrary, OHL poles are relatively

distant from each other and therefore, have a relatively high L and low C per km.

1.5.6 AC/DC Converter

A VSC-HVDC uses IGBTs as the switching elements which can be fully controlled by PWM techniques. Among several possible configurations for a three-phase VSC, the simplest one is the two-level topology comprised of six switch arms, each IGBT switch anti-parallelled by a freewheeling diode. Compared to a Modular Multilevel Converter (MMC), it has more severe problems in harmonics. In this research work, a 3-level, bi-polar half-bridge VSC-MMC-MTDC meshed grid of 4 terminals is the target MTDC grid tested as in chapter 3.

Despite numerous applications and benefits offered by the MTDC transmission system, its protection is challenging and more difficult than its counterpart HVAC system's protection. A DC system has a higher rate of change in the fault current with faster propagation of the fault within a few milliseconds. Major obstacles preventing the scalability and development of the HVDC/MTDC systems include:

- Commercial lack of high rating DCCBs
- Absence of naturally zero current crossings (faster fault propagation)
- Minimum impedance (minimum reactance) in the HVDC lines resulting into huge fault currents
- Regulation/Standardization issues
- Grounding or corrosion issues
- Massive integration of non-linear power electronic devices
- Incompatibility between the converters from different vendors
- Multiple expensive converters

On downside, in comparison to a conventional CSC-based HVDC system, a VSC-based HVDC system is extremely vulnerable to the DC side faults, particularly the worst-case solid DC line/cable short circuit fault. This less-common fault is a major threat to its operation. Most vulnerable components to this fault are the

anti-parallel diodes of the IGBT valves, because the fault current through them should not exceed 2 p.u. Minimum impedance and absence of zero current points result in huge fault currents causing severe damage to the entire system within a short time.

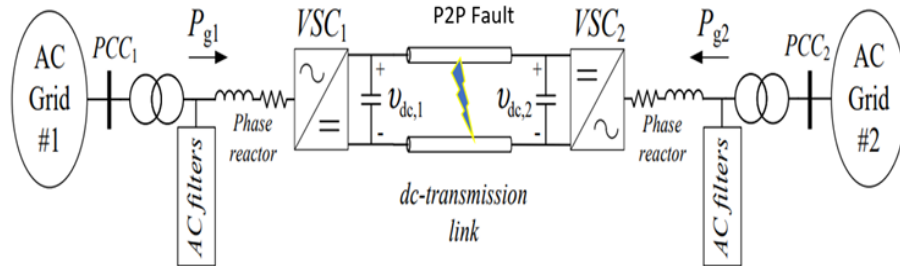


FIGURE 1.6: 2-terminal VSC-HVDC transmission link. The controlled power is the power entering the phase reactor with a positive direction towards the VSC station [98]

Fig. 1.6 shows a typical VSC-HVDC transmission link of two terminals in which the two VSC stations connect two AC systems through a DC transmission. The two AC systems are independent networks, isolated from each other, or nodes of the same AC system. A P2P fault is shown b/w the positive and negative poles of the link.

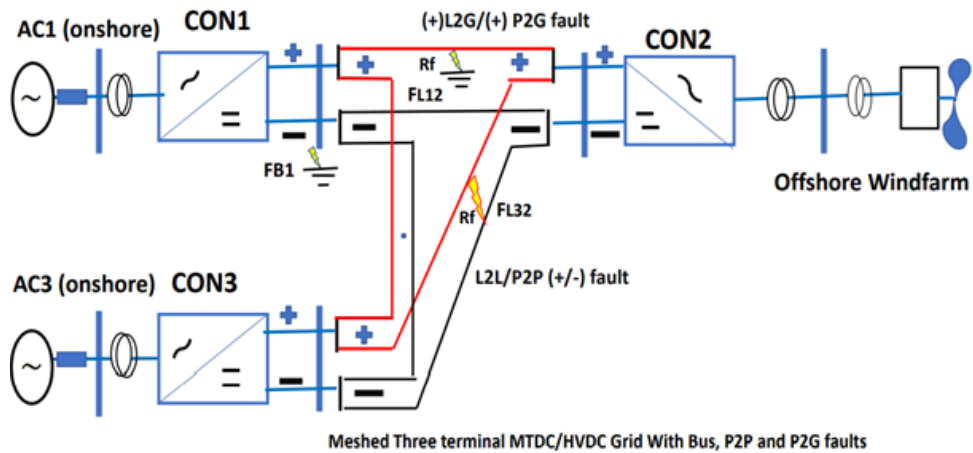


FIGURE 1.7: Block Diagram of a 3-terminal meshed MTDC grid with positive P2G and P2P faults

Fig. 1.7 shows the block diagram of a meshed 3- terminal MTDC grid, showing P2P/L2L and P2G/L2G faults. These are the most important faults which a protection scheme should consider. Protection of a DC system is more challenging and difficult than its counterpart AC system’s protection. Major hurdles include

absence of zero-current points (no frequency), minimum impedance (negligible reactance), commercial lack of high rating DCCBs, grounding /corrosion issues, and absence of a standard protocol for the HVDC networks.

Thus, a VSC-based MTDC system is extremely vulnerable to the DC faults like DC link/DC cable short circuit (P2P) faults, DC cable P2G faults, etc. DC cable short circuit (P2P) fault though less common or rare, is most damaging fault. Indeed, the IGBTs are blocked for self-protection, however, the DC fault is still feed through the anti-parallel or freewheeling diodes (uncontrolled bridge rectifier) which is a major threat to the entire MTDC system. Soon the short circuit fault current rises to a huge value abruptly within a few msec. The situation becomes more serious and severely damaging in a meshed HVDC/MTDC grid with multiple sources and multiple lines or feeders per every DC node as the fault is feed from all directions. This damaging overcurrent must be interrupted before the critical time limit (before 5 msec. or even less), otherwise even collapse of the entire grid will take place. Chapter 3 includes a comprehensive report about the development of DC cable short circuit fault current with complete fault response divided into three stages. Among the three stages, stage-2 is the most critical and challenging stage. In this stage the weakest antiparallel diodes to the IGBTs are most vulnerable components of the converters. These diodes which can only withstand a maximum current of 2 p.u. have to pass an abrupt overcurrent (high initial value) through them and IGBTs must be blocked within almost 2 msec.

According to the TW theory, the fault provoked TW travels back and forth (to and fro) along the cable from the fault point towards the converter station/detecting sensor or measuring unit. As the TW arrives the converter station at the cable end or sensor/measuring unit, it is reflected and refracted. The reflected wave travelling back to the fault point is again reflected and the similar phenomenon of reflections and refractions takes place. Due to this phenomenon of reflections and refractions, multiple peaks occur in the development of the fault current pattern as shown in Fig. 1.8(a). Consider a hybrid transmission line (non-homogeneous TL) with segments of OHLs and UGCs. A transition point is the point on it at which there is a change in the surge impedance. When an EM wave passes

through a transition point, a part of it is reflected, and a part continues to travel in the same direction. The initial wave is called ‘incident wave’, and the remaining two are called the ‘reflected wave’ and ‘refracted wave’. When a DC fault current transient (derivative) is zoomed in, a stepwise increase is seen in its development as shown in Fig. 3.6 Chapter 3.

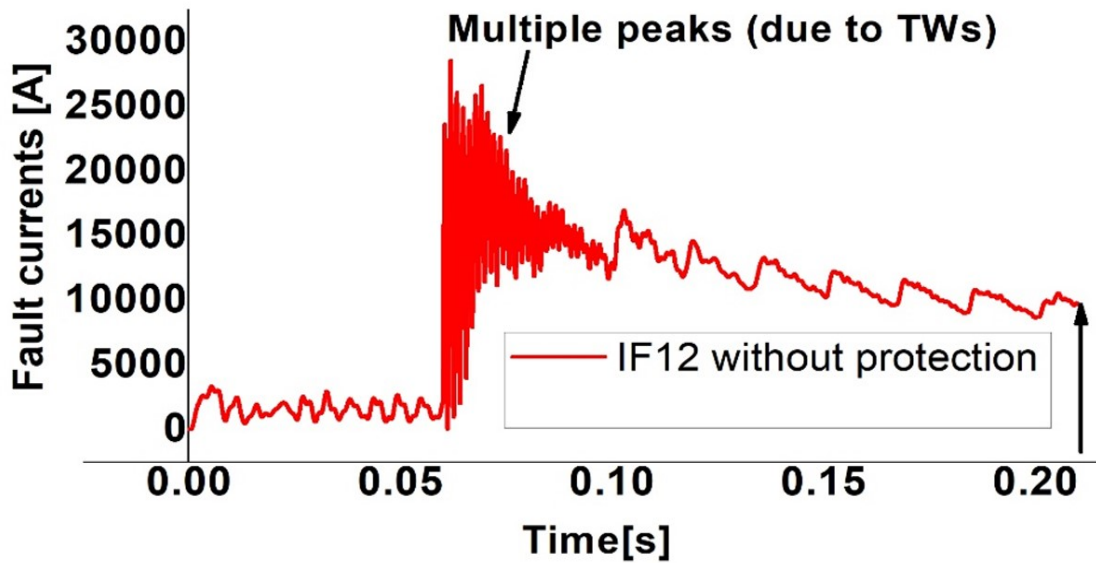
Additionally, distance of the fault point from a station’s node/ detecting sensor/-monitoring device called the fault distance and the fault impedance are the key parameters to detect and locate the fault in a TL. As the length of a TL increases, its resistance also increases causing damping (amplitude distortion) in the EM wave (the fault current transient). Therefore, if the DC cable short circuit fault is very close to a remote station’s node, it is impossible to identify the faulty line among the healthy ones within a few msec. and soon the whole system will shut down. A DC cable short circuit (P2P) fault depends on the factors like critical time limit (time required for the DC voltage to drop to zero level Fig. 1.8 (b)), DC fault current at the critical time, fault distance, line impedance, wave frequency, amplitude, and damping (attenuation factor) of the TW.

In this research work, all these important parameters useful to detect and hence, locate/isolate the fault in a TL are rigorously studied and analysed with the extensive set of MATLAB simulation results. By studying the influence of different fault distances, different fault impedances, and varied fault locations on the fault provoked DC current and voltage transients, It is concluded that in a VSC-based HVDC/MTDC system, the DC current transient (TW or derivative) contains the fault characteristics. Since, an FCL or any interruption device increases the grid impedance and affects transient (dynamic) response of a system, therefore, if the line end inductance value is increased to a large value [76,55], the cable current will eventually decrease (highly unwanted).

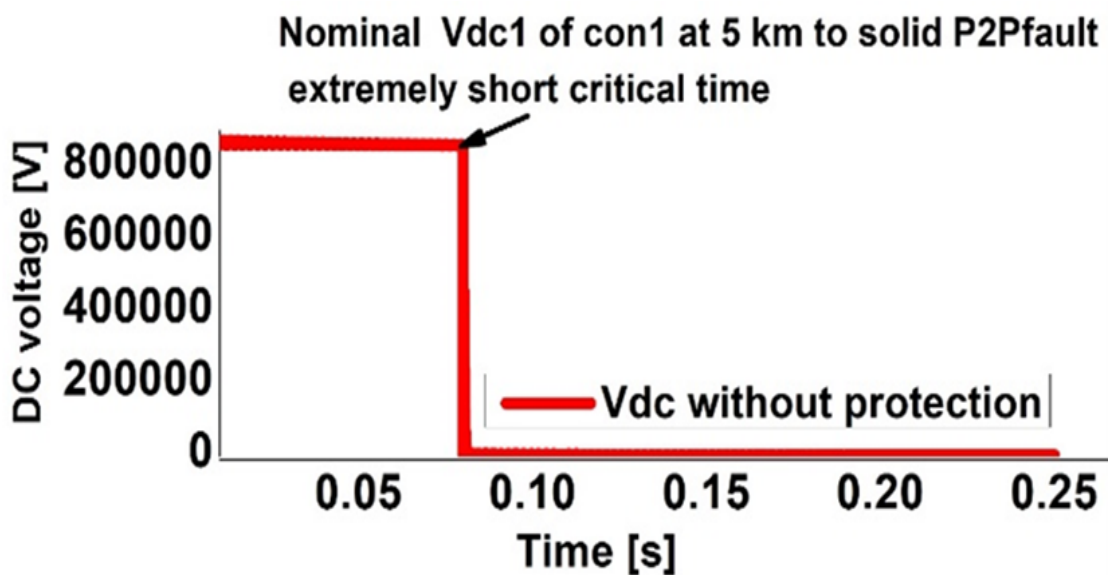
As the rectifiers (sources /energy suppliers) to the grid will block earlier than the inverters, in this scheme appropriately sized inductors (2/pole) are installed only at the DC output of sources (AC/DC) converters to limit the AC side contributions to the DC fault current and avoid damage/allow continuous grid operation during the faults. This way of active limiting technique is not reported so far in

any protection scheme proposed for a VSC-HVDC system. It allows to use limited soothing inductors.

Further sensors/current measuring units are installed on the line side of an FCL so a TW will be first incident on the sensor. In this way a compromise can be achieved.



(a)



(b)

FIGURE 1.8: (a) Huge DC fault current for a solid P2P fault at 60 msec. and at 10 km to the source Station node B1. (b) DC link voltage for a solid P2P fault at 5 km to the source node B1 (MMC1) without protection

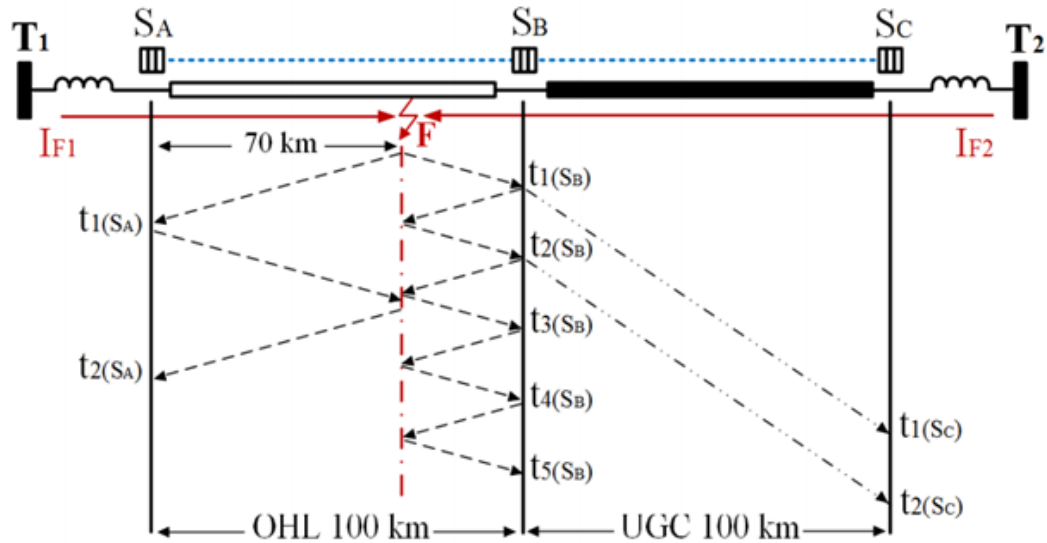


FIGURE 1.9: Bewley Lattice diagram incorporating OHL, UGC and distributed optical current sensors for the fault current development [76]

Fig. 1.9 shows a lattice diagram which indicates the general idea of the fault triggered TW reflections and refractions. In Fig. 3.6 in chapter 3 a clear TW effect (staircase waveform) is seen in the development of the DC fault current transient measured at 1 km to 10 km to a VSC source converter station. The time taken by the fault provoked current TW (associated with the attenuation or damping variable) to travel from the fault point to a station's node is denoted by τ . During simulation tests it is also seen that the closer the DC fault is to a node (source node), higher the magnitude of the DC fault current gets. Importantly also, at the fault distance ' D_f ' of 1 km to 13 km the DC voltage drops abruptly to zero or very near to the zero level. As D_f is increased beyond these distances, V_{dc} also starts increasing which shows the closeness of a station/node/sensor to the fault point respectively.

1.6 Research Objective

No protection strategy exists in the literature so far that has combined the joint performance of communication dependent current differential and TW methods based on optical sensor networks and independent DWT, current derivative data, overcurrent relays, active/passive FCLs, fast HDCCBs, ACCBs, and other simple backup plans to explore rigorously all the important aspects of the DC fault clearance time both theoretically and with numerical simulations having appropriate

data and analysis. During normal operation, a VSC-MTDC/HVDC transmission system requires no or very less communication between its interconnected terminals. Although the controllers at the stations are identical in design, but they work independent of each other (independently control both the active and reactive powers). However, during the fault conditions, communication between the converters and fault coordination is very essential in order to locate a remote station close-up fault. This means that both the communication dependent and independent schemes can be jointly implemented to protect these grids from the DC faults.

Thus, the primary goals of this PhD thesis are as follows:

- **To investigate** the general requirements of a feasible HVDC/MTDC protection scheme and hence, propose a comprehensive, robust, novel, fully selective, seamless, and cost-effective VSC-MTDC protection scheme, capable of completing the total DC fault clearance time within a few milliseconds of the critical time limit.
- **To analyze** the system's fault response especially for P2P faults in terms of critical time limit and overcurrent. To analyze the impact and influence of different fault locations, varied fault distances and fault impedances on the fault provoked DC voltage and current transients (TWs). Then after comparing with theory, explore rigorously all the important aspects of the total DC fault clearance (response) time both theoretically as well as with the appropriate data and extensive simulation results. The important aspects include:
 - Fast and unified real time fault detection
 - Accurate faulty line / segment discrimination (determination) from the healthy ones.
 - Effective fault current limiting much below the breakable levels of the hybrid DC circuit breakers.
 - Fully selective isolation of only the faulty line from the system while resuming normal operation of the healthy grid zones with little power adjustments (without shutting down the entire system).

- Accurate fault location.
- **To design** the 3-level, bi-polar half-bridge VSC-MMC-MTDC meshed grid models of 3 and 4 terminals and test in MATLAB using Sims-Cape Power systems.
- To design appropriately sized active and passive FCLs using multi-run simulation tests based on the following important specifications and parameters:
 - Timely analytic results of total contributions from the weak, medium strong, and very strong AC sources to the DC fault current.
 - Rated AC and DC voltages, Rated power, Peak currents on the healthy and faulty cables, and Current ratios.
 - Current limiting effects of the FCLs based on FCL triggering current, response (transition time), precise thresholds detections with different diode sizes, bidirectional fault trapping hybrid DCCB properties, and other issues.
- **To achieve** the DC fault clearance time of 5.1 or 5.2 ms within the critical time limit and the fault current suppression much below 1.7 kA through the coordination of bidirectional hybrid DCCBs, active/passive FCLs, converter configuration, relay/sensor threshold settings, and simple backup plans with the proposed fault discriminating, detecting, and locating methods.
- **To implement** the faults especially DC cable short circuit faults at different locations along the cables and analyze the influence of varied fault distances and fault resistances on the fault provoked DC voltage and current transients.
- **To Distinguishing** DC cable pole-to-pole faults from pole-to-ground DC faults.
- **To compare** all the simulation results obtained without and with protection devices with the previously and recently proposed HVDC/MTDC schemes in the literature and draw conclusions based on the simulation results obtained.
- **To, characterize** two ways of protecting an MTDC grid from the DC side faults into one scheme. The two ways are:
 - Shortening the overall DC fault clearance time through accurate determination of the faulty line with fast real time fault detection. Thus, allowing the concerned CBs to operate before the critical time limit.

- Extending the total DC fault clearance (grid outage) time through significant suppression of the DC fault current much below the breakable levels of the available CBs. Thus, gaining more reaction time for the fault detection, its location, faulty part isolation, and the system restoration

1.7 Main Fault Isolating Unit (Fault Clearing Unit) Used in the System Model

FCU is a series combination of bidirectional hybrid DCCB (HDCCB) and a DC resistive type- SFCL (R-SFCL) replacing the series reactor especially on DC cable pole ends at every node. FCUs are installed at the DC cable ends (2/pole or 4/cable) and 2/converter DC output. DC current measuring units (assumed as optical sensors) are distributed on π -section cables with each DC cable having a positive and a negative pole. Maximum of HDCCB current depends on factors like series reactor, DC capacitor, distance to fault D_f , fault resistance R_f and the power of adjacent AC source.

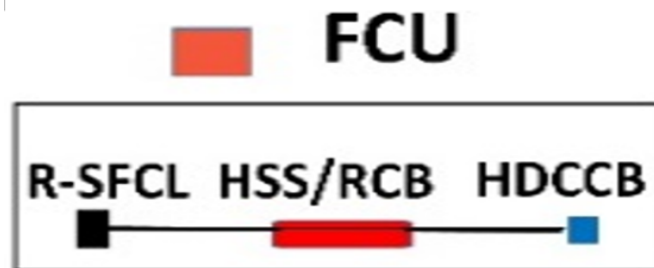


FIGURE 1.10: DC Fault Clearing unit (Fault Isolation Unit)

Larger DC capacitors like $100\text{-}200\mu\text{F}$ increase maximum HDCCB current and system inertia. However, they also improve voltage stability in the grid (suppress over-voltages while increase minimum terminal voltages). Capacitor size may only marginally affect HDCCB voltage. Therefore, four DC-node (Bus-bar) capacitors of $5\ \mu\text{F}$ to $50\ \mu\text{F}$ were added to accelerate the R-SFCL quenching.

A brief description of working of HDCCB is written in chapter 2, Fig. 2.3, page 37. It has a breaking time of 2 ms achievable. The maximum breaking current is 9 kA and anticipation is up to 26 kA. The HDCCB type used in this project

has bidirectional fault tripping capability. It coordinates well with the highly selective current differential algorithm which works well with small sized FCLs (small sized inductors). A General perspective about the parameters of FCU is briefly explained in chapter 4. For a 200 km cable length, a time delay of 1ms to 2 ms is ok with HDCCB operation.

In the existing literature so far various algorithms and efficient methods have been proposed to protect the HVDC/MTDC systems. However, the work done is mostly for HVDC links. Each of these methods, algorithms, and devices are discussed briefly in chapter 2 (literature review) of this thesis. Based on the preliminary conclusions of existing techniques and in-depth simulation results obtained the total fault processing time (fault detection, faulty line discrimination, fault current interruption, faulty line isolation) is kept within a few msec. by immediately interrupting the fault current before the critical time is reached.

1.8 Thesis Structure

Rest of the thesis is organized into four chapters. Chapter 2 Explores literature survey. Chapter 3 Includes the modelling of a meshed four terminal VSC- MTDC grid. It also explores the DC side faults especially the DC cable short circuit fault both theoretically as well as with the simulation results. Chapter 4 Includes the proposed protection scheme. The scheme is divided into two parts of theoretical analysis and the simulation results. Chapter 5 Concludes the whole report, summarizes the main findings and contributions of this thesis work. It also suggests some interesting topics for the future work.

Chapter 2

Literature Survey

2.1 Introduction

The most superior and effective solution for the reliable operation, integration, and extension of the HVDC/MTDC transmission grids is to install the high rating DC circuit breakers DCCBs at each end of a DC line. However, currently, such devices are commercially unavailable, while the proposed DCCBs (prototypes) have limited current breaking capabilities [25–30]. Indeed, extensive research, many selective algorithms, and strategies have been proposed for the HVDC networks to shorten the fault clearance time. However, the work is mostly for conventional point-to-point HVDC links or tested for small-scale grids up to the laboratory level experiments. The work is still in its immature stage, and there is no fast protection scheme with a mature science available, especially for the protection of the medium and large scale meshed MTDC grids. With the current technologies and proposed devices, it is impossible to satisfy the demand for a few milliseconds of the total DC fault clearance time (fast DC protection scheme). Following are the alternative methods which have been proposed in the existing literature so far to protect the HVDC grids:

2.2 Device Based Protection Strategies

2.2.1 AC Circuit Breakers

Slow ACCBs, lacking both speed and selectivity are practically unsuccessful in a meshed MTDC grid [31, 32]. Thus, the non-selective Hand Shake method can

cause loss of the entire DC grid (slow decaying behavior of the fault current) by tripping all the ACCBs/blocking all the converters at the same time. Also, ‘cut-trial and wait’ schemes won’t be successful in a meshed grid with multiple feeders, requiring an extraordinary strict time constraint of a few milliseconds to clear the DC fault. The ACCBs with the HB-MMCs and fast DC dis-connectors (FDs) cause loss of the entire HVDC grid by tripping all the ACCBs or blocking all the MMCs immediately once the DC fault is detected [31]. Further, in the absence of a converter, this method is incapable to detect the signs of the fault currents at a DC bus (node) lines of the converter.

Opening of ACCBs takes about 50 ms, the fault current naturally decays to zero while all the FDs open, and this process takes a very long time of 200 ms. Long interruption time due to the ACCBs exposes the DC system to high fault currents and there is only time wastage in unnecessary tripping of the healthy lines using the ACCBs and HSSs [31]. The ACCBs installed on the AC side of the converters can be used for conventional point-to-point HVDC links. Importantly also, being a mature technology with their low cost, ACCBs can be used as one of the final backup options to increase the reliability of a meshed MTDC grid with multiple sources. If the DCCBs fail in a DC line, one good option to eliminate the fault current contribution of the converter connected to the DC node having a failed breaker, is opening the converter’s ACCB, since here additional components are not needed.

2.2.2 Converter Configurations

Conventional two-level VSC’s and the half-bridge MMC’s cannot limit the fault current, because in the former capacitor discharge during the DC fault takes place even when all the IGBTs are turned off to prevent the device breakdown. In the HBMMC, although the capacitors are prevented from discharging, however, the circulating fault currents exist due to the arm inductors. One option to control the fault currents is that the antiparallel diodes on the fault paths can be replaced by the Thyristors.

Full-bridge fault blocking MMCs (FBMMCs) block the AC infeed currents. FB-MMCs with full-bridge sub-modules SMs are blocked to prevent the discharge

of sub-module capacitors and to interrupt the fault current contributed by the connected AC system. However, delivery of the active power amongst all MMCs is interrupted during the fault clearance. Such converter topologies using FB or clamp double (CD) SMs consist of a larger number of semiconductor devices and are subjected to higher conduction losses. Thus, their higher conduction losses and cost than the half-bridge converters, reduce their reliability in overhead transmission (OHL) schemes. Although the duration is shorter (<60 ms) compared to the ACCBs protection method, however, the power in-feed loss during this period is still highly undesirable in an MTDC grid. Indeed, the converter topologies and control are critical both for the fault current limiting and bypassing. Because due to the uncontrolled discharging from the capacitors and inductors, DC fault currents may not be fully limited.

Converter protection strategies can fail in ring topology grids due to the loss of selectivity and shutdown of multiple converters at a time. Uncontrollable discharging from the capacitors/inductors, and problems of restarting/restoration after the fault [33–35]. Further, some changes in topologies and /or semiconductor switches are necessary to allow a controllable switching on the fault paths, which results in increased costs.

Additionally, blocking of FBMMCs cannot prevent the current flowing through the diodes of the IGBTs from feeding a DC fault. In order to stop the energy sources at the converter side from contributing to a fault, the SMs within the MMC are bypassed. To transform a DC fault into a balanced AC short-circuit, MMCs are bypassed using Thyristors to clear the DC current gradually and then recover MMCs. Additionally, Thyristors withstand large AC currents and these methods could also be implemented for the HVDC grids. However, Thyristors cannot be turned off when their currents are different from zero. Therefore, the recovery of an MMC station from a bypassing operation is slow. Further, due to the long fault clearance duration, the AC system is exposed to a large AC current which causes more severe disturbances to both the DC and the AC systems. The concept of bypassing an MMC using its own IGBTs has only been tested in a point-to-point HVDC link and not in the HVDC grids. Because coordination of various types of

DCCBs, FCLs, with the relay/sensor threshold settings, converter configurations, network topologies, and the fault detecting/locating algorithms is extremely important to design a feasible MTDC protection scheme [36–38]. A rigorous analysis of the maximum arm and AC currents of an MMC during bypassing is required, as the IGBTs have a low current capability.

2.2.3 Proposed DC Circuit Breakers (Prototypes)

A high rating DCCB that satisfactorily interrupts extremely high fault currents within a few milliseconds is the most reliable and superior solution for the protection of an HVDC/MTDC system. However, its commercial lack is a huge challenge in HVDC/MTDC systems preventing their integration, extension, and development. There is no satisfactory HVDC Circuit breaker available so far, and hence deep research is required in this field. The HVDC circuit breakers (CB) must create artificially a current zero in order to interrupt DC current.

Additionally, the fault detecting and locating algorithms should be immune to the practical installation of various types of DCCBs, FCLs, and other components. Many HVDC circuit breaker concepts have been proposed in the existing literature. However, all have a similar structure, consisting of a commutation branch to drive the current to zero, a switching component for voltage withstand, and an absorption path to dissipate the energy.

Generally, DCCBs are classified into three categories as:

- Mechanical DC Breakers
- Solid state DCCBs
- Hybrid DCCBs
- Resonant [28]
- Superconducting [29]

The features of main topologies analyzed so far are discussed below and compared according to the literature. However, these figures may improve in future according to current interest on the development of HVDC-CBs and the considerable effort

that is being made. Thus, the interruption time, on-state losses, voltage and current rating, internal commutation time, losses, costs, and maintenance are discussed using different concepts in literature.

2.2.3.1 Mechanical DC Circuit Breaker

A mechanical DC breaker (MCB/MDCCB) is the first generation of HVDCBs and is based on the technology of AC gas breakers (both air-blast and the SF₆ ACCBs) [93-94][73]. Though in the MDCCB, a resonant circuit is used to create artificial zero-current crossing, however, speed of operation is still challenging due to extraordinary strict DC fault clearance time of a few milliseconds and maximum current.

A MDCCB has negligible on-state losses, low installation cost, but requires maintenance. Interrupting capability is (2-16) kA, voltage rating is less than 400 kV, rate of rise of fault current is (1.6-2) kA/ms, and internal current is less than 5 A to 8 A. It is always used with the FCLs (RSFCL) as it is slower than the other breakers with a clearance time of tens to a hundred of milliseconds (usually 60-100 ms). As shown in Fig. 2.1 a MDCCB has three branches, branch A (switch) in parallel with branch B (an LC resonant circuit) and branch C (a surge arrester). Indeed, MCBs have lower on-state losses and installation costs, however, their internal current commutation times are higher. These features are improved in both solid state and hybrid CB.

The switch remains closed during normal operation and paths B and C are short-circuited. However, during fault conditions, the switch opens resulting into the high voltage arc and this arc can initiate the oscillating current in loop A & B at its natural frequency. The arc is subjected to negative voltage-current characteristic and due to positive feed-back it keeps increasing till the maximum current hits the set value of current interruption. Soon the oscillating current crosses 0 and the switch interrupts the current (CB is open). Thus, the commutated current starts charging the capacitor immediately till in branch C the voltage reaches the threshold of the Surge arrester. The energy is dissipated through the surge arrester, therefore voltage across the capacitor and the commutation current, both are limited.

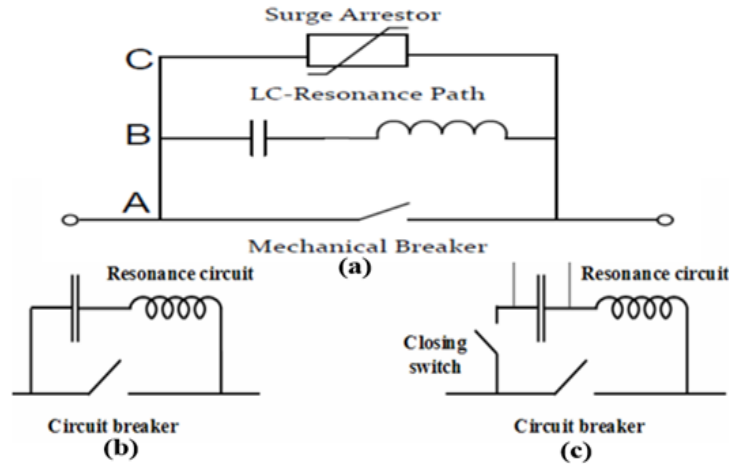


FIGURE 2.1: Mechanical DCCB (a) Air-blast MDCCB Basic Topology [93] (b) Passive type. (c) Active Type

2.2.3.2 Solid State Circuit Breaker or Semiconductor Circuit Breaker

It is fast (a fault clearance time within 1ms is achievable) [26]. Its current interruption capability is 5 kA to 19 kA (expected), voltage rating is 132 kV, rate of rise of fault current is 47 kA/ms and internal current is 0.4 A. However, compared to mechanical CB its on-state losses and installation costs are high, but maintenance cost is low. The switches used are IGBTs, gate commutated turn-off thyristors, and GTOs respectively.

Due to its fast interruption capability, IGBT breaker is a good candidate in the DCCB and is anti-parallelled with a diode (free-wheeling diode). The topology of an IGBT breaker is shown in Fig. 2.2. As can be seen there are two main paths to enable the bidirectional power flow. Each path has diode in series to prevent the current flowing through the freewheeling diodes. Series connected IGBT breaker models increase the withstand capacity of the breaker. Surge arresters/surge arrester banks (energy absorption branch) used to limit the fault current are also connected in series. The number of IGBTs should be selected according to the CB voltage and current rating. During the fault detection in a line, the concerned IGBT breaker will receive a blocking signal. When the fault current is interrupted, fast acting DC switches (HSSs/fast DC disconnectors) are opened to isolate the faulty line from the system.

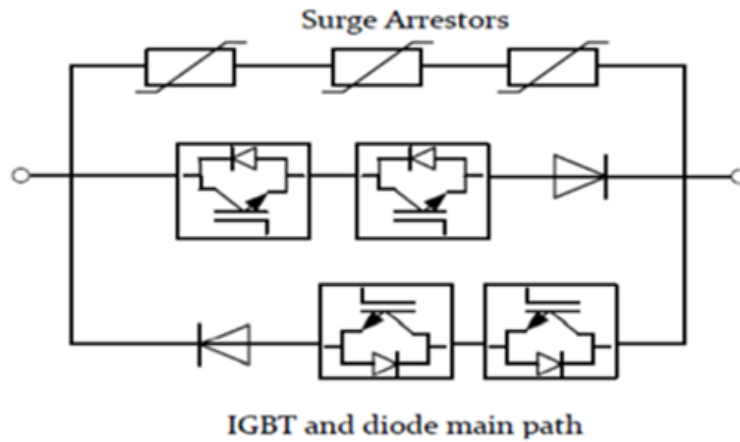


FIGURE 2.2: Semiconductor (Solid State) DCCB with IGBT Breaker Topology [39]

A proactive hybrid HVDC breaker (HDCCB) proposed has become commercially available by ABB in literature [96][75]. and combines the strengths of both mechanical DCCB and semiconductor DCCB. Thus, it offers both fast operation and low on-state losses. However, installation costs are high and maintenance is required. The fault clearance time for a proactive HDCCB is little higher than the semiconductor DCCB due to the time needed for the mechanical disconnecter. Thus, a breaking time of 2 ms is achievable. Minimum current breaking capability is 9 kA and maximum interruption capability is up to 26 kA (expected). Its voltage rating is 500 kV, rate of rise of fault current is 2.9-6.7 kA/ms, and internal current is 2 to 3 A.

The Design of a HDCCB has three sections 1) Section A consists of several groups of IGBTs connected in series and each group has a parallel surge arrester to limit the over-voltage during the fault occurrence. 2) Section B (a bypass path) consists of a fast mechanical disconnecter in series with the IGBTs and is used as the auxiliary DCCB to interrupt the current quickly. 3) Section C consists of the current limiting reactor (FCL) in series with the residual DC current breaker (RCB).

During healthy conditions, the current flows through the section B (fast mechanical disconnecter and the auxiliary DC breaker). During the fault, when a tripping signal is initiated by the controller, the auxiliary DC breaker in Section B opens quickly, driving (commutating) the current through the main breaker path/commutation branch in Section A. The fast DC disconnecter is opened as no current

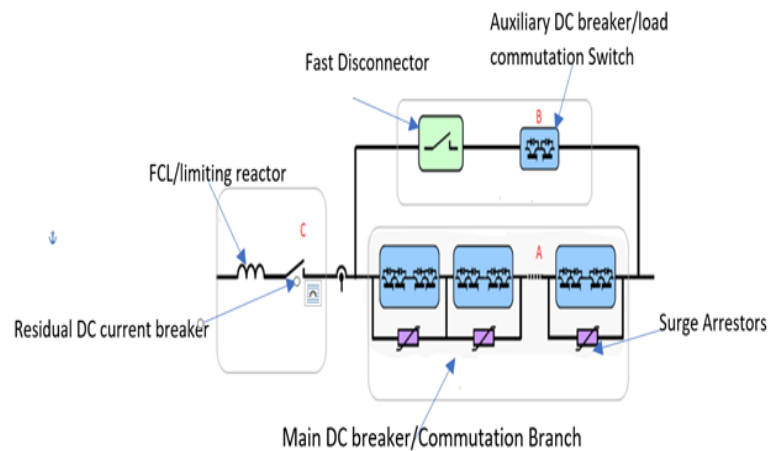


FIGURE 2.3: Proactive HDCCB Prototype from ABB (Hybrid 1 type) [96]

flows through it. Afterwards, the main DC breaker/commutation branch turns off leading to overvoltage which causes the surge arrestors/arrestor to operate. Thus, the current flows through the surge arrestors/arrestor and due to dissipation of the energy, the current gradually drops to zero. In a new solid-state DCCB (NSS-DCCB), the fault clearance within (2-5) ms by replacing the surge arrestors with an RC high pass filter action is achieved. However, again it can't be used for high voltage or current applications [31].

Another Hybrid-2 type DCCB combines the mechanical DCCBs or solid-state DCCBs and FCLs together to effectively reduce the fault current. When the fault is detected the switches in the main path are switched off and the current is driven to the second path through the FCL.

2.2.4 Various Types of Fault Current Limiters

A fast protection scheme keeps the total fault processing time within a few milliseconds by immediately interrupting the fault current before it becomes higher than the maximum current breaking capability of the circuit breakers. Although, a hybrid DCCB is a widely accepted alternative for the HVDC systems and takes a delay of 2-3 ms to isolate a DC fault. However, due to negligible impedance in the HVDC systems, even during this short time, the fault current will rise at a higher rate, particularly if there is a delay in fault detection. Therefore, another more direct approach is to limit the fault current itself and avoid damage to the

power system devices and components. By installing efficient FCLs on either AC or DC side or on both sides, the magnitude of the rapidly increasing DC fault current will be significantly reduced. In this way, the total DC fault clearance (grid outage) time is extended by gaining more reaction time for both fault detection and isolation. Reducing the fault current to significantly lower values before its interruption, not only prevents damage to the entire power system, but also brings down the ratings. Hence, this allows low cost protection devices to interrupt the reduced fault current leaving more time for fault detection, its location in the grid, faulty part isolation, and the system restoration. Inserting effective FCLs also improves the performance of ACCBs, reduces the current interruption stress on the available DCCBs, and allows the fast opening of auxiliary HSS/RCBs.

In literature, both passive and active FCLs have been introduced, such as protective inductors, saturated iron core FCLs, superconducting FCLs, solid-state impedance insertion FCLs (SSIIFCLs), solid-state bridge-type FCLs using Thyristors, PTC Resistors, liquid metals, and the LCL-VSC topology [40–49]. The DC-DC buck converters [49], fault blocking full-bridge MMCs (FBMMCs), and clamp double MMC's are also effective FCLs and can even interrupt the fault current. A buck converter becomes a surge-less DCCB if the IGBT of its upper arm is always on during normal operation and off during the fault conditions. In the DC systems, solid-state protection devices with ultrafast speeds are more suitable to limit the rapidly increasing DC fault currents. In series and bridge type solid-state FCLs selection of appropriately sized limiting inductors is one of the major design challenges. Superconductive inductors can be used in bridge-type SSFCLs in order to have low conduction losses during normal conditions. Superconductive inductors can also be used as energy storage for backup during an emergency. Usually, the DC side FCLs like protective inductors can effectively limit the fault current magnitude in Stage 1 (DC capacitor- discharge stage) and Stage 2 (diode freewheel stage) of the DC cable short circuit fault as well as during Stage 3 (grid current feeding stage). AC side FCLs limit infeed AC currents in Stage 3 (grid current feeding stage) of the fault response. However, neither the inductors on the DC side nor the FCLs on the AC side, alone can effectively protect the system

from the DC faults.

Stage-2 is the most challenging stage, in which the IGBT modules are blocked shortly by self-overcurrent protection as soon as the fault current starts to exceed a threshold level of about twice the nominal value [50]. The blocking condition of a half-bridge converter is when the arm current exceeds about 1.8 p.u. (w.r.t. peak arm current), and the conduction by all diode arms begins at this instant. Therefore, even after installing the FCLs on the AC side of the converters, the destroying overshoot current at the beginning of Stage 2 still exists. This forces the weakest diodes to pass a huge current with a high initial value through them and puts the diodes and cables at high risk. Indeed, Stages 1 and 2 are the most stringent periods to take the fault decision (trigger the IGBT block signal within 2 ms).

Now, in the existing literature, a simple approach is to connect large-sized and extra reactors of 150 mH to 200 mH in series with the DCCBs to limit the maximum DC fault current to around 3 kA to 4 kA or at the AC side of the converter to form an LCL circuit. Inserting protective inductors of suitable size between the cables and the VSC stations can effectively protect the system by limiting the capacitor discharge current, cable current, and diode current. Moreover, since the inductor's impedance is relatively low, therefore, the system efficiency is not affected too much during normal operations.

However, any FCL or interruption device increases the total grid impedance and slows down the dynamic (transient) response of the system. Therefore, increasing the size of protective inductors increases the total impedance of Stage 3, which causes a decrease in the maximum DC cable current.

Thus, various drawbacks of large-sized and extra inductors include increased grid inductance and time constant of the system, more reactive power losses, inductive kickback effects, voltage instability, increased mass and volume of a converter station, and increased cost [51–53]. Further reactor energy dissipated during the fault can cause increased DC fault current. Therefore, the single-ended methods can practically fail to locate the fault in a TL [54, 55]. Indeed, if the inductor size is increased to a very large value, the diode current would eventually drop

with the decrease in the total cable current which is highly unwanted. Actually, while sizing any FCL important parameters like the current limiting effect, dynamic slow-down effect, and the total cost of the project are very important. If the minimum sized inductors are to be used with the DCCBs, current sensors, or relays on the DC side, it has to be practically validated, which FCL on the AC side or which converter topology will co-ordinate with it to significantly suppress the fault current. A non-linear resistor such as a superconducting FCL (R-SFCL) being merely passive (resistive), does not affect the system's dynamic response. A non-linear resistor such as a superconducting FCL (R-SFCL) being merely passive (resistive), does not affect the system's dynamic response. It has low resistance during normal operations, which rises sharply after the fault due to its increased temperature resulting from the fault current. Once the fault is cleared and the temperature of an SFCL cools down, it becomes low in resistivity again. While testing, ideally the resistance of an SFCL remains zero during normal operation which jumps to high values (20~25) Ω at the fault instants and remains constant onwards. However, its drawbacks, of recovery time in seconds (>1 s), large quenching impedance, higher power consumption and energy dissipation, larger size, and high cost are highly unwanted in an MTDC grid [56, 57]. An MTDC grid requires instantaneous fault recovery, therefore, an appropriate impedance value has to be designed for a resistive SFCL to compromise with the cost and size. During testing, when the RSFCLs were installed on the DC side, the DC fault current was effectively reduced. The utmost requisite to shorten the total fault clearance time is accurate determination or discrimination of the faulty line or segment from the healthy ones with quick detection of the wavefront arrival time.

2.3 Various Methods of Faulty Line Determination and Fault Detection

The utmost requisite to shorten the total fault clearance time is accurate determination or discrimination of the faulty line or segment from the healthy ones with quick detection of the wavefront arrival time. Various efficient methods found in the literature are as follows:

2.3.1 Overcurrent Protection

Instantaneous overcurrent protection is a mature and widely used simple technique. Here the overcurrent relay measures the corresponding current and compares it to a given threshold. If its magnitude exceeds the threshold, a tripping signal is generated to trip the corresponding CB(s) and isolate the faulty line [50, 58]. However, the overcurrent protection is unsuitable for a meshed MTDC grid because it lacks selectivity, is sensitive to power production, load variations, and high impedance faults. Still due to its simplicity, cost-effectiveness, it might work as a powerful final backup plan, particularly when the fault occurs extremely close to a converter station/DC node.

2.3.2 Current and Voltage Derivative Methods

Algorithms for the fault detection and discrimination using the local measurements of current and voltage or their derivatives without using communications have been proposed in [59–65]. In the current derivative-based fault detection during a fault current derivative of the faulted line is higher than those of the other healthy lines of the grid. If the derivative exceeds a given preset threshold value, then the corresponding CBs are tripped to isolate the faulty line. However, the derivative detection method is useful mostly for point-to-point HVDC links. Fault detection based on the current derivative, though computationally efficient is not a reliable solution to protect a meshed MTDC grid with multiple power sources/nodes having multiple lines per every node. Difficulty in determining the faulted section independently as the system becomes highly meshed, sensitivity to noise, incorrect data samples, high impedance faults, and the inductor size are some drawbacks of the current derivative method. However, due to its capability of indicating the fault directions, the current derivative method with polarity principles helps to improve the selectivity of the DC protection scheme in identifying a faulty line and indeed, is a partial discriminative method. Therefore, the current derivative direction method can be used as a backup/auxiliary protection with the primary communication-based fault discrimination algorithms such as the differential protection and TW methods (type-D) in a meshed MTDC grid.

Importantly also, in a VSC-based MTDC grid, the DC voltage polarity remains

constant. Hence, the fault provoked DC link voltage transients (TWs) may give a rough estimation of the fault location in a TL, but cannot detect the wavefront [59, 62, 63, 65]. They cannot distinguish a faulty line from the healthy ones, particularly when the fault occurs very close to a station or a measuring point. Because in such cases the TW effect is not clearly visible in the DC voltage transients. In the pattern recognition method of the DC fault detection, the measured voltage is compared to an already known signal and the degree of similarity is measured by the Pearson correlation coefficient. However, the successful implementation of this method in a VSC-based HVDC grid is impossible due to the fixed DC voltage. It might fail in a VSC-based HVDC system, particularly for close-up faults. Fault detection method using the first and second current derivative local measurements with more line inductances as in [60] causes more reactive power losses [64].

2.3.3 Conventional Differential Protection and TW Principles

Relatively accurate location of the fault in a faulty line is estimated with conventional Type A (single-ended) and Type D (double-ended) traveling wave-based fault location methods. The wave velocity can either be calculated in theory or practically measured. The arrival time of the wavefront is determined with either the current derivative data or wavelet coefficient (WC) data obtained during the fault detection. A single-ended method requires the identification of two consecutive TW reflections measured at one terminal, while a two-ended method uses the first reflection only (captured and time-stamped at both the terminals). As the first reflection always provides the clearest signature, two ended method is considered more reliable.

The MTDC transmission system is basically built to transport a bulk amount of sustainable power over extra-long distances (>2600 km) for the overhead lines (OHLs) and (>300 km) for the underground cables (UGCs) with an extraordinary strict total fault clearance time of a few milliseconds.

Conventional communication-based current differential protection algorithm has high (intrinsic) selectivity. The speed need is somehow relaxed in the long cables in

discriminating a faulty line [66]. However, it is not suitable for the long/extra-long-distance power transmission due to its dependence on a communication system. The TW-based fault location and differential protection methods have a number of drawbacks such as the need for a high sampling frequency (large data storage and processing time), inherent communication delays of hundreds of milliseconds (larger than the wave propagation time), and delays associated with the encoding and decoding messages that cause measurement errors. Synchronization problems causing incorrect tripping, difficult detection of high impedance faults, frequent faults in the OHL's passing through complex terrains and operating under harsh weather conditions, amplitude distortions (attenuation of the EM waves) over long distances, the requirement of communication links and GPS installation particularly for Type-D method, failure in noisy situations, difficulty in detecting the wavefront arrival time, and difficult estimation of the propagation velocity are other drawbacks. Thus, there is a potential communication failure at any time and their reliability is not guaranteed for extra-long transmission lines/remote faults.

A fault protection method based on signal-processing with the burden of complex computations cannot be fast [67]. The differential protection method using master/slave control technique with sensors, and CPU based differential schemes can work well for bounded regions. They are not suitable for long/extra-long distances for which an MTDC network is constructed [68, 69]. The two-ended TW-based fault location method based on time-stamped voltage and current measurements sampled at 2 MHz even with noisy inputs might be very accurate. However, the fault resistances up to only 100 Ω , the need for a high sampling rate, and synchronized measurements are some of the drawbacks of this method [63].

To locate the fault in an MTDC grid, a single-ended TW-based fault location method along with two graph theory-based lemmas is proposed [70]. However, it also requires a high sampling frequency. To identify the faulted segment of a hybrid transmission line (HTL), the Type-A method utilizes both the current and voltage measurements and a support vector machine (SVM) in [71]. However, only 70 Ω fault resistance is used and the sampling frequency is not clearly specified.

The protection methods in [32, 39] are used to estimate the fault location, but no wavefront detection is given.

The differential protection scheme proposed in [72] uses a comparison of the current of each line terminal and mechanical DC breakers. However, assuming the use of fault-tolerant converters in order to permit low-speed fault isolation, only one criterion of a fixed preset threshold and no other criteria, make the algorithm vulnerable to noise [73]. In [74] the derivative of DC voltage utilized to quickly detect and locate the DC faults is not successful in the VSC-based MTDC grids. Also, in this method, the converter DC voltage immediately after the fault is assumed to remain unaffected. Additionally, highly resistive faults are not considered in this method. Both non-unit methods in [53, 74], do not consider the influence of power reversal and the transmission medium. The performance of the fault detection method based on capacitor discharge is poor under highly resistive faults [39].

2.3.3.1 Optical Sensor Schemes

Most of the drawbacks and challenges associated with the conventional differential protection and TW methods can be eliminated with Type-D TW-based fault location and differential protection methods, utilizing the measurements obtained from the distributed optical sensors on the hybrid transmission lines (HTLs) [75]. These optical schemes accurately discriminate a faulty segment, are robust to high impedance faults, and require neither a high sampling frequency nor an accurate GPS time stamping as synchronized measurements are ensured. Optical sensor networks can be installed on any TL regardless of the number of segments or sensors, as they are completely passive networks. Every optical sensor network operates independently and is not affected by the operation of any other sensing network. Distributed optical sensing technology interrogates all sensor data using a single measurement/fault locator station (Data Acquisition point) and relative robustness to noise is also ensured.

Indeed, optical sensing technology can facilitate high flexibility in the operation of a VSC-based MTDC network. Because a VSC-MTDC network implements the damage-resistant cross-linked polyethylene (XLPE) cables of high mechanical

strength, which are mostly buried except in the case of deep oceans. Therefore, in these cables, the reason for the fault is mostly due to mechanical damage. Technically, the connection between the overhead lines and the underground cables takes place at the “transition joint pits” where the actual onshore installations, current measurements, protective and control equipment are realized. Thus, in a VSC-based MTDC network, an optimum number of optical sensors can be equidistantly distributed on long TLs. Optical sensors can be installed around the transition joints, where the conductor connections take place and the current measurements realized.

Hybrid Fiber Bragg Grating Technology (FBG) is used to build the voltage and current sensors. Each hybrid transmission medium requires only one optical measurement interrogator and one fault locator station at one end (as the method is single-ended by nature). Each fault location scheme operates independently to facilitate higher flexibility. Pre-simulated DC cable fault currents at the corresponding sensing locations along the transmission line are used to produce replica voltage waveforms. These voltage traces (which represent the DC line currents) are physically input to the optical sensors. The FBG peak wavelengths are then recorded for all corresponding voltages. The sampled data obtained from the Optical Interrogator system is stored on a PC for further analysis (signal processing, plotting) by the protection algorithm in Simulink/ MATLAB. However, the higher sampling rates can be achieved when an alternate interrogator such as a solid-state based on an Array waveguide grating (AWG) with the scanning frequencies of greater than 100 KHz achievable, is used to further improve the fault location.

An FBG sensor shown in Figure 2.4 is formed by periodic modulation of the refractive index along an optical fiber core over a length of 5-20 mm. Bragg wavelength is given as:

$$\lambda_B = 2\sigma_{eff}T \quad (2.1)$$

where $\sigma_{eff}T$ is the effective refractive index multiplied by grating period of FBG section.

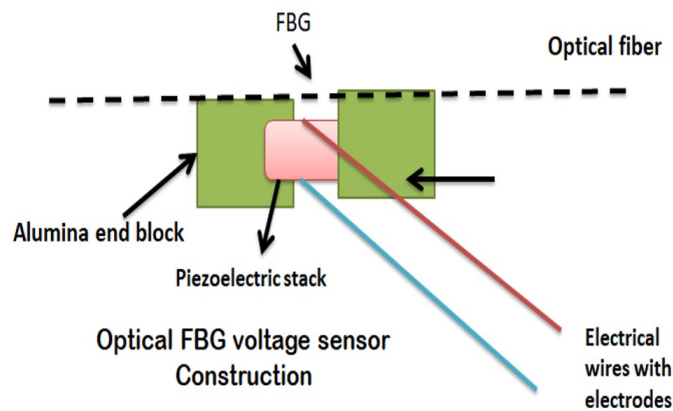


FIGURE 2.4: Optical FBG sensor construction [55]

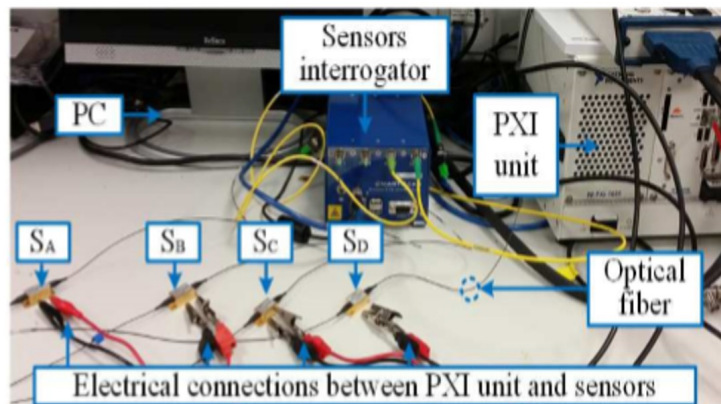


FIGURE 2.5: Fiber Grating Sensor Experimental Implementation taken from [55]

The voltage applied to a piezoelectric stack is converted to strain on the FBG and causes a shift in its peak wavelength calibrated to the voltage. If the piezoelectric component is replaced with the magnetostrictive transducer, a DC current sensor is realized. Light composite insulators guide an optical fiber between the sensors (installed directly on the conductor) and the pole which is at the ground potential. The optical fiber (black solid dashed line) as shown in Fig 2.4 above, is placed alongside the HVDC line or integrated within the conductors or wrapped around the conductors. Strain = longitudinal piezoelectric charge constant \times E (electric field = voltage across the piezoelectric material V / length (l) of the material). However, the reliability of these communication-dependent optical schemes is reduced for long and extra-long-distance power transmission. A communication-based fault discrimination/location algorithm practically fails for

the detection/location of a remote station close-up fault. Long overhead TLs passing through the complex terrains and operating under harsh weather conditions are often subjected to the faults. Hence, a permanent telecommunication shutdown with a remote sensor/breaker failure is potential, which is a major cause of the MTDC/HVDC outages. A worst-case close-up solid P2P fault at a remote station requires expensive backup plans.

Continuous wavelet transform (CWT) is not suitable for quick fault detection in a non-stationary random signal with multiple peaks, as it consumes both time and memory space. CWT is more accurate in off-line fault location for which high speed is not required, except in the case of permanent short circuit faults [75, 76]. Fig. 2.5 shows the diagram of experimental set-up utilized for practical validation of the optical sensing scheme taken from [55]. Here four FBG optical voltage sensors have been used along a 300 km transmission line. Pre-simulated fault currents at corresponding four locations along the transmission line are used to produce replica voltage waveforms (generated directly from a multifunction data acquisition card). These voltage traces represent the DC line currents, are physically input to the optical sensors and the sampled data obtained from the optical interrogation system is stored on a PC for processing by the protection system algorithm developed in Simulink. The FBGs are optically connected to a commercial Smart-Scan interrogator (Smart Fibres) offering a scanning speed of 2.5 kHz over a spectral range of 1528-1568 nm.

In the existing literature so far extensive research and experiments have been done to protect the HVDC/MTDC grids. Some focus on locating the fault, some focus on detecting the fault, while some focus on isolating the fault. Other approaches are limiting the fault current by introducing various kinds of FCLs. However, firstly the proposed work is mostly for conventional HVDC links or tested for small-scale grids up to the laboratory level. Secondly the core design demand for clearing the DC fault within a few msec. has not yet been fully satisfied by any proposed scheme or existing technology especially in a meshed MTDC grid. So far not much research has been explored both theoretically as well as with the appropriate results to combine all the important aspects (fault detection, fault

current suppression, interruption and isolation, fault location) into one scheme especially in a meshed VSC-MMC-MTDC grid. Most of the recently proposed protection strategies and approaches for the VSC-HVDC/MTDC systems have unfeasible technical specifications, lack reliability, mature science, and robustness. Traditionally, many schemes of protecting VSC-HVDC grids by installing ACCBs on the AC side have been proposed. ACCBs along with the fast DC disconnectors and current derivative direction method is proposed in [32-33]. However, such schemes are suitable to protect the point-to-point HVDC links.

As mentioned before, during a DC cable short circuit fault the fault current rises rapidly and abruptly to a huge value, making the fault clearance time extremely demanding within a few msec. of the critical time limit (less than or up to 5 msec). Slow ACCB (200 msec) lacking both speed and selectivity is practically unsuccessful in a meshed HVDC/MTDC grid with multiple sources/feeders.

Further, "Split /wait" and trial methods are unsuccessful in a meshed MTDC grid because it requires instantaneous operation and therefore, time wastage in incorrect tripping of the healthy lines would cause total collapse of the grid. Additionally, blocking all the converters simultaneously will cause shutdown of the entire grid. However, ACCBs can be installed as a final backup plan with the primary protection scheme on the AC side of the converters to increase the reliability of a protection scheme as here additional components are not needed. This is possible only if the DC fault current is significantly reduced.

A mechanical DCCB (MDCCB) is slow with fault clearance time of (70 msec -100 msec). Therefore, it needs a combination of effective FCLs and fault co-ordination. A semiconductor or solid -state DCCB (SSDCCB) is fast as the clearance time within 1 ms is achievable. However, it has the challenges like need of effective fault coordination, high on-state losses and cost, and small breaking capability. The hybrid DCCBs Type 1 and Type 2 called Prototype HDCCBs combine the strengths of both the mechanical and semiconductor DCCBs. They are both fast (2 msec) and have low losses. Their breaking capability from 14-26 kA is anticipated. However, still high costs/maintenance, need of effective fault coordination/FCLs, limited breaking capability are major hurdles. Commercial lack of

high rating DCCBs is still a major challenge preventing the development of meshed HVDC/MTDC grids. No doubt zero-crossing can be artificially created using a resonant circuit, however, none of the existing DCCB technology is satisfactory to fulfill all the requirements for a feasible DC fault protection scheme mainly due to huge fault currents and extraordinary strict requirements of the total DC fault response time. Thus, effective FCLs, properly sized inductors, precise sensor/relay threshold settings and more research testing is required in the limiting/breaking technology.

Fault blocking FBMMCs can't prevent the AC infeed to the DC fault/delivery of active power is interrupted. Higher losses and cost reduce their reliability in OHL schemes. Can fail in ring topology grids. The DC Fault current is not fully limited (uncontrolled discharge from capacitors/inductors, problems of restoration after the fault). Recovery from bypassing is slow. Power in-feed loss for about 60 ms causes severe disturbances to both DC and AC systems.

MTDC transmission system is basically built to transmit a bulk amount of sustainable electricity over long and extra-long HVDC transmission lines (greater than 300 km submarine /UGCs and greater than 2600 km OHLs). Massive integration of non-linear power electronic devices in an MTDC system increases its complexity and decreases its reliability especially for long distance power transmission. Therefore, the deployment of the MTDC/HVDC grids and their reliable operation depends on the adequate performance of their protection scheme during the faults.

Recently proposed distributed optical current sensing schemes might eliminate most of the drawbacks of conventional differential protection and travelling wave methods [76][55]. However, the dependence of these schemes on a communication system is a major threat to their reliability for long-distance power transmission. There is a potential communication shutdown for long distances. In these schemes, most of the research is on the faulty segment discrimination. They have inability to discriminate the high impedance faults above 100Ω and there are limited results/flow charts.

There are no in-depth simulation results available especially for high impedance

faults above 400Ω with distributed differential current measurements based on optical sensing. In optical schemes, there is no description about diode and cable sizing which are the most vulnerable components of a VSC-HVDC system during the DC line/cable short circuit fault. A larger line reactor (200 mH) in series with a DCCB is beneficial only in terms of active limiting of the current. In single-ended schemes [55], the installation of large-sized and extra limiting inductors at the station terminals can cause failure of these schemes to locate the fault.

In single ended optical scheme AC voltages taken is 400 kV at 50 Hz [55] and in double ended optical scheme [76] fault coordination is not described. Main objective of these optical schemes is on fault location and discrimination. However, the fault location is mostly done offline with the data obtained from the fault detection. Further in the single ended optical sensing scheme, there is no description about breaking the fault currents above 9 kA.

Optical schemes have no brief description about proper FCLs, very strong AC sources, sources and loads, and alternate protection devices if the Hybrid DC-CB/sensor fails. Importantly also, to design a feasible MTDC protection scheme, coordination of various types of DC circuit breakers, FCLs, with the relay/sensor threshold settings, converter configurations, network topologies, backup plans, and the fault detecting/locating algorithms is extremely important.

However, in the previous schemes including optical sensing schemes, there is no brief description about how to achieve an effective fault coordination in a meshed VSC-based MTDC grid. Since, the DC fault clearance time of a few milliseconds (high speed of operation) is the key requirement for the MTDC protection scheme, therefore, in-depth research and analysis of the faults, particularly DC cable short circuit fault is very important in a VSC-based MTDC system.

Additionally, in the optical sensing schemes there is not much description about fast fault detection in real time. Modern world is the digital world and every complicated network like a meshed MTDC grid requires real-time digital system (RTDS) for fast fault detection. The HVDC/MTDC systems are also prone to various cyber attacks, therefore, intelligent, and powerful digital signal processing

tools like the Discrete Wavelet Transform (DWT) or the Stationary Wavelet Transform (SWT) are very practical for the fault detection and location in these systems. These orthogonal wavelets have very nice localization properties in time-frequency space and are perfect signal processing tool to achieve three - dimensional analysis of a non-stationary random signal with abrupt changes/multiple peaks. Further, if these real-time and denoising schemes are used with other efficient algorithms, even many hidden anomalies in the HVDC/MTDC systems can be detected.

The CWT is more accurate in off-line fault location for which high speed is not required, except in the case of permanent short circuit faults [76]. Importantly also, the fault location can be estimated only with the data obtained during the fault detection. Indeed, fast real-time fault detection is the utmost requisite for the HVDC/MTDC protection scheme to detect the fault, discriminate the faulty part, locate the fault, and trip the concerned breakers.

A communication-based fault discrimination algorithm needs to be aided with selective FCLs, fast isolation tools, and other partially discriminative methods which indicate the fault directions like the current derivative polarity method. The Current Derivative Data method is an efficient method to locate the fault but only in ideal situations, which is practically impossible.

This method is useful mostly for point-to-point HVDC links in ideal situations. Fault detection based on the current derivative, though computationally efficient is not a reliable solution to protect a meshed MTDC grid with multiple power sources/nodes having multiple lines per every node. Difficulty in determining the faulted section independently as the system becomes highly meshed, sensitivity to noise, incorrect data samples, high impedance faults, and the inductor size are drawbacks of the current derivative method. However, due to its capability of indicating the fault directions, the current derivative direction principles help to improve the selectivity of the DC protection scheme in identifying a faulty line and indeed, is a partial discriminative method. Therefore, the current derivative direction method with a short time window (Minimum samples) can be used as one of the backup plans with the primary communication-based fault discrimination algorithms such as the current differential protection and TW methods (especially

type-D) in a meshed MTDC grid.

The overcurrent protection is unsuitable for a meshed MTDC grid because it lacks selectivity, is sensitive to power production, load variations, and the high impedance faults. However, due to its simplicity, cost-effectiveness, and instantaneous operation, it might work as a powerful backup plan, particularly to clear an extremely close-up fault to a remote converter station/DC node. Also, the time delay in communication can be minimized with backup overcurrent protection and severe damage to the system caused by the huge fault currents can be prevented early.

Algorithms for the fault detection and discrimination using the local measurements of current and voltage or their derivatives without using communications have been proposed. However, in a VSC-based MTDC grid, the DC voltage polarity remains constant. Thus, the fault provoked DC link voltage transients (TWs) may give a rough estimation of the fault location in a TL, but cannot detect the wavefront. They cannot distinguish a faulty line from the healthy ones, particularly when the fault occurs very close to a station or a measuring unit/detecting sensor. Because in such cases the TW effect is not clearly visible in the DC voltage transients as can be seen in the simulation results in chapters 3 and 4.

Fault detection method using the first and second current derivative local measurements with more line inductances cause more reactive power losses. Increasing the size of protective inductors increases the total impedance of Stage 3, which causes a decrease in the maximum DC cable current.

Indeed, if the inductor size is increased to a very large value, the diode current would eventually drop with the decrease in the total cable current which is highly unwanted. While sizing any FCL important parameters like the current limiting effect, dynamic slow-down effect, and the total cost of the project are very important. If the minimum sized inductors are to be used with the DCCBs, current sensors, or relays on the DC side, it must be practically validated, which FCL on the AC side or which converter topology will co-ordinate with it to significantly suppress the fault current.

2.4 Research Gap

The MTDC/MTHVDC transmission system is an optimal solution and cost-effective power transmission network to minimize the global energy crisis largely. However, protection of a DC systems is more challenging and more difficult than its counterpart AC system's protection.

In an MTDC/HVDC system the total DC fault clearance time (overall DC fault response time) is restricted to a few msec. (within 5 msec. or less as in CIGRE Benchmark B4) to protect the system from the damaging overcurrent. However, based on the existing literature so far and preliminary conclusions:

- Most of the research work done in literature is on HVDC links/laboratory type small HVDC grids.
- The proposed strategies and approaches so far have unfeasible technical specifications. These strategies have a lack of feasibility and robustness. There is no feasible protection scheme with a mature science available for an MTDC grid, particularly for a meshed VSC-based MTDC grid.
- So far there is no protection scheme available that can clear the DC fault within 5 msec. or less especially for a meshed VSC-MTDC grid.
- Thus, the core design demand for a feasible MTDC/HVDC protection scheme, capable of completing the total DC fault-clearance-time within the critical time limit of a few msec (5 msec or less) is a key technical Gap in both research and practice so far.
- This key technical challenge is holding back the development and scalability of this global grid. despite its numerous benefits and applications.

2.5 Problem Statement

Despite being a major enabler and promising technology for the future Super-grid, a VSC-based HVDC system is extremely vulnerable to the DC side faults, particularly the worst-case solid DC line/cable short circuit fault. This less-common

fault-type is a major threat to the operation and future development of this network. In a VSC- HVDC/MTDC grid, during a solid P2P fault, even when all the IGBTs are blocked for self-protection by the local overcurrent protection control, it is impossible to prevent the AC grid from feeding the fault via the antiparallel (freewheeling) diodes. Local self-control blocks the IGBTs as soon as the fault current exceeds the threshold level of about twice the nominal value. This leads to the formation of an uncontrolled diode bridge rectifier and the AC power remains injected into the DC grid through these freewheeling diodes. This fault has the impact of over-current in both the symmetrical mono-polar and bipolar systems. The antiparallel diodes are the most vulnerable components during the freewheeling period and put the converters and cables at a high risk. Additionally, the IGBTs can usually withstand just twice the rated current to remain in the safe operating area.

The problem becomes more severe in a meshed VSC-MTDC grid with multiple power sources and multiple lines (feeders) per every node. Minimum impedance in the HVDC lines, commercial lack of high rating DCCBs, absence of naturally zero-current points (no frequency), grounding or corrosion issues, absence of a standard protocol for the HVDC networks, capacitive behaviour, and various time delays of several milliseconds due to the fault provoked TWs.

All these factors in general make the protection of the HVDC system more challenging and difficult than the HVAC system's protection. Additionally, as the number of line connections increases at a DC node, the overall current interruption stress on the CBs of its faulted line increases accordingly.

All the devices and components experience large currents as the MTDC grid feeds the fault from all directions. The worst-case fault scenario is a close-up solid P2P fault to a remote source station. The short circuit fault current reaches a huge peak value within a few milliseconds with a significant drop of DC voltage almost to the zero level. Thus, accurate determination and hence, isolation of only the faulty line or its faulty segment becomes too difficult or impossible. If the DC fault is not cleared within a few msec. of the critical time limit (within 5 msec. or less), entire MTDC grid will collapse due to the destroying overcurrent.

Based on the existing literature and preliminary conclusions, the proposed strategies and approaches so far have unfeasible technical specifications. There is no feasible protection scheme with a mature science available particularly for a meshed VSC-based MTDC grid capable of clearing the DC fault within the critical time limit of a few msec.

Thus, an alternate MTDC protection scheme aided with efficient sub-protection methods and backup plans is required to improve the overall performance of the optical sensing scheme [76] for long-distance electrical power transmission. Hence, a feasible fault discriminating, detecting, locating, limiting, and isolating scheme is proposed in this research thesis. The scheme combines the joint performance of both the communication dependent optical schemes and other efficient independent auxiliary methods into one scheme. The scheme explores rigorously all the important aspects of the DC fault clearance time including quick fault detection, accurate faulty line determination, relatively accurate fault location, significant fault current limiting much below the breakable levels of the available CBs, and fast isolation of only the faulty line without shutting down the entire MTDC system.

All these important aspects are explored in-depth both theoretically as well as with appropriate simulation results. All the general requirements of a feasible protection scheme like robustness, novelty and selectivity, reliability, less susceptibility, and the cost-effectiveness are included in-depth. Further the scheme is not only applicable to a meshed 4-terminal VSC-MTDC grid, but its general methodology can be implemented to other large scale meshed HVDC/MTDC grids with any number of terminals as well.

2.6 Research Contribution

Indeed, the optical sensing schemes can facilitate a high flexibility in the operation of a VSC-based MTDC network. However, their dependence on a communication system is a major threat to their reliability and performance for long distance power transmission. Therefore, a major contribution of this research thesis is

to enhance the reliability and improve the performance of these optical schemes for long and extra-long distances. This is achieved by aiding them with other independent sub-protection schemes and simple mature backup plans. The scheme is applicable to even large-scale meshed MTDC grids with several added benefits than the previously proposed schemes. Fault coordination and DC fault clearance within the critical time limit of a few msec. are the main focuses. Technical feasibility of the scheme can be verified using the simulation results. The proposed algorithms can also be verified using RTDS systems for an MTDC grid.

Various contributions of the proposed scheme include as follows:

- The scheme is comprehensive. No protection strategy exists in the literature so far that implements the joint performance of current differential algorithm along with TW principles using the measurements obtained from distributed current measuring units (optical sensors) on the TLs, fast fault detection with DWT, overcurrent protection, current derivative sign principles with a short time window, effective active and passive FCLs, half bridge-VSC-MMCs, HDCCBs, and other fast isolation tools.
- All the important aspects of the total DC fault clearance time are thoroughly explained with detailed flow charts and a comprehensive report of a feasible DC protection scheme is prepared. An optimized scheme is developed which is capable to complete all the general requirements of a feasible MTDC/HVDC protection scheme.
- Accurate discrimination of a faulty line/segment using differential current algorithm based on multipoint distributed optical sensor measurements on transmission lines in three ways:
 1. Differential current sums at each node
 2. Series differential currents on every TL, Difference of currents at the two ends of a DC link
- Measurement of the differential current sums at every node not only determines a faulty line, but also its faulty segment. Hence, this method of measurement is faster than the previously proposed series methods [76, 55]. A meshed MTDC grid with both source and load terminals is tested.

- Unified and fast (real-time) detection of the DC fault (detection of the wave-front arrival time) using the DWT. To enhance the performance, backup plans with the Differential protection and the DWT include RSFCL quench detection, overcurrent protection (for extremely closeup P2P faults), current derivative direction method with a short time window, and precisely large thresholds much above the noise level
- The scheme is a fully selective scheme, as only the faulted line is isolated from the system, without shutting down the entire system. Its selectivity is guaranteed by precise and large threshold settings, RSFCL quenching criteria, the DWT, and the differential protection.
- In the proposed scheme, large and extra inductors are avoided. All the fault discriminating, detecting, and locating methods are coordinated with bidirectional HDCCBs, small inductors, R-SFCLs, half bridge VSC-MMCs, ACCBs, and the other passive components to compromise with the cost and size of the network components
- The scheme is cost-effective, as the differential protection along with other fault detecting/locating methods coordinate well with the HDCCB (constant breaking time of 2 ~ 3 ms), small sized inductors, RSFCLs, HB-VSC-MMCs, ACCBs, and other passive components. The DC fault current is significantly reduced to below 1.7 kA before its interruption. Hence, low cost (low rating) protection devices like HSSs/RCBs and MCBs in series with the RSFCLs can be installed to interrupt the reduced DC fault current easily
- For continuous operation of the grid, properly sized series inductances of 10 ~ 70 mH (2/converter) are added at the DC output of only AC/DC (source) converter stations (1 /each pole) to limit the AC infeed currents and avoid the converter blocking/allow continuous operation
- The proposed scheme operates the HDCCBs before the critical time limit and protects the system from the damaging overcurrent in a meshed VSC-MMC- MTDC grid. The total DC fault clearance time achieved is 5.1 msec. to 5.2 msec., which proves its novelty and hence, the scheme is fast scheme

- Reliability of the scheme is guaranteed. Because the primary communication-based fault discrimination and location algorithms are aided with other efficient sub-protection methods and mature back up plans. Even if all the protection methods fail from the DC side, the Converter's AC-side ACCBs trip and clear the fault. After limiting the DC fault current significantly, fast isolation is not required and even mechanical DCCBs can be installed as the isolation tools. A reliable option to eliminate the AC side fault current contributions. No additional components and after limiting the fault current significantly, fast isolation is not required. No need of FCUs at the converter terminals
- The scheme is robust, as it is capable to discriminate the DC side faults from the AC side faults, noises, load changes and the other external disturbances. Fast fault detection, accurate faulty line determination, significant DC fault current limiting, and quick faulty line isolation guarantee its robustness. Selectivity of differential current measurements is reduced in case of high impedance faults. Thus, it is aided with the RSFCL quench detection and the DWT
- Seamlessness of the scheme is achieved through an RSFCL quench detection and using the DWT. Only the RSFCLs installed on the faulted line quench and the line is isolated by tripping the concerned CBS. The remaining healthy grid zones can keep operating safely after the fault clearance. Thus, any type of the DC system can be connected to any type of the AC grid
- Measuring the differential current sums and using only Type-D TW-based fault location method, requires a smaller number of equidistantly distributed optical sensors. Thus, cost-effectiveness of the scheme is further achieved. Since, an optical sensor link is used between the two-line ends, therefore, a continuous data transfer with bidirectional communication only during the fault events can boost the speed need for long distances
- In the scheme relatively accurate fault location is measured in a meshed MTDC grid by utilizing the current derivative data (short time window) and the travelling wave methods.

-
- In the proposed scheme expensive back-up plans are avoided. Overcurrent relays, RSFCL Quench Criteria, Current Derivative Sign method all are used to mitigate downsides of both the differential protection and the WT.
 - Simple mature backup plans like overcurrent relays, neighboring HDCCBs/sensors and RSFCLs, are used. Operating overcurrent relay at a node to disconnect the station avoids damage to the system in case of diode oversizing. Through proper coordination of overcurrent relays, even MDCCBs in series with the RSFCLs will work well as the isolating devices.

TABLE 2.1: Comparison Table with Specific Parameters and Authors

Ref. No	Technique	Parameters and Cons	Authors
[33]	ACCBs (Han-shake method)	<p>Interruption time within 50-100ms and can be as long as 200 ms.</p> <p>Leads to shut-down of entire grid by blocking all converters</p> <p>VDC = +/-200 kV</p> <p>ACCB operation time = 50 ms</p> <p>Submodules per arm 200 [-]</p> <p>Submodule resistance (on) 0.908 mΩ</p> <p>Converter arm inductor 100 mH</p>	L. Tang and B.T. Ooi
[32]	ACCBs and FDD-C/HSS	<p>Link end inductor 10 mH</p> <p>FD operation 10 ms</p> <p>Link 12 OHL 200 km</p> <p>Link 23/24/14 Cable 100/150/100 km</p> <p>Per Unit Base Voltage 400 kV</p> <p>Per Unit Base Current 2 kA</p>	<p>R. Dantas, J. Liang, C. E. Ugalde-Loo, A. Adamczyk, C. Barker, and R. Whitehouse, 2017 and 2018</p> <p>J. Candelaria and J.D. Park</p>

[73],[93],[94]	MDCCB	<p>60-100 ms</p> <p>Interrupting capability is (2 -16) kA, voltage rating is less than 400 kV, rate of rise of fault current is (1.6-2) kA/ms Fault clearance time within 1 ms achievable.</p>	<p>E. Kontos M. K. Bucher C. M. Franck</p>
[26]	Solid State CB	<p>current interruption capability is 5 kA to 19 kA (expected), voltage rating is 132 kV, rate of rise of fault current is 47 kA/ms and internal current is 0.4 A.</p> <p>A breaking time of 2 ms is achievable.</p> <p>Minimum current breaking capability is 9 kA and maximum interruption capability is up to 26 kA (expected).</p>	<p>Yang J, Fletcher J E O'Reilly J, M. Hagian D. Jovtic</p>
[75][96]	Hybrid DCCB	<p>Its voltage rating is 500 kV, rate of rise of fault current is 2.9-6.7 kA/ms, and internal current is 2 to 3 A.</p> <p>A 500 kV HVDC CB prototype has been developed in 2018</p>	<p>J. Hofner, B. Jacobson C. Franck</p> <p>D. Jovcic, G. Tang, H. Pang</p>

- [31] New solid-state DCCB (NSS-DCCB) Fault clearance time within 2 to 5 ms
 150-200mH Single-ended (Type-A) methods can fail for fault location with large sized inductances. The parameters of single-ended optical scheme are AC voltage 400 kV
 K. Sano and M. Takasaki, 2013
- [55] Single-ended optical sensing scheme for fault location (distributed optical sensor differential current measurements on TLs) AC frequency 50 Hz
 X/R ratio of AC networks 10
 AC short-circuit level 40 GVA
 AC transformer reactance 0.2 p.u.
 DC line external inductance 150 mH
 D. Tzelepis, A. Dysko,
 G. Fusiek,
 J. Nelson, P. Niewczas,
 D. Vozikis,
 P. Orr, N. Gordon, and
 C. D. Booth,

		AC voltage 400 kV	
		AC frequency 50 Hz	
		AC short-circuit level [Ss.c] 40 GVA	
		DC voltage 800 kV	D. Tzelepis, G. Fusiek,
		DC line external inductance 150 mH	A. Dysko,
[76]	Double-ended (Type	MMC number of sub-modules /arm 400	P. Niewczas,
	D TW-based method)	MMC arm inductance 0.1 p.u.	C. Booth, and
	Novel fault location	Parameters of UGC and OHL	X. Dong,
	in mtde grids with	Resistance [Ω /km] 0.015 0.0146	
	non-homogeneous	Inductance [mH/km] 0.96 0.158	
	transmission lines	Capacitance [μ F/km] 0.012 0.275	
	utilizing distributed		
	current sensing tech-		
	nology		

2.7 Summary

In this chapter different fault discriminating, limiting, detecting, isolating, and locating methods have been introduced in detail. However, most of the research work done in the existing literature is on point-to-point HVDC links or tested for small-scale grids up to the laboratory level experiments. There is no feasible protection scheme with a mature science available, especially for the protection of medium and large scale meshed MTDC grids. With the current technologies and proposed devices, it is impossible to satisfy the demand for a few msec. of the total DC fault clearance time.

So far there is no protection scheme available in the existing literature that can complete the total DC fault-clearance time within 5 msec. or lesser (CIGRE B4 benchmark in 2013 [78]), especially in a meshed VSC-based MTDC grid. This key Technical Gap is addressed in this research thesis and the proposed protection scheme for a meshed MTDC grid can clear the DC cable short circuit fault within 5.2 msec.

Chapter 3

Critical DC Faults in an MTDC Grid

3.1 Grid Modelling

Based on the CIGRE B4 benchmark in 2013 [77], first two-terminal HVDC-link, then three-terminal, and finally four-terminal meshed MTDC grids were developed in MATLAB. Initially, tests were carried with Mono-polar, Bi-polar 2-level, and 3-level VSC-HVDC links, 300 km to 600 km long, and the AC voltages were varied from 230 ~ 800 kV. Nominal AC power and frequency of 4 to 10 GVA and 60 to 50 Hz with line-end inductances of 10 to 15 mH, and DC side capacitors up to 120 μ F were used. Then 3-level, bi-polar half-bridge VSC-MMC-MTDC meshed grids of 3 and 4 terminals were developed as shown in Fig. 3.1. Both source and load terminals were taken and extensive simulations were carried with all the configurations. The current measuring units (assumed as optical sensors) were distributed on π -section DC cables with each cable having a positive and a negative pole. The fault clearing units (FCUs) were inserted as 4/cable (2 for each pole) and 2/converter (1 for each pole). An FCU consists of a bidirectional HDCCB combined with a resistive type DC-SFCL (R-SFCL) replacing the series reactor especially on the DC cable ends at every node and high-speed switch (HSS)/ RCB

[43]. The R-SFCL quenches after the fault and passively limits the fault current. Weak, medium strong, and very strong AC sources were tested.

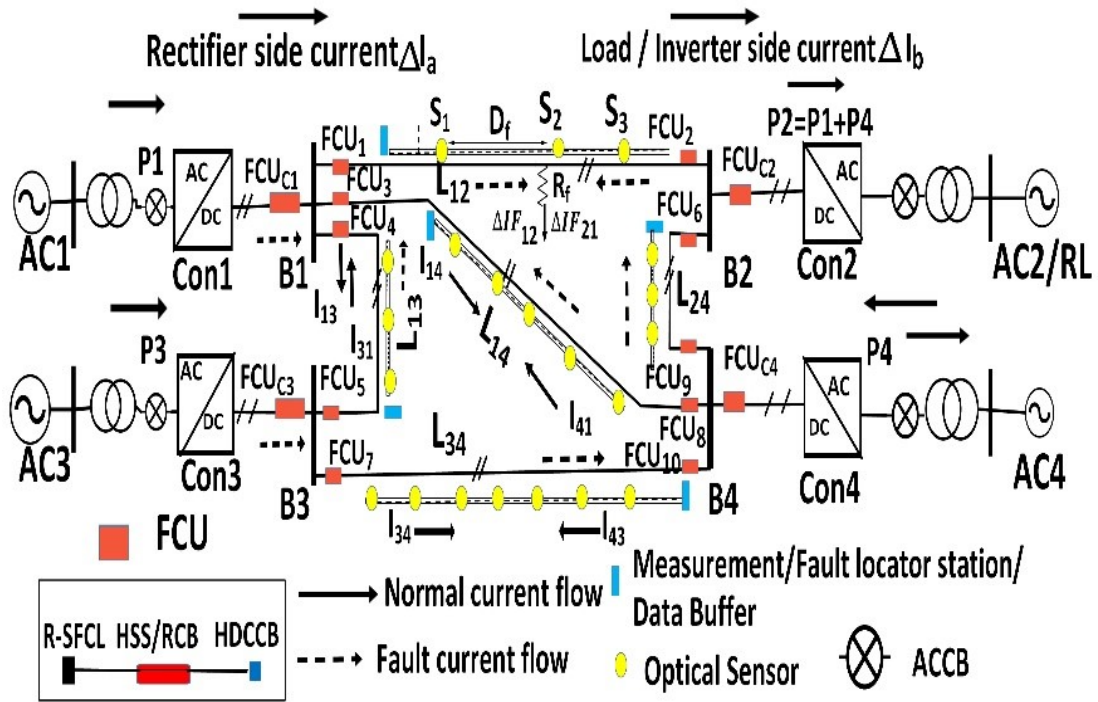


FIGURE 3.1: A four-terminal meshed MTDC grid with optical sensor networks, fault locators and protection devices.

Larger DC capacitors of 100-200 μF increase the maximum CB current and the system inertia. However, they also improve voltage stability (suppress over-voltages while increasing minimum terminal voltages) in the grid. Therefore, four DC node capacitors of 5 to 50 μF (1/ node) were added to accelerate the quenching of the R-SFCLs due to the discharge currents.

The system parameters used are listed in the table 3.1. During testing, the R-SFCLs effectively limited the DC cable short circuit current when installed on the DC side. Taking the concept that an arm overcurrent criterion is used to block the IGBTs of a VSC, which means that the Rectifier (source) IGBTs will block earlier than those of an Inverter, extra and large sized reactors were avoided. The potential benefits of both the active (appropriately sized inductors) and passive (R-FCLs) were utilized to effectively suppress the fault current. A larger line reactor in series with a DCCB is beneficial only in terms of active limiting of the maximum fault current [40–42]. However, considering the drawbacks of extra and

large-sized DC inductors and assuming the breaking capability of an HDCCB up to 9 kA, properly sized series inductors of 15 to 50 mH (2/converter) were added at the DC output of only AC/DC (rectifier) converter stations. These actively limited the rate of rise of the AC infeed currents and allowed continuous operation of the grid without a converter blocking during and after the fault. Discharge from every healthy DC cable was passively limited by two R-SFCLs one at the end of the cable itself and the other at the end of the faulted cable. This makes the possibility of the DC protection devices with significantly reduced current ratings.

TABLE 3.1: Simulation Parameters

S.no.	Parameters	Value
1	AC Voltage and AC Frequency	230 kV to 800 kV, 50 to 60 Hz
		10-200 μ F,
	DC-side Caps, Resistive-load,	150 Ω -200 M Ω ,
2	Line-Reactors, Power	10-15 mH (for two terminal links
	Consumption, Nominal Current	only,bipolar/mono-polar/2level
		/3level),500 MW, 2 kA
3	DC Voltage, DC Bus Capacitors	up to \pm 860 kV, 10-120 μ F
	(1/node)	
4	DC-Cables	180 km -600 km/120 km/300 km
	(L12/L13/L14/L34/L24/L32)	/180 km/90 km/300 km
	Series Inductor 2/ (AC/DC) or	
5	source converter output	10 mH – 70 mH
	(active current limiting)	
		min $R_{SFCL} = 0.01 \Omega$
6	R-SFCL (passive current limiting)	to max 25 Ω ,
	4/DC cable, 2/converter if needed	trigger $I_q = 3$ kA
7	AC Transformer Leakage	0.15 p.u. to 0.2 p.u.
	Reactance	
8	R_f, D_f (Fault)	0 Ω -500 Ω ,
		1 km-600 km

Table 3.1 continued from previous page

S.no.	Parameters	Value
9	FCU 4/line & 2/Converter	HDCCB, operation 2 ms, breaking capability up to 9 kA
10	Converter Technology	Half-bridge 3-level -VSC-MMC
11	Converter Blocking (dip/trip), Threshold detection point	2.5-2.9 kA (blocking condition Arm current exceeds 1.8 p.u)

While designing a properly sized soothing inductor, important parameters which were taken into consideration include contributions from the weak, medium strong, and very strong AC sources to the DC fault current, rated AC and DC voltages, rated power, peak currents on the healthy and faulty cables, current ratio, and the current limiting effects of inductors and RSFCLs. The DC surge arrestors performed better to reduce the over-voltages, especially during the P2G faults in symmetrical mono-polar configuration. In this configuration during a P2G fault, DC fault current is reduced due to the high impedance grounding of the surge arrestors hence, reducing the interruption stress on the HDCCBs. While in low impedance grounding high currents and low voltages were produced during the faults.

Further, the two R-SFCLs per source converter DC output were omitted based on the maximum contribution to the fault current from each source converter. Four AC circuit breakers (ACCBs) were inserted on the AC sides of the converters as one of the backup options to increase the reliability of the scheme.

3.2 MTDC Faults

Different system configurations like symmetrical monopole configuration (high impedance grounded), bipolar systems (low impedance grounded), and asymmetrical monopole are created by grounding of a DC system. Therefore, the impact of a fault in a DC system depends on the type of fault and on the type of grounding in the system. Important faults to be taken into account while designing a reliable HVDC protection scheme include:

1. Positive line/pole to ground (+L2G/+P2G) fault
2. Negative line/pole to ground (-L2G/-P2G) fault
3. Positive line/pole to negative line/pole (\pm L2L/P2P) fault

As an HVDC system is symmetrical (monopole/bi-pole), the first two types of the fault are together called as DC line/cable ground fault, or line/pole-to-ground L2G/P2G fault. The third fault is called the DC line/cable short circuit or line-to-line/pole-to-pole (L2L/P2P) fault. Let us discuss each one as follows:

3.2.1 DC Line to Ground or Pole to Ground (L2G/P2G) Fault

The overhead line transmission due to open-air exposure is prone to L2L and L2G faults. Line-to-ground fault in overhead lines (OHLs) is highly probable with the impact of overvoltage in symmetrical Monopole (high impedance grounded) configuration and overcurrent in Bi-pole (low impedance grounded) systems. The P2G fault in a cable system is also probable with the impact of overvoltage in symmetrical Monopole and overcurrent in Bi-pole systems. In symmetrical monopole configuration, P2G fault causes a rapid discharge of the faulty pole capacitor to the ground leading to an imbalance of the DC voltage between the positive and the negative poles. Due to the capacitor discharging, the current flows via ground back to the healthy pole and finally to the source leading to over-voltage in the healthy pole. Indeed, in the symmetric monopole HVDC network, a P2G fault may result in an overvoltage as high as twice the nominal voltage. Since a P2G fault results in a low or limited fault current as the current is forced through the high impedance grounding or surge arresters. Therefore, DCCBs with a limited current interrupting capability can be installed in the symmetric monopole grid. A P2G fault is not as serious as a P2P fault, because in the P2G fault over-current is not prominent. For such faults, a DC protection scheme requires investigations on DC breaker requirements and the rating of the system components like cables and diodes. For such over-voltages leading to high cost, the fault clearing time for the voltage rebalancing, and energy dissipated in the bus/line surge-arresters need rigorous study. Importantly also, the doubled floating voltage persists even after

clearing the P2G fault. This requires that every time the fault occurs, the whole HVDC grid has to be shut down and the healthy poles have to be discharged/re-energized. In an HVDC grid being de-energized following P2G fault clearing, particularly in symmetrical mono-polar systems, several options for eliminating the voltage imbalances or restoring the DC voltage include: 1) Using earthing switches combined with discharge resistors to earth both poles before the DC voltage is restored. 2) Using converter control to drive the voltage of both poles to zero. In an HVDC grid in order to restore the DC voltage without de-energizing the grid, options for removing voltage imbalances include: 1) Using dynamic-breaking-systems (DBs) or choppers to reduce the over-voltage on the healthy pole. 2) Using converter control to rebalance the poles if a device at the converter’s AC terminals is present to allow zero sequence currents.

3.2.2 Simulation Results of P2G Faults

Fig. 3.2 (a) to (d), shows the current and voltage profiles for an internal P2G fault triggered at different times and locations in a three-terminal meshed MTDC grid.

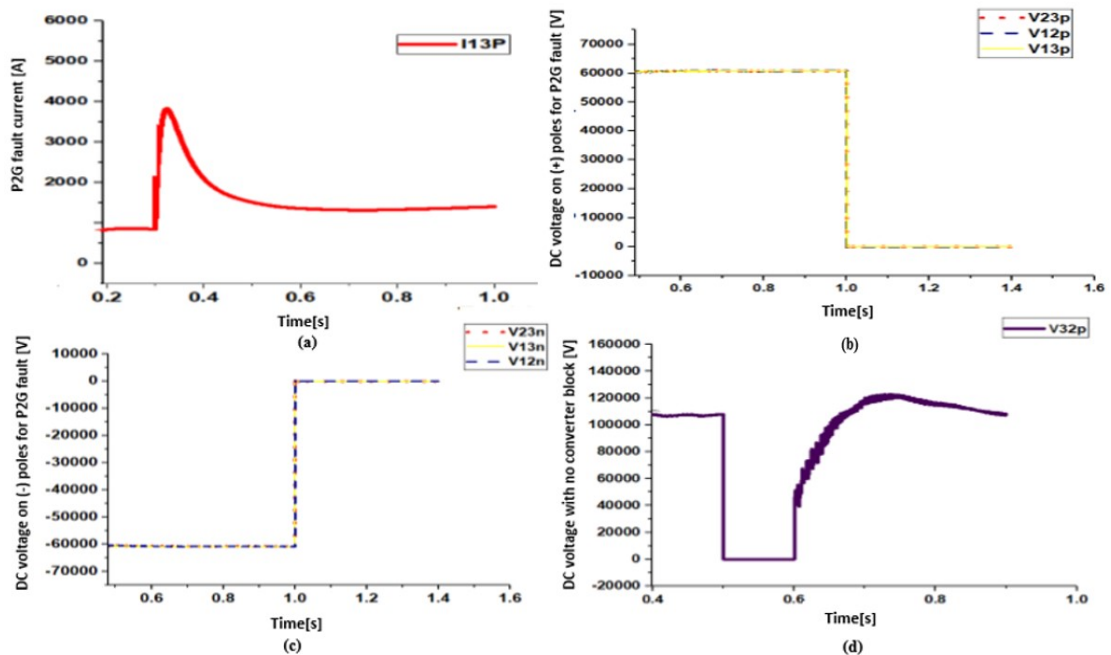


FIGURE 3.2: (a) DC fault current profile for an internal P2G fault incepted at 0.3 s in the positive pole of link L_{13} . (b) DC voltage profile at the positive poles. (c) DC voltage profile at the negative poles. (d) DC voltage profile at the positive pole for an internal P2G fault at 0.5 s with no converter blocking after the fault for a three terminal meshed grid.

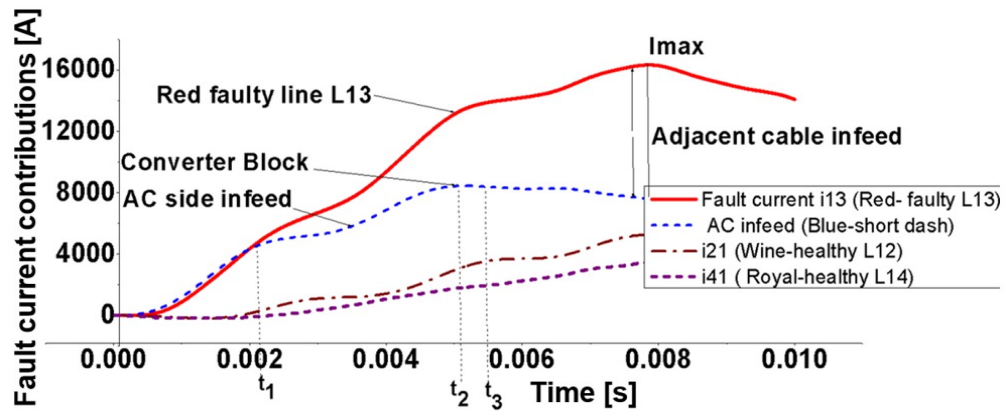


FIGURE 3.3: Total contributions to the fault current for a P2G fault in L_{13} at 1 km to B_1 without protection. Faulty cable L_{13} current (solid red curve), MMC_1 DC current (blue short dash) and healthy cable currents (wine and royal) for a four terminal meshed grid.

Fig. 3.3 shows the total contributions to the DC fault current for a P2G fault at 0.5 ms in the cable L_{13} and at 1 km to the source node B_1 of the four terminal meshed grid (Fig. 3.1). The current rise rate through the FCU_4 is highest (red solid curve). During the period b/w $t_1 \cong 2.3$ ms and $t_2 \cong 5.24$ ms, major contribution to the fault current is the AC infeed via MMC_1 . MMC_1 side arm current decays from t_2 onwards, however, the current through the faulty cable L_{13} keeps on increasing. This is because after the converter blocks at time t_2 , currents through the adjacent healthy cables L_{12} (wine-dash-dot) and L_{14} (royal-dash) are significant from t_2 onwards due to prominent discharges. Now if the current breaking capability for the HDCCB at the converter output is increased up to the maximum fault current contribution from one converter, then the R-SFCLs (2/converter) placed at the converter output could be omitted. Since P2G faults are not of major concern in this research work, therefore extensive simulation results were not performed.

3.2.3 DC Line to Line or Pole to Pole (L2L/P2P) Fault

This fault is probable in OHLs and improbable or less common in cables with the impact of overcurrent in both the symmetrical monopole and bi-pole systems and is a major threat to the operation of a VSC-based HVDC grid. Indeed, a high vulnerability of VSC's to a solid DC line/cable short circuit fault, demanding an extraordinary strict fault clearance time of a few milliseconds, has remained

a core technical challenge in both research and practice so far which needs to be addressed.

During this fault, even when all the IGBTs of the submodule are blocked for self-protection by the local control, it is impossible to prevent the AC grid from feeding the fault via the freewheeling diodes which form an uncontrolled bridge rectifier.

In a VSC-based HVDC system, complete solid DC cable short circuit fault response is divided into three stages.

1. Stage 1: DC capacitor discharge stage, where the DC capacitor gets discharged through the fault and dominates the fault current in first a few time-instants
2. Stage 2: Diode freewheel stage, most challenging and critical stage, where the IGBTs are blocked for self-protection and the freewheeling diodes work as an uncontrolled bridge rectifier
3. Stage 3: Grid current feeding stage (AC infeed stage) where the connected AC grid feeds the fault via the diode paths

Usually, DC side FCLs like protective inductors can effectively limit the fault current magnitude in Stage 1 (DC capacitor discharge stage) and Stage 2 (diode freewheel stage) of the DC cable short circuit fault as well as during Stage 3 (grid current feeding stage). AC side FCLs limit infeed AC currents in Stage 3 (grid current feeding stage) of the fault response. However, neither the inductors on DC side nor the FCLs on AC side, alone can effectively protect the system from the DC faults. As already discussed, that any FCL or interruption device increases the grid impedance and hence, affects to the amplitudes of the fault provoked reflected and refracted TWs. During the transient period, the magnitudes of the reflected and incident waves depend on the size of the DC limiting reactor. Larger the inductor size, smaller the incident wave transmitted into rest of the system.

Thus, for minimum sized inductors on the DC side, practical testing of which FCL on the AC side or which converter topology co-ordinates with these in effective reduction of the DC fault current is must. Co-ordination between the types of FCLs installed on both sides of the converters, their effect on the system dynamics, DC-CBs, relay threshold settings, converter configuration, network topology, and the

fault detecting or locating methods is extremely important. Further immunity of the proposed fault detecting / locating principles against the practical installation of any FCL is of critical importance.

Therefore, the research work presented in this thesis co-ordinates with the minimum-sized inductors, HDCCBs, ACCBs, DC resistive-type superconducting fault current limiters (R-SFCLs), and the half bridge VSC-MMCs to effectively reduce the huge DC fault current below the breakable levels of the HDCCBs. Stage-2 is the most challenging stage, in which the IGBT modules are blocked shortly by the local overcurrent protection control as soon as the fault current starts to exceed a threshold level of about twice the nominal value [50]. The blocking condition of a half-bridge converter is when the arm current exceeds about 1.8 p.u. (w.r.t. peak arm current), and the conduction by all diode arms begins at this instant. Therefore, even after installing the FCLs on the AC side of the converters, the destroying overshoot current at the beginning of Stage 2 still exists and forces the weakest diodes to pass a huge current with a high initial value through them.

This puts the diodes and the cables at high risk. Indeed, Stages 1 and 2 are the most stringent periods to take the fault decision (trigger the IGBT block signal within 2 ms). The AC power of the connected AC grid remains injected into the DC grid through the freewheeling diodes which can only withstand a maximum current of 2 p.u. Therefore, in a meshed MTDC grid with multiple power sources and multiple lines or feeders per every node, all the devices and components experience large currents to feed the fault. As the number of line connections increases at a fault related node, the overall current interruption stress on the DCCBs of its faulted line increases accordingly.

During the fault occurrence, capacitive behavior, propagation delays of TWs, wavefront detection delay, synchronization delay, data processing delays, and the interruption or isolation delays take place. Thus, the DC fault current contributed by infeed from multiple power sources and due to the minimum surge impedance of the grid reaches to a huge peak within a few milliseconds with a significant drop of the DC voltage almost to zero level. If this fault is not cleared quickly before the critical time limit of a few milliseconds, collapse of the entire grid may take

place. The rate of rise of the short circuit fault current is extremely high, particularly when the fault is very close to a source station/node. This fault is indeed a worst-case fault scenario, if it occurs very close to a remote source station. Since an MTDC grid feeds the fault, therefore, accurate identification and isolation of only the faulted line or its faulty segment becomes impossible.

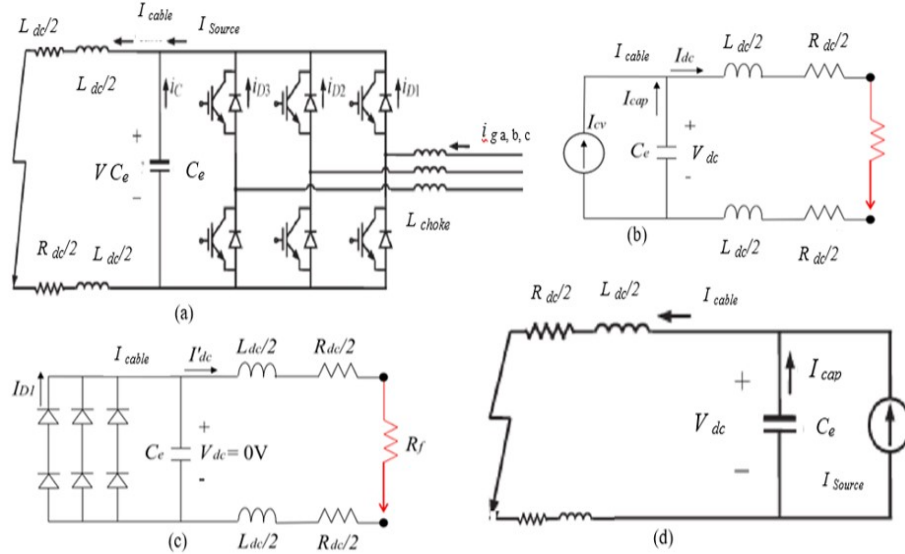


FIGURE 3.4: DC Cable Short Circuit Fault Equivalent Circuits of MMC DC side (a) the converter model (b) DC Capacitor discharge stage. (c) Diode free-wheeling stage. (d) Grid current feeding stage.

The DC cable short circuit fault response depends on two key factors: (a) The time duration taken by the DC voltage to drop to zero or the combined sub-modular capacitance to discharge through the fault known as the Critical time limit. (b) The cable current at the critical time. These two factors are utilized to indicate the total fault processing time required in the protection scheme, in sensor settings and can be used to indicate the fault distance D_f .

The meshed MTDC grid shown in Fig 3.1 with MMC_j and MMC_k as the number of terminals, has I_{jk} ($j, k = 1, 2, 3, 4, \dots, N$) DC currents measured at each terminal respectively. The DC current measuring units S_1 to S_n were distributed on all the cables of the grid. Each cable consists of m segments ($m=1, 2, \dots, n-1$).

Fig. 3.5 shows the events taking place during the occurrence of an internal P2P fault within the protection zone of the cable L_{12} . The DC current measuring units were distributed on π -section cables and each cable L_{12} , L_{13} , L_{14} , L_{34} , L_{32} and L_{24}

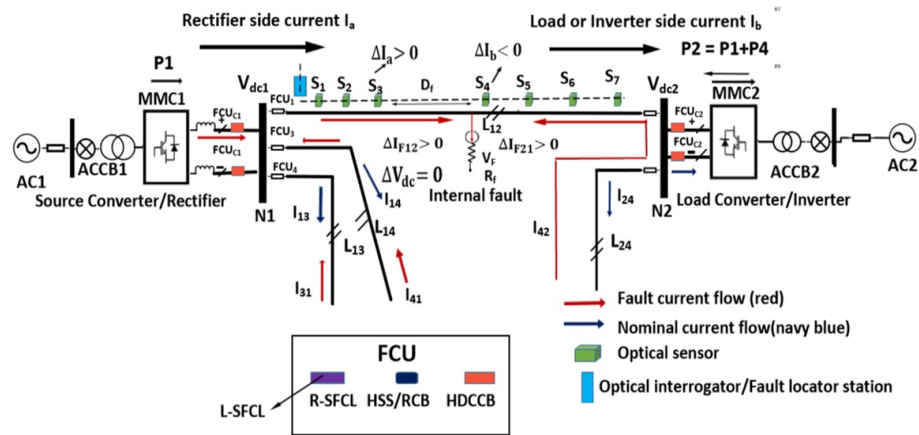


FIGURE 3.5: Internal and external faults using series of the differential current measurements with the current direction principle based on optical sensors.

represented as a single line has a positive and a negative pole respectively. Due to the symmetry of the system, P2P faults were mostly simulated in the cable L_{12} at different distances and the current measuring units were distributed as 4 to 7 on it respectively. P2G faults were simulated in different cables for a three terminal meshed grid and in the cable L_{13} of four terminal meshed grid (Fig. 3.1).

Since an MTDC grid especially mesh type, relies on a specific direction and magnitude of the DC fault current [31], and the identification of a faulty part makes use of fast transients of current, voltage or power following the DC fault. In literature, the DC link anomalies like overcurrent, undervoltage, overvoltage are used to indicate the fault occurrence. According to the travelling wave principle, a fault causes sudden change in the voltage level at the fault point in a transmission line. This can be viewed as an imaginary voltage source with opposite polarity to the pre-fault voltage. This shortly provokes voltage and current transients (TWs) to travel along the cable in both directions.

Before propagating into the other elements connected to a DC bus, the incident TW first reaches to DCCBs and FCLs at the ends of the faulted line. A part of this incident wave propagates through these while a large portion of it is reflected [78, 79].

The fault provoked current transients (TWs or surges) on a charged power line are reflected forward and backward b/w the terminals and the fault point causing

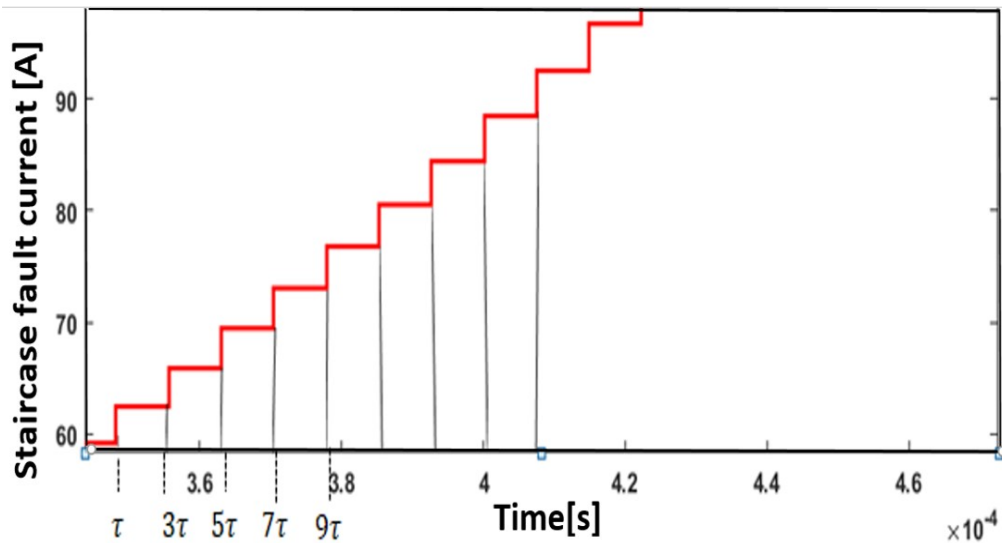


FIGURE 3.6: A clear TW effect seen in the development of DC fault current at a distance of 1 to 10 km to a VSC converter station.

multiple peaks or stepwise increase in the fault current development like a staircase waveform till they attenuate to zero. The travelling wave effect can be seen in Fig. 3.6.

In the existing literature so far, following a DC fault, fast transients of current, voltage and power are used to identify the faulty sections. However, when the fault occurs close to a DC bus (converter), TW surge is not clearly visible in the DC voltage transients. Importantly also, in a VSC-based MTDC system, the DC voltage polarity remains constant, therefore, the voltage signals cannot distinguish a faulty line from the healthy ones, particularly when the fault occurs close to a converter station. In the existing literature so far, following a DC fault, fast transients of current, voltage and power are used to identify the faulty sections. However, when the fault occurs close to a DC bus (converter), TW surge is not clearly visible in the DC voltage transients. Importantly also, in a VSC-based MTDC system, the DC voltage polarity remains constant, therefore, the voltage signals cannot distinguish a faulty line from the healthy ones, particularly when the fault occurs close to a converter station. Thus, in a VSC-based MTDC grid, the current transients or TWs contain information about the fault characteristics. Therefore, in this research work, the DC fault current transients are taken as the object signals for the fault detection and its location in a TL.

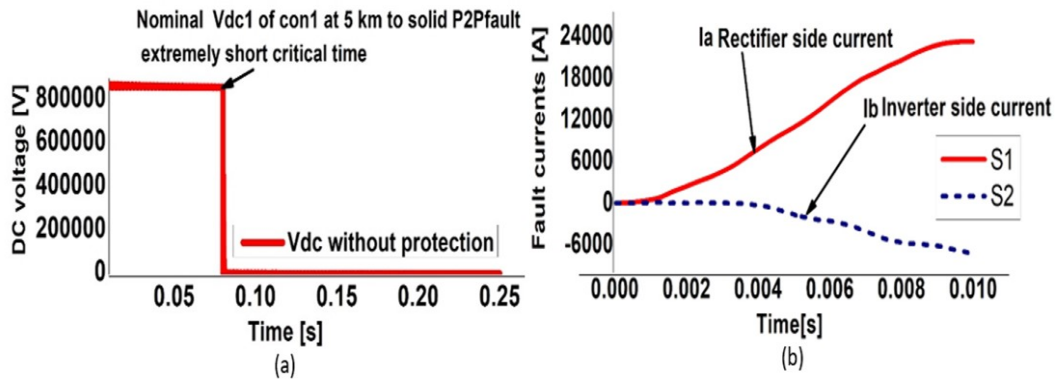


FIGURE 3.7: (a) HVDC link voltage without protection for a solid P2P fault at a distance of 5 km to the source node B_1 (MMC_1). (b) Current reversal b/w S_1 and S_2 oriented for the positive current flow from the sending MMC_1 to the receiving MMC_2 terminal due to an internal mid-line P2P fault in the cable L_{12} without protection.

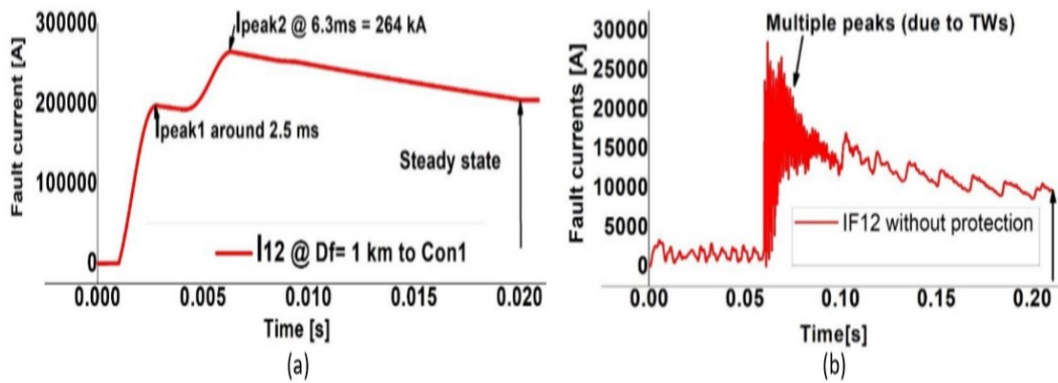


FIGURE 3.8: a) Huge P2P fault current at a distance of 1 km to the source node B_1 for strong AC source (800 kV). (b) DC fault current with multiple peaks without protection.

3.2.4 Simulation Results of P2P Faults

Maximum of the HDCCB current depends on factors like series reactor, DC capacitor, distance to fault D_f , fault resistance R_f , and power of the adjacent AC source. While simulating the P2P faults in this research work all the important factors like critical time limit, highest interruption current, maximum current breaking capability of HDCCB used, sizing of the FCLs, maximum contribution of weak and strong AC sources to the DC fault current, peak currents in the faulty and healthy cables were taken into account. Also, the influence of distance to the fault location D_f and the fault impedance R_f on the DC current and voltage transients

were rigorously analyzed in the meshed MTDC grid and a comprehensive report was prepared.

The P2P faults were simulated at different distances D_f to the terminal (MMC1)/ sensor S_1 in the cable L_{12} with different fault resistances R_f and using different L_{12} lengths. A sudden rise in the DC current or its derivative and a drop in the DC voltage are the early symptoms of a P2P fault. During the normal operation, currents at each end of a segment or transmission line are almost identical. However, during the fault conditions line current splits into load and fault currents so a clear difference occurs between them. As shown in Fig. 3.1 and Fig. 3.5, both the sensors S_1 and S_2 are oriented for the positive current flow from sending MMC_1 to the receiving MMC_2 terminal.

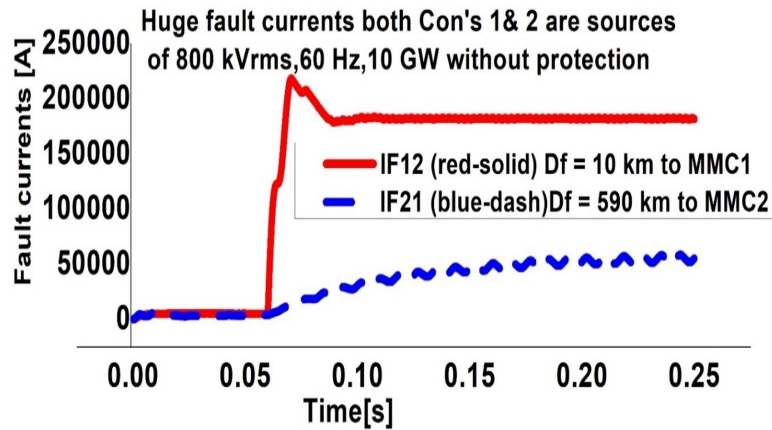


FIGURE 3.9: Influence of different distances to a solid P2P fault on the DC fault current transients showing the damped transient (blue dash).

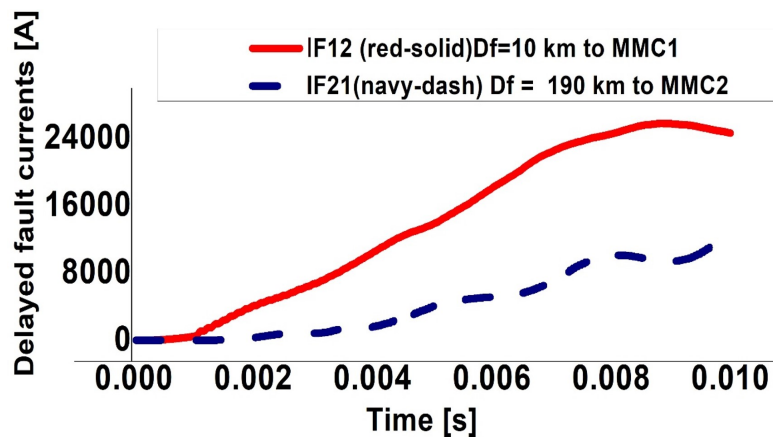


FIGURE 3.10: Delayed fault current profile for a solid P2P fault at 1 ms in L_{12} with B_1 at 10 km and B_2 at 190 km to the fault without protection.

Due to an internal mid-line P2P fault in the cable L_{12} b/w the pair S_1 and S_2 , current reversal takes place through them as shown in Fig. 3.7 (b). Thus, for an internal fault within the protection zone of the line L_{12} , I_a the rectifier side current through S_1 ascends, and I_b , the inverter side current through S_1 descends. Thus, the partial discriminating property of the current derivative direction method when used alone is verified. Therefore, this method is used as one of the back-up plans in the proposed scheme to locate the fault in a TL along with the TW principles.

Distance of the converter station/detecting sensor to the fault location ' D_f ' in a TL, is one of the key factors affecting to the rate of rise of the DC fault current derivative, DC voltage transients, and hence, is another important parameter to locate the fault in a TL. Indeed, fault induced current /voltage transient is a function of fault location in a TL. Since, the resistance of a TL (conductor) increases as its length increases therefore, attenuating the current magnitudes of the EM waves. Hence, the closer a station and or/sensor is to the fault point, the higher the frequency change / magnitude of the fault current derivative and its corresponding (wavelet co-efficient) gets.

Indeed, the highest DC fault current occurred for a solid P2P fault in the cable L_{12} at a distance of 1 km to the source node B_1 as can be seen in Fig. 3.8 (a). The wave front or surge arrival time is estimated as the instant when the current derivative exceeds a preset and large threshold level. When the fault occurs extremely close to a station's node (1~5 km), the current derivative surpasses the threshold level quickly and makes the critical time much shorter. However, as ' D_f ' increases, magnitude of the fault current derivative and its corresponding WC decreases (damping occurs) as shown in Fig. 3.9 and 3.10. Thus, due to the attenuating effect of long TLs on the fault current transients, it is impossible to locate a remote station close up fault quickly even with the optical schemes [75] or the wavelet transform. In Fig. 3.9 and Fig. 3.10, as the distance of the converter MMC_2 increases from the fault location, attenuation (damping) occurs in the fault current I_{F21} (blue-dash curve) and (navyblue-dash curve). With the proposed protection, these huge fault currents are limited, interrupted, and the faulty line L_{12} is isolated within a short time as is seen in chapter 4. Off course,

even with the wavelet transform (WT) it becomes difficult to detect the fault and hence, locate it in the TL with a damped transient (remote station faults). In other words, due to the attenuating effect of long TLs on the fault current transients, it is impossible to locate a remote station close up fault.

As already shown, that in a VSC based MTDC grid, the DC fault current surges exhibit a clear stepwise TW effect for close up faults to the nodes or the detecting sensors. Now, the merit of partial discriminative property of the current derivative polarity method indicates the fault directions and selectively identifies a faulty line. Therefore, in the research work, selecting a short time window of a minimum number of samples with large and precise threshold settings, current derivative method performed much better to locate the fault in a TL. Current derivative direction method combined with the differential protection and Type-D TW-based methods based on the optical sensor communication links, even reduces the communication errors as is seen in chapter 4. During testing when the distance to P2P fault D_f was 1~10 km, the fault current exhibited a clear TW effect when zoomed in represented as the stepwise increase in its development and rose sharply making the critical time much shorter as shown in Fig. 3.6 and Fig. 3.8 (a and b).

Fig. 3.8 (a), explains all the three important stages of a solid P2P fault in the DC cable L_{12} . It shows the timely development of a huge fault current through the HDCCB1 for a solid P2P fault in the cable L_{12} at 1 ms and at 1 km to B_1 . Both the terminals 1 and 2 were very strong AC power sources of 800 kV with the nominal power/ frequency of 10 GVA/60 Hz in a 2-level bipolar 3-terminal grid. There are two peaks visible clearly, one at 2.5 ms and the other at 6.3 ms. During the first 2.5 ms, fault current pattern is determined by the DC capacitor discharges and the current surges (Stage 1). In Stage 3, the AC contribution keeps on increasing and recharges the DC capacitor (capacitors) until the peak arrives. After this discharging into the fault takes place, and the maximum $HDCCB_1$ current I_{peak2} is arrived at 6.3 ms. Gradually the DC capacitor contribution decreases until the steady-state at around 20 ms arrives. The DC capacitor is still charged and discharged in the steady-state, but without any contribution to the fault current.

In chapter 4, these huge fault currents are interrupted quickly and the total DC fault clearance time of around 5.2 ms is achieved.

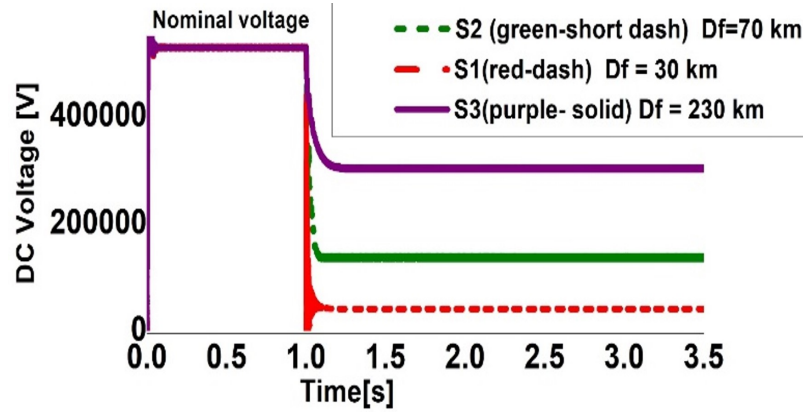


FIGURE 3.11: Influence of varied distances to a solid P2P fault on the HVDC link voltage transients without protection.

The influence of different distances to a solid P2P fault on the fault induced DC voltage transients was also tested. DC voltage sharply dropped to or very near to the zero level for a solid P2P fault at 1 to 13 km to the node/measuring unit, and the TW effect was not clearly visible in such cases. However, as the distance ‘ D_f ’ increased, DC voltage also increased above the zero level, thus indicating the nearness (closeness) of a converter station/sensor to the fault point. Therefore, the DC link voltage transients can fail to detect the wave-front arrival time, particularly for a solid close-up P2P fault to a station or sensor because of not exhibiting a clear TW effect. However, DC voltage transients can be used to estimate the fault location in a TL in the VSC-based MTDC grid.

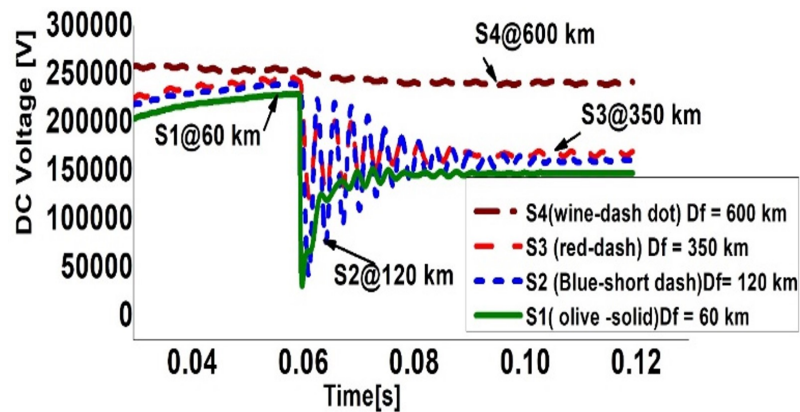


FIGURE 3.12: Influence of varied distances to a solid P2P fault on the HVDC link voltage transients. Damped oscillations due to TWs without protection in the faulty line.

A solid P2P fault simulated in the cable L_{12} at a distance of 1~5 km from the source node B_1 as shown in Fig. 3.7 (a) shows extremely short critical time duration and abrupt drop of DC voltage to zero with no TW effect seen. Fig. 3.11 and Fig. 3.12, show the influence of different distances of sensors to a solid P2P fault in the cable L_{12} on the fault induced DC voltage transients. As the distance of a sensor to the fault location increases, the corresponding DC voltage transient also increases. Except for the distances of 1 km-13 km, DC voltage did not drop to zero.

Fig. 3.11 shows the DC voltage profile for an internal P2P fault in the cable L_{12} with a 2-level bipolar VSC based HVDC link. Both the terminal MMC_1 and MMC_2 AC voltages used were 400 kV with the nominal power and frequency of 10 GW and 60 Hz respectively. The DC capacitor range was 70 to 120 μF , R_f was 0.01 Ω , and the inductances used were 10 mH. Three current measuring units (sensors) were distributed on the line and a P2P fault was triggered at 1 ms, at a distance of 70 km to S_2 and 30 km to S_1 . As the distance to fault increased, DC voltage also increased above the zero level.

Fig. 3.12, shows the converter DC output voltage profile on the cable L_{12} at different distances to the P2P fault for a bipolar four terminal meshed 3-level half-bridge VSC-MMC-MTDC grid. Damping oscillations are seen in the voltage transients of the faulty line L_{12} due to the TW effects. The converter blocks at the threshold (drop of DC voltage) and conduction by all the arms begins at this time.

In order to detect the high impedance fault, R_f was increased from 0.01 Ω to 500 Ω for a P2P fault at 1 ms in the cable L_{12} (180km) with $B_1(MMC_1)$ at 1 km. Variation of the differential current profile with increasing fault resistance showing corresponding 'Haar-2' wavelet coefficient magnitudes and damping effect was observed. Both the fault current and the WC magnitudes decreased with the increasing fault resistances and the fault distances due to the damping effect of both. However, with the DWT it was easy to detect a high impedance fault as can be seen in chapter 4. The WC remained constant up to 5 Ω but beyond this

value it kept on reducing. However, the WC remained well above the threshold level and the WCs of the healthy line currents.

3.2.5 Important Findings

Following are the important findings from the simulation results of the DC faults, particularly the pole-to-pole fault:

1. The DC fault has to be cleared before the critical time limit (in theory before 5 ms).
2. The DC fault current transients are the perfect signals to analyze the DC faults in a VSC-based MTDC grid. Because they exhibit a clear TW effect when zoomed in and hence, contain information about the fault characteristics.
3. The protection of a transmission line is based on the correct tripping of the corresponding DCCBs, while the tripping action of a DCCBs depends on the current waveforms during the fault. If the short circuit fault current is not cleared before the critical time, collapse of the whole grid may take place. The basic concept to differentiate between the internal and external faults and identify the ‘selected DCCBs’ (to be opened) and ‘non-selected DCCBs’ (which remain closed) is based on the magnitude and sign of the DC fault current derivative after the fault start time respectively.

The fault location D_f is the distance from the fault point to a monitoring terminal/detecting sensor and can be evaluated in-terms of its location in the MTDC grid, distance, and the fault impedance or resistance R_f .

3.2.6 Summary and Discussions

In this chapter critical DC faults in a VSC-based MTDC grid are illustrated with both theory and simulation results, particularly the DC link/cable short circuit fault. Despite being a major enabler for the Super-grid due to its considerable features and benefits, a VSC-HVDC system is highly vulnerable to the DC faults especially the rare DC cable short circuit fault. This fault is mainly caused by the environmental conditions, insulation breakdown, electrical stresses, and aging.

A worst-case scenario is a solid DC cable P2P fault extremely close to a remote source station. To better analyze the fault characteristics and design a feasible protection scheme against such faults, the fault provoked DC current transients are taken as the target signals as they exhibit a clear TW effect when zoomed in. A rigorous analysis of the P2P fault is done in terms of its location in the four terminal MTDC grid, distance from a source station or a detecting sensor, and the fault impedance. It is found that all these parameters affect the fault response. Two important parameters of a P2P fault (a) time taken by the DC voltage to drop to zero (critical time) and (b) the line current at this time are investigated. It is noted that the closer the P2P fault is to a monitoring sensor and/or source station, the higher the magnitude of the fault current gets. As the fault distance increases the signal damps. Additionally, it is also concluded that the fault provoked DC link voltage transients (TWs) may give an estimation of the fault location in a TL, but cannot detect the wave-front in a VSC based MTDC system. Important aspects of the total DC fault clearance time include faulty line determination, fault detection, fault current interruption, faulty line isolation, and fault location. The core requirement in protection of the system is to isolate the fault before the current exceeds the maximum current the IGBT diodes can sustain (within a few milliseconds). Thus, among important aspects, it is concluded that the utmost requisites are the fast fault detection and isolation.

Because if these two aspects, especially quick detection of the surge arrival time are fulfilled, alternate methods and backup plans can be implemented in the grid to cover other aspects and protect it. Quick fault detection shortens the overall DC fault clearance time comprising of faulty part identification, fault detection, its location, and isolation of the faulted line.

However, with the existing technologies the key requirement of a few milliseconds of the total DC fault clearance time is not fully satisfied. Thus, more reliable and efficient fault discriminating/detecting/locating methods have to be investigated. If the available isolation tools are aided with the appropriate FCLs and efficient backup plans fast isolation can be made possible. With efficient FCLs, the fault current magnitude can be limited to a reasonable range, thus making the time

constraint less strict in an MTDC system. Because after significantly reducing the fault current fast isolation is not needed. Thus, other available mature and simple protection devices can be used to interrupt and isolate the fault.

The four-terminal meshed VSC-MTDC model presented in this chapter is the basis of this project in which all the important objectives of the proposed scheme (DC fault detection, faulty line/segment determination, significant fault current limitation, fault location, and selective isolation of only the faulty part) are implemented. Each possible way is rigorously explored and based upon the results a comprehensive and robust HVDC/MTDC protection scheme is proposed in the following chapter.

Chapter 4

Proposed Scheme

For a conventional point-to-point HVDC link, high rating DCCBs at the line ends are not mandatory, because the ACCBs/MCBs with the associated FCLs are adequate devices to clear the fault. However, in a meshed MTDC grid, almost every DC node (bus) has multiple cables/lines connected to it. During normal operation sum of the currents entering/leaving a node is zero by KCL. However, during the fault conditions especially during the freewheeling period of a close-up P2P to a converter station, the converter blocks within a few milliseconds after the fault trigger and the DC voltage drops almost to the zero level. Soon the DC fault current contributed by the capacitor discharges, infeed from multiple connected sources/feeders, and due to the minimum surge impedance of the grid reaches to a huge peak within a few milliseconds. Now if this rapidly rising fault current is not interrupted quickly before the critical time limit, collapse of the entire grid may take place.

From the previous literature [31], if the current derivative is positive at the fault detection time, fault is potentially internal to a DC link and if it is negative then the fault is external to a link. However, these statements are valid only for a current measuring unit/sensor oriented for the positive current flow from a source converter station towards the DC link (seen by the sending end of the line towards the receiving end). For example, an internal P2P fault triggered at 1ms between S_1 at 10 km from the fault point and S_2 at 40 km in the cable L_{12} (Chapter 3) lead to

the current reversal between them, indicating the partially discriminating property of the current derivative direction method. Thus, determining a faulted line from the healthy ones at a fault related node simply with the overcurrent protection principle, FCLs, fault current derivative principles, etc., is not a reliable solution. For a meshed MTDC grid, in order to fulfill the promise of “sustainable electricity” DCCBs are the mandatory devices to clear the fault quickly and selectively isolate the faulted line, while continuing normal operation of the healthy grid zones.

Thus, based on the existing literature particularly the optical sensor schemes, this thesis work proposes an alternate, cost-effective, robust, and a fully selective DC protection scheme. The scheme is applicable to even large scale meshed MTDC grids, with several added benefits as compared to previously proposed strategies and algorithms. The scheme utilizes the joint performance of both the communication dependent and independent methods and combines two ways to protect an MTDC grid from the DC side faults respectively.

In one way, the overall DC fault clearance time is reduced due to the accurate discrimination of the faulty line with fast fault detection. Hence the concerned CBs are allowed to operate before the critical time limit. In the other way, the total DC fault clearance (grid outage) time is extended by significantly reducing the DC fault current to or below the breakable levels of the available CBs. Thus, more reaction time is gained for both the fault detection and isolation. Off course, the proposed scheme is a fast scheme as the total fault processing time is kept within a few milliseconds by immediately interrupting the fault current before it becomes higher than the maximum current breaking capability of the HDCCB.

The proposed scheme includes all the important aspects of a feasible DC protection scheme. Each aspect is explored rigorously both theoretically and with the simulation results which are found to be accurate as follows:

1. Accurate determination of a faulty line utilizing the differential current algorithm based on the distributed optical sensor measurements on TLs. The differential protection coordinated well with a hybrid DCCB (constant breaking time of 2~3 ms) and very small inductors. Both the source and load

terminals were tested and three ways were explored to accurately determine a faulty line or its faulty segment.

2. Fast real-time detection of the wave-front (surge) arrival time utilizing the independent digitalized wavelet transform (DWT).
3. Significant reduction of the DC fault current below the breakable levels of the hybrid DCCBs (HDCCBs).
4. Fully selective isolation of only the faulty line, instead of shutting down the entire MTDC grid.
5. Fault location in an MTDC grid utilizing the current derivative data along with Type A and Type D travelling wave methods.

4.1 Fast Fault Detection

Since the protection of a transmission line is based on the correct tripping of the corresponding DCCBs, while the tripping action of a DCCBs relies on the current waveforms during the fault. Continuous wavelet transform (CWT) is not suitable for quick fault detection in a non-stationary random signal with multiple peaks, as it consumes both time and memory space. CWT is more accurate in off-line fault location for which high speed is not of high priority, except in the case of permanent short circuit faults. Analytic wavelets are best suited for time-frequency analysis as these wavelets do not have negative frequency components. Some of the analytic wavelets suitable for continuous wavelet analysis include Morse Wavelets, Bump Wavelets, and Analytic Morlet Wavelet.

CWT outputs are the coefficients which are a function of scale (frequency) and time. They have finer time resolution which is very important to have a high accuracy in the TW- based fault location method. CWT is not discussed briefly in this thesis work, as the primary focus is on the application of Discrete Wavelet Transform (DWT) very practical for real-time fault detection.

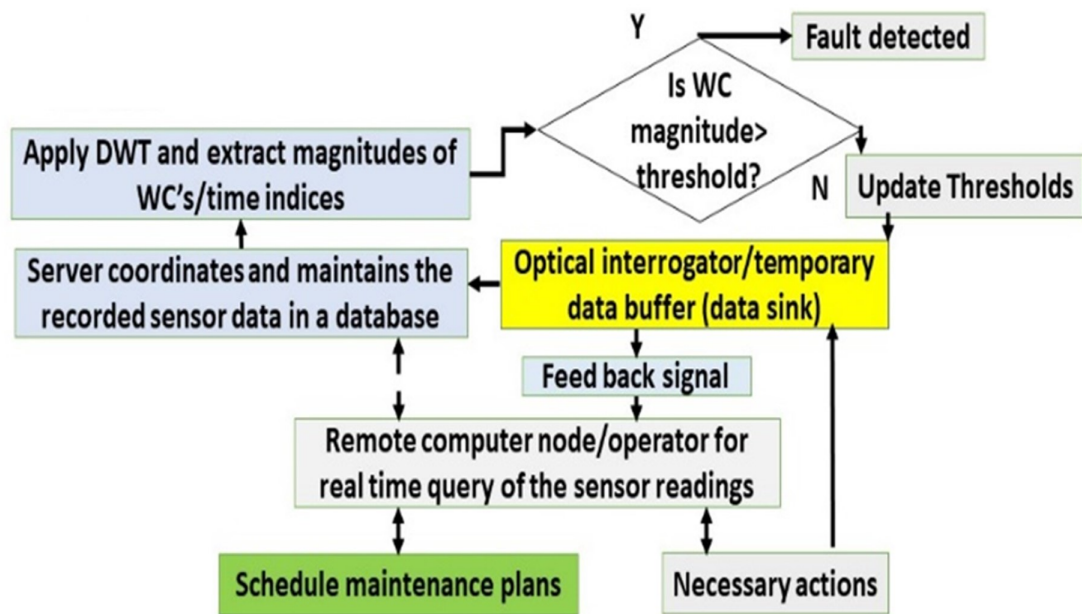


FIGURE 4.1: Flowchart for rapid fault detection using DWT (DSP).

Rapid (real time) fault detection is the utmost requisite for a feasible DC protection scheme to fulfill the core requirement of fast speed of operation. Indeed, the fault detection not only detects the wave front, but also discriminates the faulty line and determines which breakers to trip quickly. Thus, it shortens the overall DC fault clearance time comprising of faulty part identification, fault detection, its location, and accurate isolation of only the faulted line.

To days world is a digital world and by introducing intelligent real time digital systems (RTDS) in an MTDC network, detection of wave-front arrival time is fast. Fig. 4.1, illustrates the flowchart for real-time detection of the fault generated surge arrival time. Here the optical sensor data is periodically collected in a run-time input temporary buffer (an Optical Interrogator). Then the collected sensor data from the buffer is transmitted to a computer server, to permanently maintain all the sensor readings in a database for further analysis and coordination. The sensor data in the server can be remotely or wirelessly queried by an operator in order to collect the results/issues/updates if required and interact with the available resources to direct the necessary actions to be taken. At the same time a remote operator can also manage the operation of the entire transmission system by interacting with the maintenance plans.

4.1.1 Why the Wavelet Transform

Fourier transform FT, though a powerful tool for signal and data analysis does not address efficiently to the high frequency abrupt changes (used for the fault detection) in a non-stationary random signal with multiple peaks [80–82]. Because the sine waves representing the data in this analysis are not localized in time or space and oscillate forever. This transform relies on a single basis function. Although, Short-Time-Fourier-Transform (STFT) is able to analyze a non-stationary signal in time -frequency domain, but its window size is fixed leading to high frequency and time uncertainty of the events [83]. Off course good frequency resolution can be obtained using a longer window but at the expense of time resolution and vice versa.

Therefore, a new class of intelligent, independently discriminative, and powerful signal processing tool more effective than the STFT, called the wavelet transform or wavelet analysis (WT) is used to accurately analyze the signals and images exhibiting abrupt changes [84–90]. Real world data or non-stationary continuous-time signals, often exhibit slowly changing oscillations accompanied with abrupt changes. These abrupt changes are important parts of the data in terms of the information they give.

Various attractive features and benefits offered by the wavelet transform include:

1. Simultaneous time and frequency localization capabilities for real world data and non-stationary continuous-time signals consisting of slowly varying components accompanied with abrupt (high frequency) changes.
2. Communication independent DWT is a suitable fault detection technique particularly in a VSC-based meshed MTDC grid which requires less or no communication between its interconnected Terminals. The WT allows each terminal to independently determine its faulted line (without the need of a communication channel or inter-terminal communication) using simple local DC current measurements.
3. With the WT, correct tripping of even remote CBs becomes possible

4. Unlike sinusoids that extend to infinity, a wavelet exists for a finite duration i.e., a wavelet is a rapidly decaying wave-like oscillation that has a zero mean.
5. The availability of a wide range of wavelets in different sizes and shapes is a key strength of the WT. Choosing a right wavelet depends on the application the wavelet is used for.
6. The WT in response to the dynamics of a non-stationary signal, automatically changes the window size.
7. Ability to capture a high frequency (abrupt change) for the fault detection by generating a high wavelet coefficient WC.
8. Consistently high WC's of the faulty line currents and consistently low WC's of the healthy line currents further assist in quick detection of either the internal or external faults. The WT allows the healthy terminals to recognize that the fault is outside their protection zone, since the WCs of their currents remain consistently low.
9. Fast DWT is used as the main detecting scheme in this research work. DWT is further aided with the current derivative direction method and an SFCL quench criteria. For better performance, the mother wavelet and the transform level are selected very carefully.

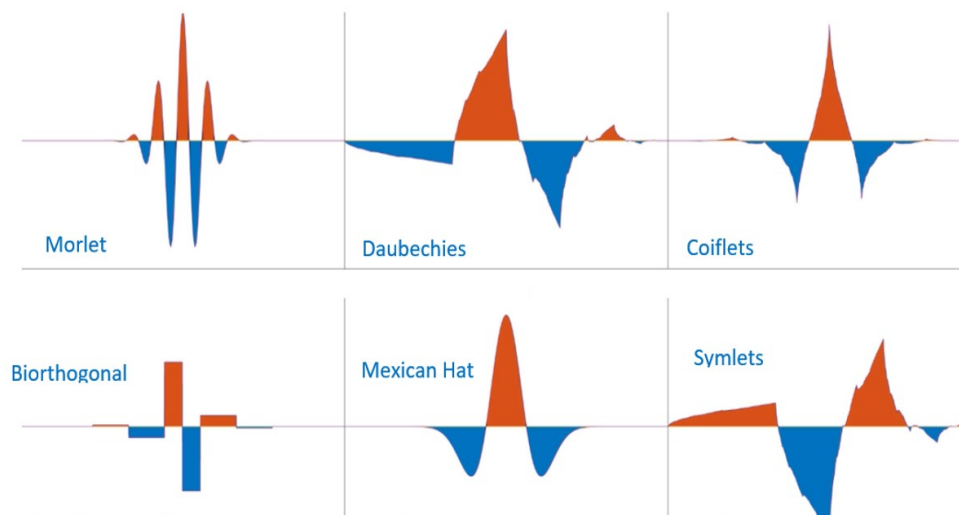


FIGURE 4.2: Various types of the mother wavelets in WT.

In the WT an input given function signal is decomposed into different output levels of resolution called the wavelet coefficients (WCs) or scales by an analyzing function called the mother wavelet MW denoted as ' $\phi(t)$ '. The wavelets (baby wavelets) are scaled and translated (dilated) copies of a finite-length or fast-decaying oscillatory mother wavelet (transformation function). A mother wavelet (MW) is a basis for various transformation process. A MW can be thought as a windowed function that shifts (moves) along the time-series signal from time $t = 0$ to time $t = T$. The portion of the signal in that window is multiplied by the MW and then integrated over all times to get the wavelet coefficients (WCs). Widely used mother wavelets are 'Haar Wavelet' and 'Daubechies (db) Wavelet' respectively. The WC is the cross-correlation of the fault signal and the MW, the higher the WC, the closer the signal matches to the chosen MW. Therefore, precise and large threshold settings (much above the noise level) and the selection of a correct MW that has the closest (best) match with the fault current pattern are the key requirements in the WT to avoid wrong fault detection, boost high accuracy in the TW-based fault location method, enhance correct DCCBs to trip, and avoid false tripping of the healthy lines. Unlike a sine wave, a wavelet has a band pass characteristic in the frequency domain with the key concepts of Scaling and Shifting.

The wavelet transform is an intelligent signal processing tool and explores new ways to reduce the computational complexity in order to achieve better noise reduction performance. Capabilities of wavelet include revealing data aspects, discontinuities in higher derivatives, breakdown points, and self-similarity which are impossible with the other techniques. Fig. 4.2 shows a number of wavelets to extract information from different kinds of data like music, images, etc. Time-frequency analysis of the wavelet transform means which frequency at what time.

Morlet Wavelet: Gaussian modulated sinusoid/Gabor wavelet/Sine-wave tapered by Gaussian/Complex exponential (carrier) multiplied by a Gaussian window (envelope) are its definitions. This wavelet is closely related to human perception both hearing and vision. This wavelet decomposition has an oscillatory or sinusoidal component and is important for time-frequency analysis of non-stationary

signals such as neural time-series data (neurology/neurosciences)

Applications

- Time-frequency analysis of brain oscillations like EEG
- Discrimination of abnormal heart-beat behavior in the ECG
- Music transcription.

Its function is like windowing function of the STFT. It is square integrable and has no energy at zero frequency (band pass). However, unlike STFT (where the frequency resolution is same over all frequencies), its frequency resolution is proportional to the bandwidth (decreases at higher frequencies and increases at lower frequencies). Thus, higher time resolution at higher frequencies and lower time resolution at lower frequencies. These wavelets in a bunch are characterized by different frequencies (band of different colors seen in MATLAB).

Daubechies Wavelets: These wavelets come under a family name of orthogonal wavelets (DWT) for decomposition of a signal in time-frequency scale plan and is characterized by a maximal number of vanishing moments. Denoising involves decomposition of a signal at level N by selecting a particular wavelet function. Applying soft or hard thresholding methods, a denoised version of an original input signal is obtained by thresholding the detailed coefficients for each level from 1 to N. The original signal containing all useful information for the purpose of diagnosis is decomposed and the noise is removed using Daubechies wavelet filtering technique. The original signal is improved by reducing side lobes and increasing main lobes (which contain most useful information). The signal to be decomposed is analyzed at different frequency bands with different resolution. The decomposition takes place by transmitting the signal to a series of low-pass and high-pass filters. They are also perfect wavelets for the fault detection (address signal discontinuities) and can solve fractal problems in mathematics. Commonly used Daubechies are db1 to db10. In this research work db1 to db6 were used.

They are also good for digital image processing. Orthogonal functions have very nice localization properties in time-frequency space.

Symlet Wavelets (orthogonal wavelets DWT): These are modified version of Daubechies wavelet with increased symmetry (least asymmetric). These wavelets like Daubechies have applications in the fields of medical, image processing, and mathematics. Symlets (sym2 to sym10) are usually used to denoise digital images, ECG and EEG signals. Both Daubechies and Symlet Wavelet filtering techniques are used to minimize MSE and improve SNR of the ECG/EEG signals. By improving the SNR, exact diagnosis of the heart disease becomes possible. The analysis is done by passing the low and high frequency components in the noisy ECG signal through a series of low-pass and high-pass filters with different cut-off frequencies. Soft and hard wavelet threshold values are used.

Coiflet wavelets: These are discrete wavelets and compactly supported wavelets with highest number of vanishing moments. The Coiflet has two vanishing moments. The wavelet function has $2N$ moments equal to 0 and the scaling function has $2N-1$ moments equal to 0. The two functions have a support of length $6N-1$. They are also used in image processing applications.

Biorthogonal Wavelets: Like those of orthonormal wavelets are used to decompose and recover functions. Except for the Haar Wavelet, all other orthogonal wavelets are unsymmetrical which generates phase distortions in image compression. By using Biorthogonal Wavelets this problem can be eliminated.

Mexican Hat (Ricker wavelet): Extension of the Gaussian-Mexican Hat wavelet pair, is the negative normalized second derivative of a Gaussian function. It finds applications in detection purposes.

A given MW has a duration or Scaling which corresponds to stretching or shrinking the signal in time and a location or time shift ' τ '. The scaling is expressed mathematically as in equation 4.1 below.

$$\varphi(t/s)S > 0 \quad (4.1)$$

Where ‘S’ a positive value, is the scaling factor and corresponds to how much the signal is scaled in time. For a wavelet ‘S’ is inversely proportional to frequency ‘f’ and the constant of proportionality is called the center frequency of the wavelet. Mathematically:

$$F_{eq} = C_f / S_{\partial t} \tag{4.2}$$

Where ‘ C_f ’ is the center frequency of the wavelet, ‘S’ is the wavelet scale, and ‘ ∂t ’ is the sampling interval. Therefore, a larger S results in a stretched wavelet which corresponds to a low frequency. A smaller S results in a compressed wavelet which corresponds to a high frequency. A stretched mother wavelet of low frequency with a large-scale factor helps in capturing the slowly varying changes in a signal. A compact mother wavelet of high frequency with a small-scale factor helps in capturing the abrupt change for the fault detection as shown in Fig. 4.3. In other words, large windows are used to obtain the low frequency components of the signal while small windows are used to obtain or reflect discontinuities. A wavelet is shifted to align with the feature in a signal that is desired. Shifting a wavelet means delaying or advancing the onset of the wavelet along the length of the signal. For example, $\phi(t-k)$ means that the wavelet is shifted and centered at ‘k’. According to the Pearson product-moment formula, the correlation coefficient leading to selection of a suitable MW is given mathematically in equation 4.3 where IF_k the fault signal and ϕ_k is the chosen MW.

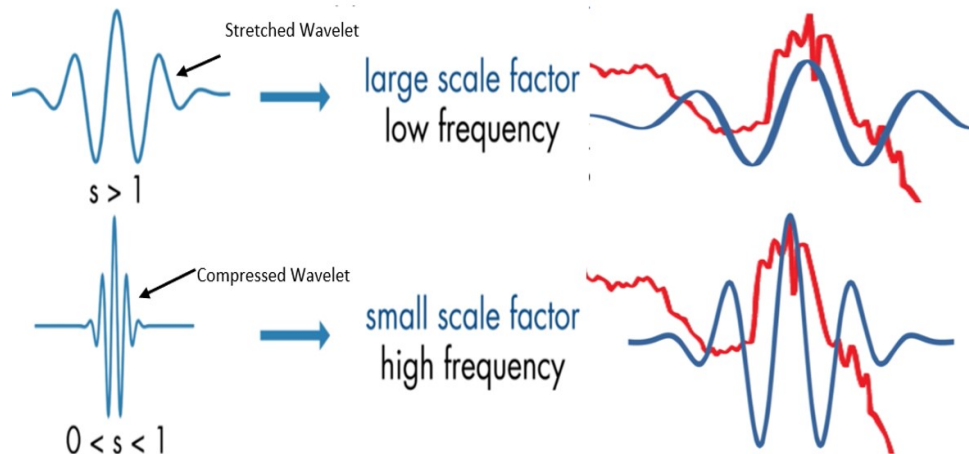


FIGURE 4.3: Compressed and stretched wavelets to detect high and low frequencies in a non-stationary continuous time signal.

$$r = \frac{\sum_{k=1}^n (IF_k - IF_{ava})(\phi_k - \phi_{ava})}{\sqrt{\sum_{k=1}^n (IF_k - IF_{ava})^2 (\phi_k - \phi_{ava})^2}} \quad (4.3)$$

The WT is generally categorized into following types:

1. Continuous Wavelet Transform (CWT), defined as the convolution of the signal and the scaled and shifted MW.
2. Discrete Wavelet Transform (DWT), the discrete or digitalized form of CWT.
3. Stationary Wavelet Transform (SWT), also known as the time-invariant wavelet transform.

4.1.1.1 The Discrete Wavelet Transform (DWT)

Communication independent DWT with the key applications of de-noising and compression of signals/images, is a digitalized WT in which the wavelets are discretely sampled.

DWT is a suitable fault detection technique in a meshed MTDC network. It is used to represent many naturally occurring signals and images with fewer coefficients, hence offers lower computational burden. The base scale in DWT is set to 2 i.e., scaling of 2^n . In other words, due to the decomposition process, the input signal must be a multiple of 2^n where ($n = 1, 2, 3, 4, \dots$) is the number of levels. Different scales are obtained by raising this base-scale to integer values as translation $2^n m$ ($m = 1, 2, 3, 4, \dots$). This process is often called as dyadic scaling and shifting. This kind of sampling eliminates redundancy in coefficients. The output of the transform yields the same number of coefficients as the length of the input signal so the DWT requires less memory. DWT offers several applications and benefits in science, engineering (image processing in digital and in UWB wireless communications), mathematics, computer science, and medical (analog filter bank in biomedical signal processing for design of low power pacemaker). A key advantage of the DWT over the Fourier transform is temporal resolution to capture simultaneously both the frequency and location (time) information. Therefore, it is used as a primary technique to detect the arrival time of the fault generated surge (TW) or wave-front in this research work.

In the DWT, a proper technique for isolating the time components of a non-stationary signal with low computational costs is the wavelet decomposition. Here the DWT of a discrete-time signal $x[n]$ is calculated by passing it through a series of low-pass filters (LPFs) and high-pass filters (HPFs). The filter bank structure as shown in Fig 4.4. is used to obtain the forward DWT coefficients. First the samples are passed through the LPF with the impulse response 'g' resulting in a convolution of the two. The signal is also decomposed simultaneously using the HPF 'h'. The outputs $y[n]$ from the LPF are the approximation coefficients and from the HPF are the detail coefficients. The filter output of LPF is subsampled by 2 and further processed by passing it again through a new LPF and HPF with half the cut-off frequency of the previous. In other words, the original signal (x) decomposes through two complementary filters and emerges as two signals. The process is iterated with successive approximations being decomposed in turn. Therefore, one signal is split into many lower resolution components and the process is called as Multi-resolution Analysis (MRA) or Multi-resolution signal decomposition (MSD).

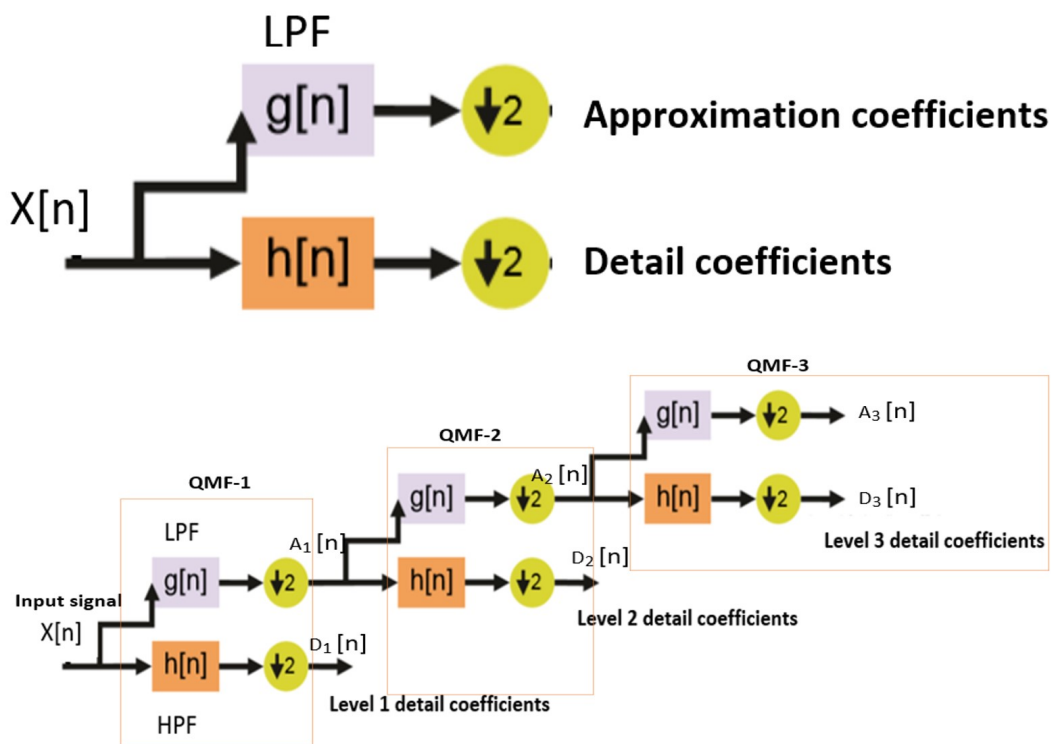


FIGURE 4.4: DWT with wavelet tree (MSD) decomposition for the three levels of detail showing Filter Bank.

$$y[n] = (x * g)[n] = \sum_{k=-\infty}^{\infty} x[k]g[n - k] \quad (4.4)$$

$$y_{low}[n] = \sum_{k=-\infty}^{\infty} x[k]g[2n - k] \quad (4.5)$$

$$y_{high}[n] = \sum_{k=-\infty}^{\infty} x[k]h[2n - k] \quad (4.6)$$

Approximation coefficients are the high scale (low frequency) components of the signal while detail coefficients are the low scale (high frequency) components of the signal. The two filters are known as quadrature mirror filters. HP and LP filters are derived from the MW and the scaling function considered. In the HVDC systems, compact MWs of high frequency with a small scale-factor ‘S’ such as ‘*Haar-6*’ and Daubechies ‘*db1-4*’, are the two types of widely used MWs. These are suitable for the fault detection and hence, its location in an MTDC grid. They perform better to localize the high frequencies in the fault current transients particularly ‘*Haar*’ (shorter processing time) with a minimum delay of around 1 ms.

4.1.1.2 Simulation Results of the Fault Detection with the DWT

In the DWT a fault is detected when the magnitude of the detailed wavelet coefficient exceeds a specified and large threshold level. Higher the absolute value of the WC, the closer the chosen mother wavelet matches to the fault signal pattern. DWT using both *Haar* and *Db4* of 6 levels as the MWs were tested out for different fault locations. Discriminative nature of WT allows each terminal to independently identify its faulted line by simply monitoring the local DC current. Faults were created on all the DC cables to obtain the WCs for the positive pole DC currents. Fault is detected when the faulted line current registers a high WC suddenly because WC values are almost zero before and after the fault.

In Fig. 4.5, using DWT, suddenly a high WC is registered for a solid P2P fault b/w S_1 at 10 km and S_2 at 20 km to the fault in the cable L_{12} , before installing the

FCU's (without protection). The fault is shortly detected at 270th sample value using 'Haar -6' as the MW and WC's are almost zero before and after the fault. Indeed, the detection time is reasonably short and using de-noising property of the DWT the steady state coefficients can be reduced in the signal. In Fig. 4.6, a P2P fault in the cable L_{12} at 1 km to MMC_1 and 179 km to MMC_2 with $R_f = 0.01 \Omega$ registered high WCs for I_{12} & I_{21} . The maximum value is 1.3896e-05 with the index of 9000 with Db-3 MW at level-2 decomposition.

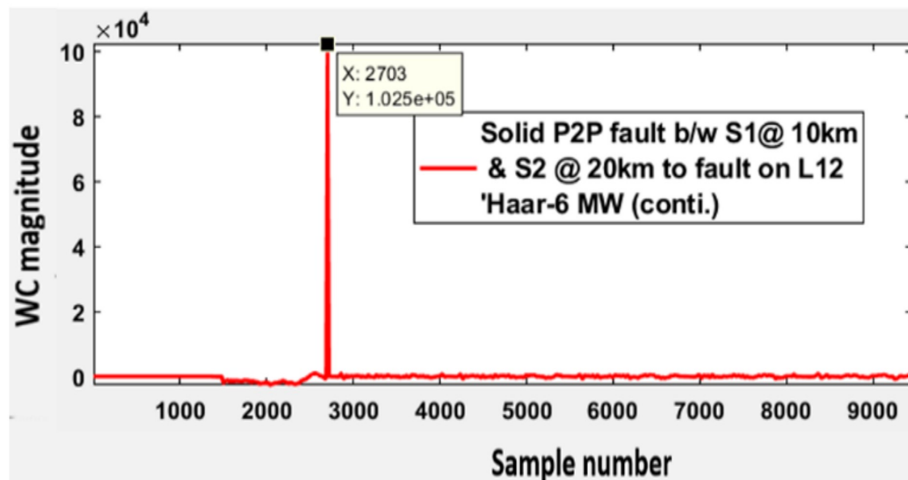


FIGURE 4.5: Suddenly a high WC 'd6' registered for a solid P2P fault b/w S1 at 10 km and S2 at 20 km to the fault in the cable L_{12} . The fault is shortly detected at 270th sample value with Haar-6 as the MW without protection. WCs are almost zero before & after the fault.

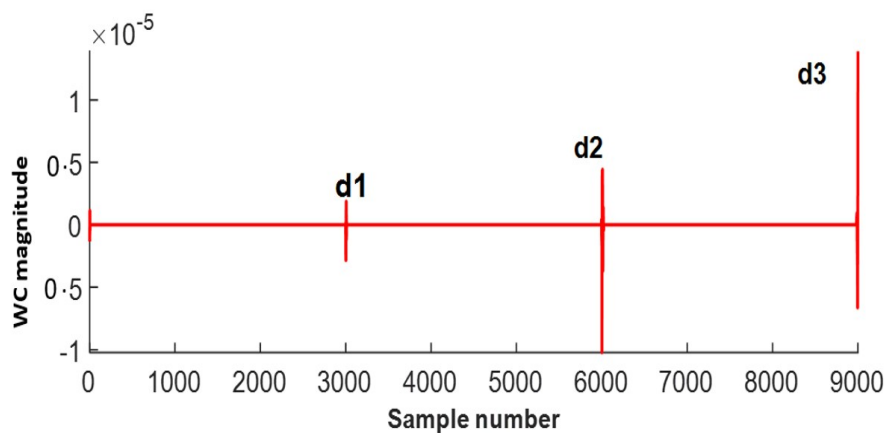


FIGURE 4.6: A P2P fault in the cable L_{12} at 1 km from B1 and 179 km from B2 ($R_f = 0.01 \Omega$) registered high wavelet coefficients for I_{12} and I_{21} . Maximum value is 1.3896e-05 with the index of 9000 using db-3 level-3 as the MW. The Fault inception time of 0.08s was translated to 9000th sample value (highest coefficient magnitude).

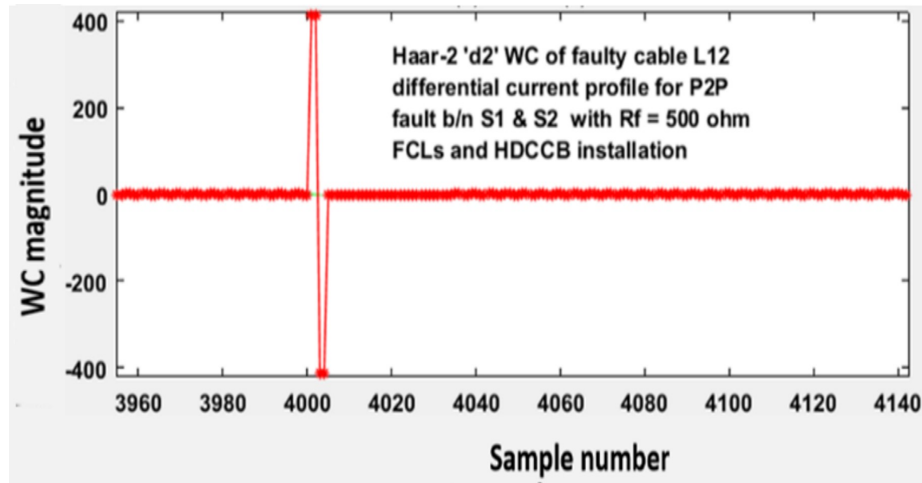


FIGURE 4.7: With protection after installing FCU's and using $R_f = 500 \Omega$ WC on the faulty cable reduced greatly but its value still stayed well above the WC's of the healthy cable currents and the threshold levels.

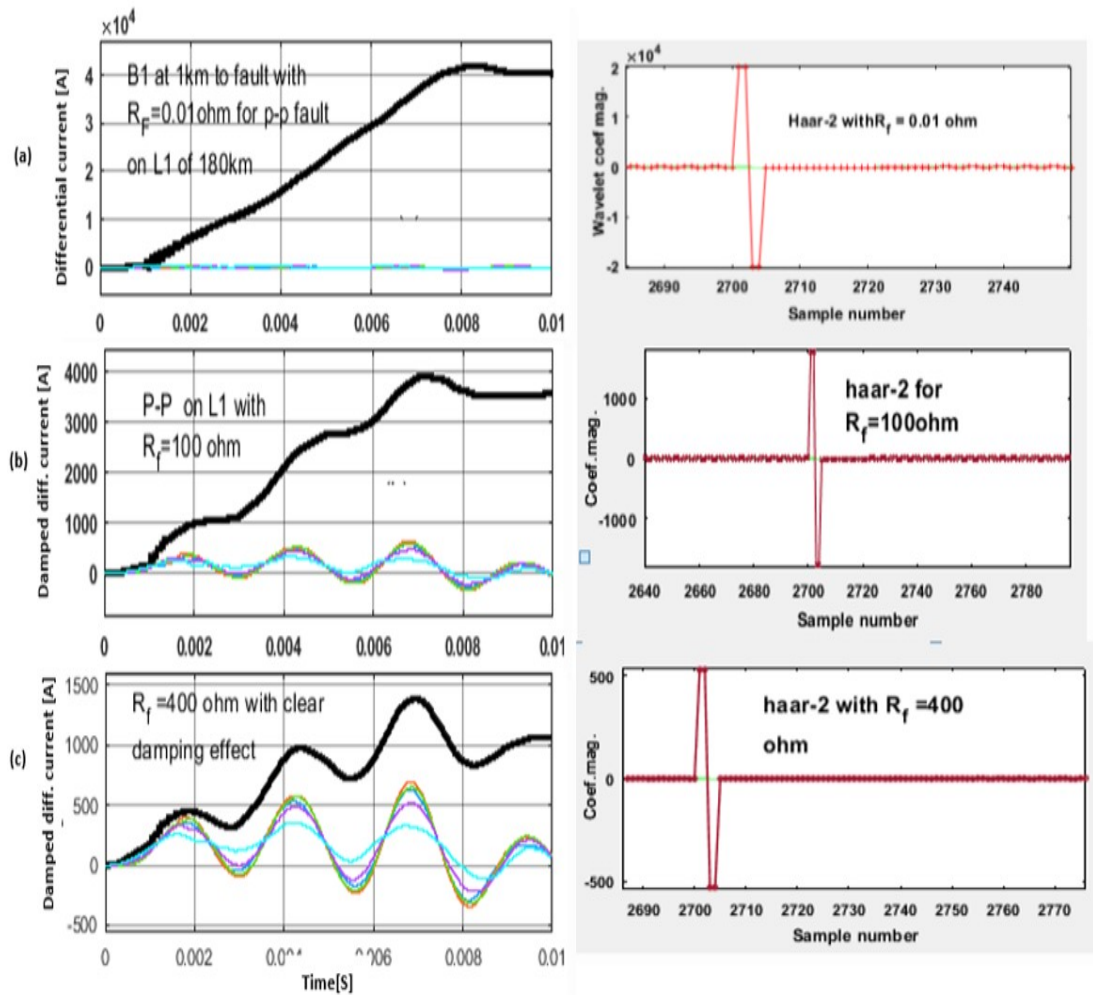


FIGURE 4.8: Variation of Differential current profile with the increasing fault resistances showing corresponding *haar-2* coefficient magnitudes (right) and damping effect for P2P fault in the cable L_{12} (180 km long) for a four-terminal grid with B_1 (MMC_1) at 1 km to the fault location.

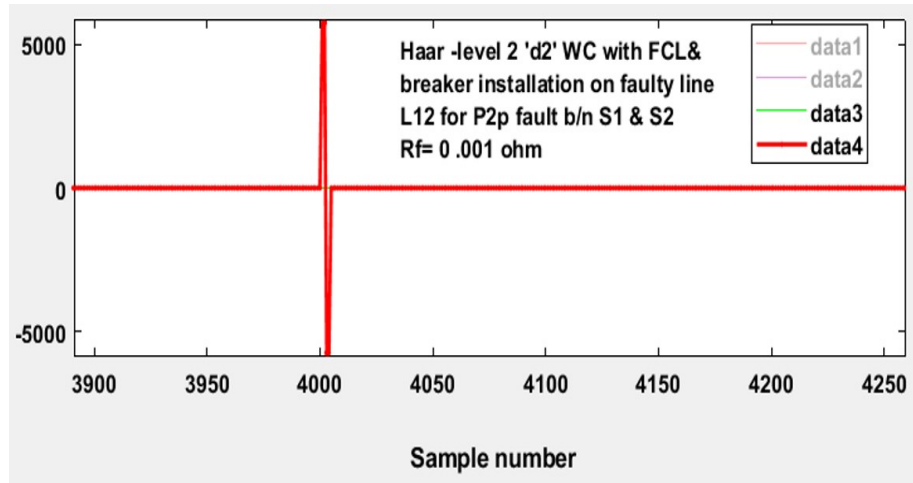


FIGURE 4.9: WCs of the differential current profile in the faulty cable L_{12} for a solid P2P fault with ‘Haar-2’ as the MW after installing the FCUs (with protection)

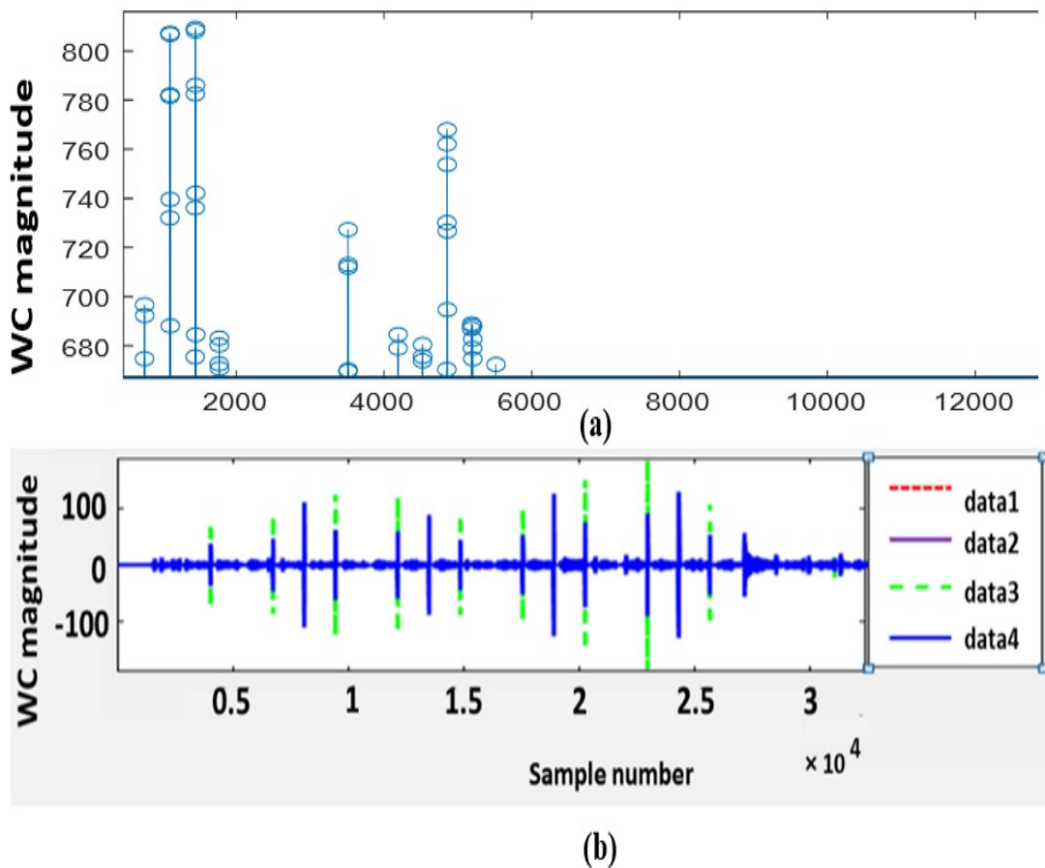


FIGURE 4.10: (a) WCs of the differential current profile for a solid P2P fault in the cable L_{12} , on the healthy cables having consistently low magnitudes without FCUs (without protection). (b) Consistently low WCs of the differential current profiles on the healthy cables further reduced after installing FCUs (with protection).

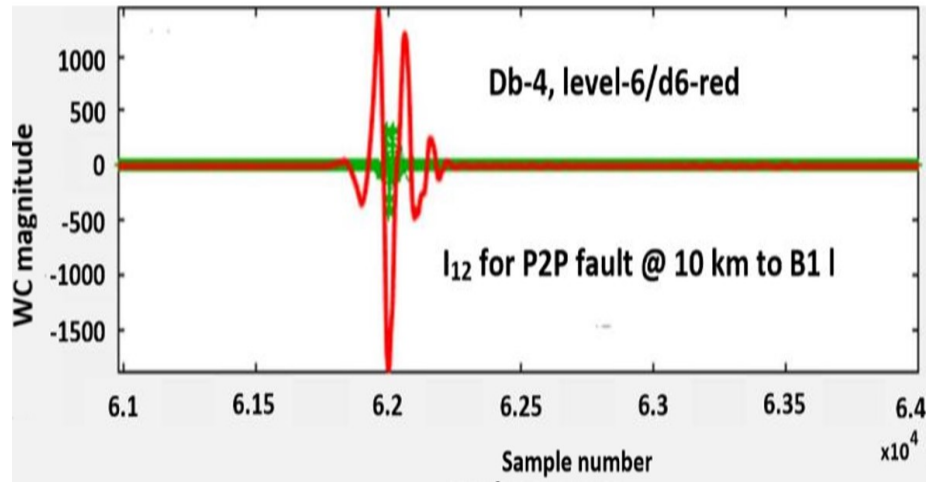
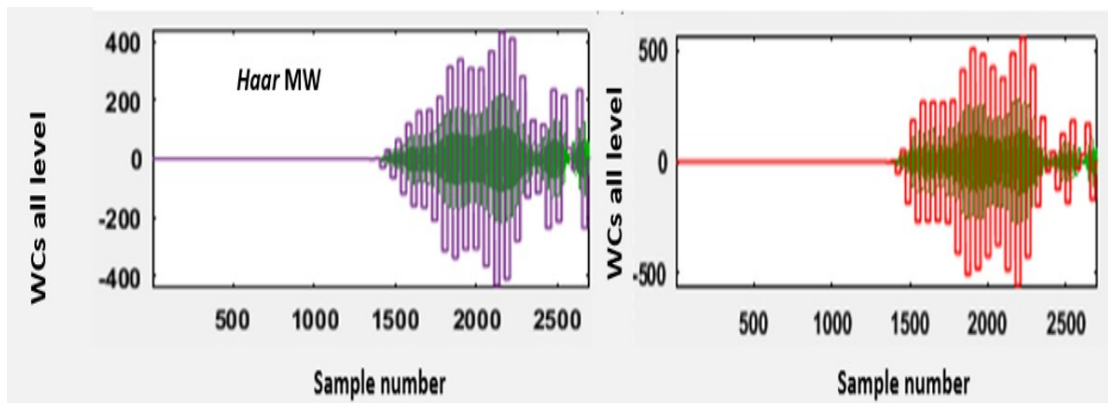
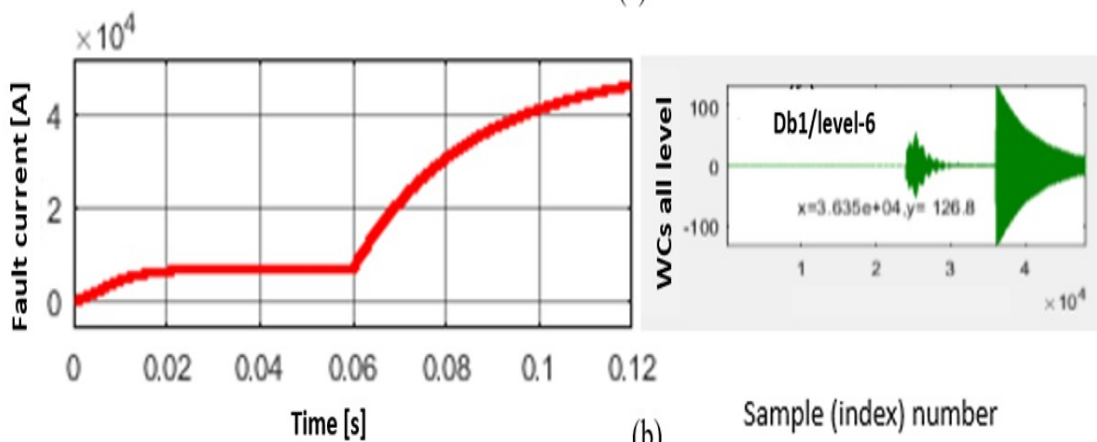


FIGURE 4.11: A Solid P2P fault at 10 km to B_1 in the cable L_{12} (600km long) generates a high WC ‘d6’ (red-solid curve). WCs are almost zero before and after the fault. WC’s of a damped transient are shown by green-solid curve.



(a)



(b)

FIGURE 4.12: (a) Consistently high WCs of the faulty line current (purple and red). Consistently low WCs of the healthy line currents (green, yellow etc.). (b) Huge P2P fault current with the fault start at 60 ms (red-curve left) and corresponding WCs (green right).

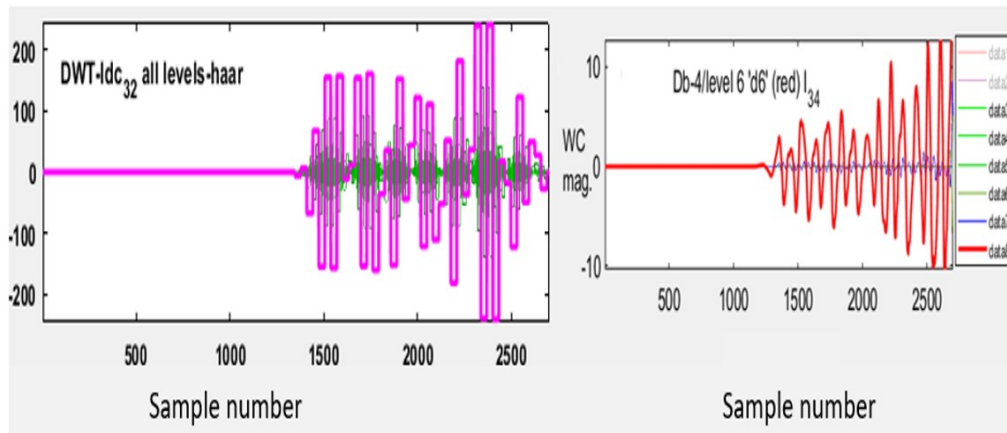


FIGURE 4.13: Consistently high WCs of the faulty line (dark-pink-left) and faulty segment (red-right). Consistently low WCs of the healthy lines (green, orange, left) and healthy segments (blue, green, light green, etc., right).

The smaller the fault impedance R_f value, the larger the fault current magnitude (shorter the critical time), and vice versa. In order to study the influence of DC fault resistance on the magnitude of the fault current or the WC and detect a high resistance P2P fault in the cable L_{12} , R_f was increased from $0.01 \sim 500 \Omega$. Magnitude of both the fault current and its WC decreased due to the damping effect of large R_f as shown in Fig. 4.23, Fig. 4.7, and Fig. 4.8 respectively. In Fig. 4.23, with a series of differential current measurements, it is impossible to discriminate a faulty segment (red-solid curve) from the healthy ones initially, due to the damping effect of large R_f . However, in Fig. 4.7 and Fig. 4.8 with the DWT, indeed, the WC magnitude reduced greatly with protection and using R_f of 500Ω . But even then, the WC magnitude remained well above the WC's of the healthy cable currents and threshold level, therefore, clearly discriminating a faulty segment/line from the healthy ones and detecting the high impedance fault. Without protection the WC remained constant up to 5Ω but beyond that it kept on reducing. However, it remained well above the coefficients of the healthy line currents.

Fig. 4.11, shows the detection of a near solid P2P fault at 10 km to the source node B_1 (red-solid curve). Variation of the WCs of I_{12} (red-curve) and I_{21} (green-curve) with the location of P2P fault (D_f) in the cable L_{12} is shown. As the distance of node B2 increases from the fault point, the WC magnitude of I_{21} decreases due to the damped transient (green-curve).

Table 4.1 lists the detailed WC magnitudes, indicating the closeness of a P2P fault in the cable L_{12} to the fault related nodes B_1 and B_2 . Despite diminished sensitivity, the fault can be successfully detected for all distances evaluated.

In Fig. 4.12 (a), it is seen that the WC (in purple and red) is for most of the time having the largest magnitude and therefore, is less sensitive to noise. Thus, consistently high WC's of the faulty line currents and low WC's of the healthy line currents distinguish between the internal and external faults. In Fig. 4.12 (b), it is noticed that the steady state DC currents essentially do not yield zero wavelet coefficients. The value falls between a certain level above which the threshold level is selected. Additionally, denoising property of the DWT used to remove the noise in the signal also reduces the steady state WC.

TABLE 4.1: Detailed Wavelet-Coefficient magnitudes using *Haar-3* as the mother-wavelet (MW)

D_f to B_1	10 km	100 km	180 km	199 km
B1(faulty)	135.3	39.56	46.07	40.55
B2(faulty)	21.38	38.07	55.62	512.3
B3(healthy)	1.21	2.39	4.972	8.809
B4(healthy)	0.8176	1.599	6.07	8.78

4.1.1.3 Important Findings about the DWT

The application of the DWT to detect the fault and independently (locally) discriminate a faulted line among multiple lines at a fault related DC node in a 4-terminal meshed MTDC system has been analyzed and validated with the simulation results. “*Haar1-6*” and “*Db1-6*” were adopted as the MWs because they showed the closest match to the fault current pattern and were able to detect the fault with a minimum delay of around 1 ms. Influence of the fault distance D_f , fault location in the grid, and the fault resistance R_f on the magnitudes of the WCs was evaluated.

Although the WC magnitude decreases as the fault distance and resistance are increased, however it still remains well above the threshold level and WCs of

the healthy line currents by a large margin. DWT is insensitive to the other disturbances like transients caused by the load change, and AC side faults.

Hence, DWT allows to achieve the robustness as it distinguishes the DC fault from various other types of disturbances. With the DWT even with the delay introduced by filtering, the detection time can still be reasonably short.

However, on the downside need of high sampling rate, large memory and processing time, and difficulty or even impossibility to detect the fault when a damped transient is concerned, are some drawbacks associated with the WT. Therefore, in the research work presented in this thesis, these shortcomings of the WT can be overcome (mitigated) by combining it with the differential current measurements based on optical sensor networks, TW-based type-D fault location method, current derivative sign principles, and the SFCL quench detection. Since the noise yields a non-zero WC, therefore, precise and large threshold settings much above the noise levels and selection of a correct MW that has the best match with the fault current pattern are the key requisites in the WT to avoid wrong wave-front detection. Denoising property of the DWT which provides better tolerance against noise reduces the steady-state WC respectively. In future implementation of the DWT with other efficient algorithms may be helpful to detect even the hidden anomalies in a meshed network.

4.2 Proposed Effective Fault Current Limiting

As already mentioned, that even after installing the FCLs on AC side of the converters, the threatening overshoot current at the beginning of Stage 2 of the P2P fault puts the VSC diodes and cables at a high risk. Now the selection of a suitable converter configuration and topology for an MTDC network is based on the analysis of its technical and economic benefits. In the scheme the MTDC grid consists of half bridge modular multilevel converters (HBMMCs). These converters are more widely implemented in VSC-based MTDC networks than the full-bridge modular multilevel converters (FB-MMCs). The cost-effectiveness of the scheme is further achieved by coordinating the differential protection based on

distributed current measuring units and other fault detecting/locating methods with the HDCCB (constant breaking time of $2 \sim 3$ ms), small sized inductors, RSFCLs, HB-VSC-MMCs, ACCBs, and the other passive components. The DC fault current is significantly reduced to below 1.7 kA before its interruption, which compromises with the cost and size of the network components. Hence, low cost (low rating) protection devices like HSSs/RCBs and MCBs in series with the RSFCLs can be installed to interrupt the reduced DC fault current easily. Through this coordination, damage to the system, incorrect tripping of the healthy lines, measurement errors, and induced noise/ fluctuations caused by the external faults are avoided. Proper size of the inductor was chosen using multiple run simulation-based analysis.

4.2.1 Effective DC Fault Current Suppression Results

In the literature so far, DC fault current is limited to around $3 \sim 4$ kA, however, at the expense of large sized and extra inductors. To practically verify this, DC fault current was reduced to 3.387 kA by inserting 200 mH inductors, 4/each DC cable and 2/each converter in a meshed 4-terminal grid as shown in Fig. 4.14.

However, in the proposed scheme, bi-directional HDCCB is coordinated with active inductors (properly sized inductors 10-50 mH 2/DC outputs of only source converters), passive R-SFCLs, half-bridge VSC-based MMCs to significantly reduce the huge DC fault current much below the interruptible levels (1.7 kA and less) as shown in Fig. 4.15, Fig. 4.16, and Fig. 4.26 respectively.

A proactive hybrid DCCB (HDCCB) combines the advantages of both the mechanical MCBs and semiconductor SSCBs such as fast current interruption and negligible or low power losses. A HDCCB is composed of a load commutation switch (LCS) built using several IGBTs, an ultrafast dis-connector (UFD) and a main breaker (MB) which consists of several hundreds of IGBTs and surge arresters. The performance of a HDCCB depends not only on the network parameters, but also on the fault detecting and locating schemes. Since an MTDC grid mainly relies on selectivity for the DC fault analysis and hence, requires a highly selective algorithm. Current differential protection based on optical sensor networks with bidirectional communication during the fault events coordinates well

with type-D TW-based method and proactive nature of the bidirectional HDCCB (with constant breaking time of 2 ms achievable). Resistive-SFCL does not affect to the system dynamics and significantly reduces the fault current on DC side.

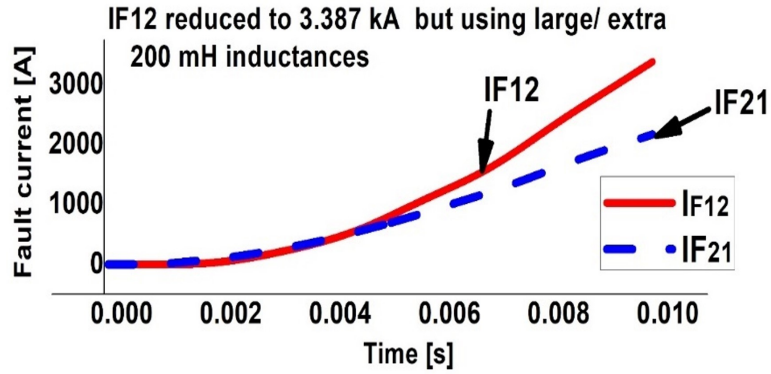


FIGURE 4.14: DC fault current limited to 3.387 kA with extra inductors of 200 mH 4/each cable and 2/each converter in a meshed MTDC grid.

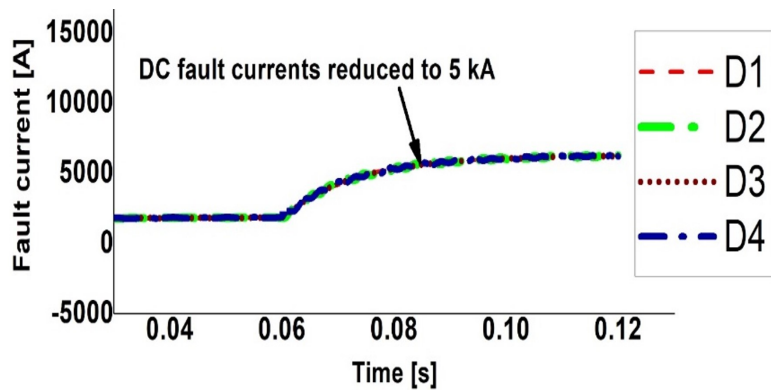


FIGURE 4.15: Fault current reduced to 5 kA with 30 mH inductors at the DC outputs of only AC/DC converters with protection in the scheme.

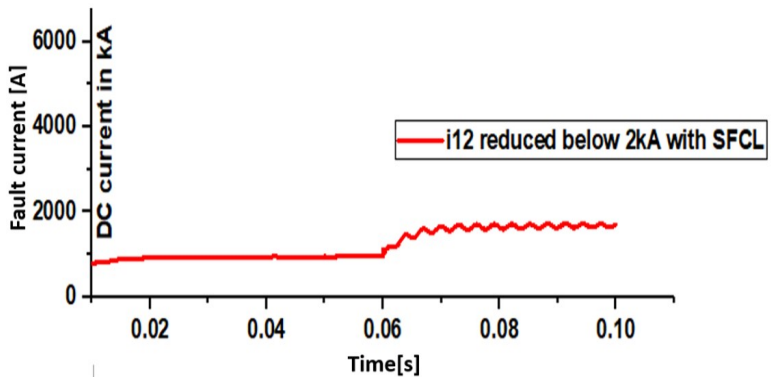


FIGURE 4.16: Fault current reduced to 1.7 kA with 50 mH inductors at the DC outputs of only AC/DC converters with protection in the scheme.

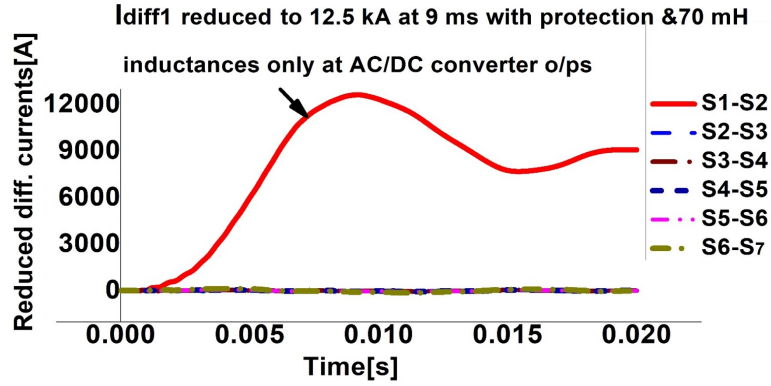


FIGURE 4.17: Huge differential current derived from the faulted pair S_1 and S_2 is reduced to 12.6 kA with protection in the scheme.

The optimum length of an R-SFCL mainly depends on the rated voltage, opening time of the associated DCCB, current limitation to be achieved, and the maximum admissible temperature of 300K. Thus, the cost of an R-SFCL is determined by its critical current and length. Now if the rated line current is 2 kA, then the R-SFCL quenching current is $I_q = 1.5 \sim 3 \times \text{line rated} = 3 \text{ kA}$. Current to be limited is:

$$I_{cable} < I_{lim} < I_q \quad (4.7)$$

For $I_q = 3 \times 2 \text{ kA} = 6 \text{ kA}$, Fig. 4.15 and Fig. 4.26 satisfy equation 4.7 criterion, i.e. $2 \text{ kA} < 4.8 \text{ kA} < 6 \text{ kA}$. R-SFCL is modeled as a generic-type DC SFCL considering the four parameters, such as response time of 2 ms, a minimum impedance of 0.01 Ω during the normal operation which jumps to a maximum value of 20 to 25 Ω at the fault instants, and triggering current of 3 kA respectively.

The intensity of the DC fault current was determined based on the strength of the connected AC power system. Therefore, the range of the AC source voltage and frequency tested was 230 kV to 800 kV and 50 Hz to 60Hz. Considering the merits of both passive R-SFCLs and active reactors, HDCCBs were combined with both these FCLs to gain more reaction time hence, eliminating the need for fast isolation. Cable lengths taken were from 200 km to 800 km and more.

Figures 4.15-4.17 show the effective limitation of the DC fault current according to the intensity of the connected AC sources. In Fig. 4.15 a solid P2P fault was

triggered at 60 ms in the line L_{12} . With the proposed active/passive limitation and multirun simulation process, the fault current is significantly limited to 5 kA from 15 kA by adding 30 mH inductors 2/ DC output of only sources along with the installed FCUs. In Fig 4.16 for the same solid P2P fault, the fault current is significantly limited to 1.7 kA from 15 kA by adding 50-70 mH inductances 2 per only source converter's DC output along with the installed FCUs on the DC cables.

Fig. 4.17 shows the effective limitation of the DC fault current in the target 4-terminal meshed VSC-MTDC grid. A solid P2P fault was incepted at 1 ms in the segment b/w sensors S_1 and S_2 of the cable L_{12} (180 km). The S_1 was at 10 km to the fault point and the S_2 was at 20 km to the fault. Other healthy cable lengths were L_{13} of 120 km, L_{32}/L_{14} of 300 km, L_{34} of 180 km and L_{24} of 90 km. Current measuring units on these cables were seven on L_{12} , five on L_{13} , eleven on L_{14}/L_{32} , seven on L_{34} , and four on L_{24} with 30 km separation b/w each adjacent pair.

The huge $I_{diff1}(t_0)$ differential current derived from the faulted pair S_1 and S_2 (red-solid curve) as in Fig. 4.22, was effectively reduced to 12.5 kA by adding 70 mH series inductors at the DC output of sources (rectifiers) as 2/converter or one inductor per each pole. The FCUs were inserted in the DC cable ends.

The I_{diff1} (red solid curve) due to the solid P2P fault at 1ms on segment b/w S_1 at 10 km & S_2 at 20 km on L_{12} (200 km) was further reduced to 11.8 kA by inserting 80 mH inductances 2/ source (AC/DC) converter DC outputs.

After installing the FCLs important findings are as follows:

1. The installation of FCLs slows down the transient response of the system resulting into reduced magnitudes of all the WCs. Off course the WC magnitude reduced greatly with protection and using the fault resistance R_f of 500 Ω . But even then, the WC magnitude remained well above the WC's of the healthy cable currents/threshold level, therefore, clearly discriminating a faulty segment/line from the healthy ones.

2. Before installing any type of FCL an appropriate size of the FCL can be designed through a set of parameters obtained by studying the results of contributions from weak, medium strong, and very strong AC connected sources to the DC fault current, rated AC and DC voltages, rated power, peak currents on the healthy and faulty cables, and the current ratio. Based on the peak currents on faulted and healthy cables and the current ratio, a positive and large enough threshold value much above the noise level should be selected for the fault detection before installing the FCLs. Then after obtaining the simulation results with the designed FCLs and their current limiting effects, the threshold value should be selectively found again. The threshold value should then be tallied with the value obtained without installing FCLs.
3. If the new threshold value does not match properly with the value obtained without installing the FCLs, the experiment should be repeated with another combination of FCL configurations and their locations. For example, during testing when the RSFCLs were inserted on the AC side of the converters their current limiting effect was not satisfactory. However, when they were installed on DC cables, DC fault current was effectively limited in all the three stages of P2P fault response. Thus, due to passive nature of an RSFCL with significant current limiting capability it can avoid the overcurrent of stage 2 also.
4. Nonlinear RSFCL is indeed, effective in limiting the fault current preferably installed on the DC side and can avoid the overcurrent of 2nd stage too. However, its drawbacks such as the recovery time in seconds ($>1s$) is highly unwanted in an MTDC grid due to the instantaneous faulty recovery. Further, while quenching SFCL needs larger impedance R_{SFCL} to significantly limit the DC fault current and causes higher voltage drop/ power consumption and greater energy dissipation across the SFCL with higher size and cost. SFCL cost depends on its quench current and optimum length. Optimum length mainly depends on the rated voltage, opening time of the associated HDCCB and maximum admissible temperature (around 300 K).

On the other hand, a saturated iron core inductive-type-SFCL has almost instantaneous recovery time within 1-2 ms desirable in an MTDC grid.

4.3 Determination of a Faulty Line

Flow chart to accurately determine a faulty line is shown in Fig. 4.18. Since an MTDC grid feeds the fault and causes the current to flow from all locations in the direction of the fault. Therefore, the basis used is the differential protection combined with the current derivative polarity (sign) principles. DC current flowing into or out of the cable from each side at every node (both the fault related and non-related) is measured during the fault occurrence to obtain the algebraic sum. A precise and large enough threshold is set to accurately determine the faulty line.

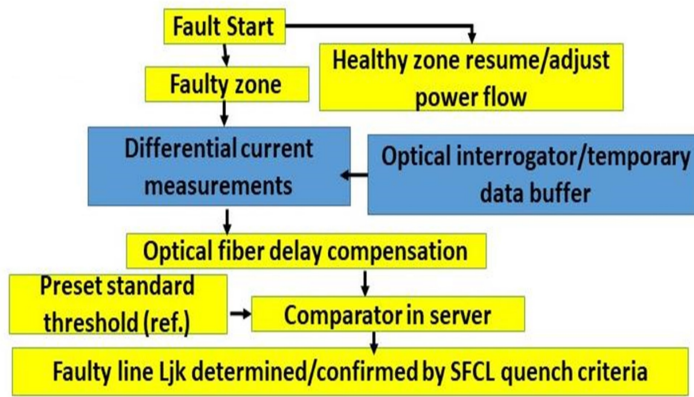


FIGURE 4.18: Faulty line or faulty segment discrimination flow chart.

In a VSC-based MTDC grid with j and k terminals, determination of an internal solid P2P fault in a charged power line extremely close to a source station's node depends on the following criteria.

1. Fault currents I_{Fjk} and I_{Fkj} or their derivatives at the fault detection instant t_0 are positive (ascending behavior) since an MTDC grid feeds the fault.
2. For a solid P2P fault very close to a station node or detecting sensor, DC voltage is at zero level and the highest fault current occurs with a clear TW effect in its development when zoomed in. The fault current or its derivative surpasses the threshold level very quickly and sharply rises to a huge value making the critical time limit much shorter.

Thus, a faulty line L_{jk} b/w the two source nodes B_j and B_k of Fig. 3.1 (Chap. 3) is accurately discriminated by measuring the current flowing out of or into every DC cable from each side at every node to obtain the algebraic sum as shown in Fig. 4.19. The current sum is the sum of the real-time local transient data, and a history data of the remote measurement. Thus, the current sum measured at B_j at the time of t_0 ms, is the sum of the current I_{jk} flowing out of B_j measured locally at the real-time of t_0 ms, and the current I_{kj} flowing out of B_k and into the cable L_{jk} measured at τ ms before t_0 ms or vice versa. Similar current sums on both sides of every cable at buses B_1 to B_4 were measured respectively. Since the input signals are the local current and the remote line current, therefore, due to the distributed optical sensor current measuring arrangement on the TLs there is no need of accurate GPS time stamping between the two signals. Importantly also, measurement of the differential current sums at every node not only discriminates a faulty line, but also its faulty segment. Therefore, this method of measurement is faster than the series method as in [54, 75]. Since the algorithm relies on the optical sensor communication link b/w the two-line ends, therefore, a continuous data transfer with bidirectional communication only during the fault events, can greatly relax the speed need for long distance power transmission. Measuring differential current sums at every node, along with Type-D TW-based method, requires a smaller number of equidistantly distributed optical sensors (usually one sensor installed around the transition joint). This further aids in achieving the cost effectiveness of the proposed scheme.

Thus, the differential current sum measured on the faulted cable L_{jk} with both MMC_j & MMC_k as sources is given in equation 4.8.

$$U_{jk}(t_0) = I_{jk}(t_0) + I_{kj}(t_0 - \tau) \quad (4.8)$$

$$U_{kj}(t_0) = I_{jk}(t_0 - \tau) + I_{kj}(t_0) \quad (4.9)$$

In terms of current derivative:

$$U_{jk}(t_0) = dI/dt_{jk}(t_0) + dI/dt_{kj}(t_0 - \tau_w) \quad (4.10)$$

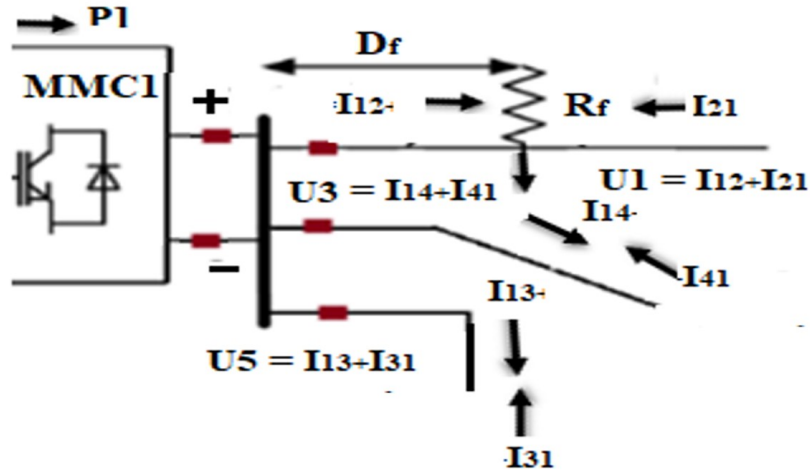


FIGURE 4.19: Discriminating a faulted line from the healthy ones at the fault related node B_1 taking both MMC_j & MMC_k as sources in an MTDC Grid.

To measure the currents I_{jk} & I_{kj} at the same time, sensor (j) will buffer the local current for τ ms until the sample from the other remote cable end sensor (k) is received. In terms of the current derivative, τ_w ms is the minimum window size selected. Let the absolute values of the current sums on (+) pole ends of the cables L_{12} , L_{13} and L_{14} measured at the fault related source node B_1 and denoted by U_{12} , U_{13} and U_{14} respectively are the elements of a row vector such that:

$$U = [U_{12(peak)}, U_{13(peak)}, U_{14(peak)}] \quad (4.11)$$

In order to discriminate a faulty line L_{12} from the healthy ones at B_1 , verify the highest peak such that:

$$[M, I] = \max(U) \quad (4.12)$$

Where ‘M’ is the highest peak of the differential current sum derived from the faulted line L_{12} , and I is the index value at that peak respectively.

4.3.1 Determination of a Faulted Line Between a Source and a Load Terminal in an MTDC Grid

Sum of the currents entering or leaving a node is zero during normal operation according to KCL. However, the fault in a charged power line, splits the line

current between the load and the fault currents. Differential protection is highly selective in discriminating and a faulty part is discriminated from the healthy ones simply by measuring the difference b/w the faulty and the healthy part current magnitudes. Since the DC line reactance (impedance) is negligibly small, therefore, the bus voltage collapses to zero for close up faults depending on the power supply and grounding impedance. Let us take MMC_j as the power source terminal and MMC_k , as the load terminal. The faulty line L_{jk} between them is accurately discriminated by measuring the difference of two currents at its each end as in equation 4.14. Consider the positive current flow in the cable L_{12} from the source MMC_1 terminal to the load MMC_2 terminal in Fig. 3.1 and Fig. 3.5 (Chap. 3). For an internal fault within the protection zone of the cable L_{12} , the events that occur are:

$$\delta I_a = \delta I_{F12} + \delta I_b \text{ or } \delta I_{F12} = \delta I_a - \delta I_b \quad (4.13)$$

$$I_{diff} = I_{Ljk(in)} - I_{Ljk(out)} \quad (4.14)$$

$$I_{diff} = I_{line/seg(in)} - I_{line/seg(out)} \quad (4.15)$$

4.3.2 Determination of a Faulty Segment

For a non-homogeneous TL consisting of m number of segments ($m = 1, 2, \dots, n-1$) with ‘ n ’ number of series current measuring units (optical sensors) distributed along it, a faulty segment of it is accurately discriminated from the healthy ones by measuring a series of differential currents between every adjacent sensor pair S_m and S_{m+1} . Constant communication delay τ ms through the fiber optic link is determined using the speed of TWs and the distance b/w the adjacent sensors S_m and S_{m+1} respectively such that:

$$I_{diffm}(t_0) = i_{sm}(t_0) - i_{sm+1}(t_0 - \tau) \quad (4.16)$$

Where $I_{diffm}(t_0)$ is the m -th differential current derived from the two adjacent sensors S_m and S_{m+1} . In case of external faults outside the protection zone of the line L_{12} or its faulty segment, the differential current is very close to zero, while

for an internal fault a highest value of differential current is derived.

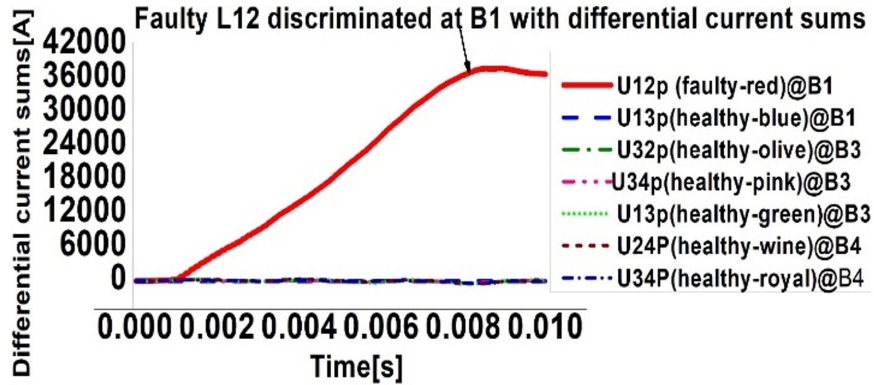


FIGURE 4.20: A Faulty line L_{12} (red-solid curve) 300km long discriminated for a solid P2P fault at 1ms b/w S_1 at 10 km and S_2 at 40 km at B_1 by measuring the differential current sums without protection.

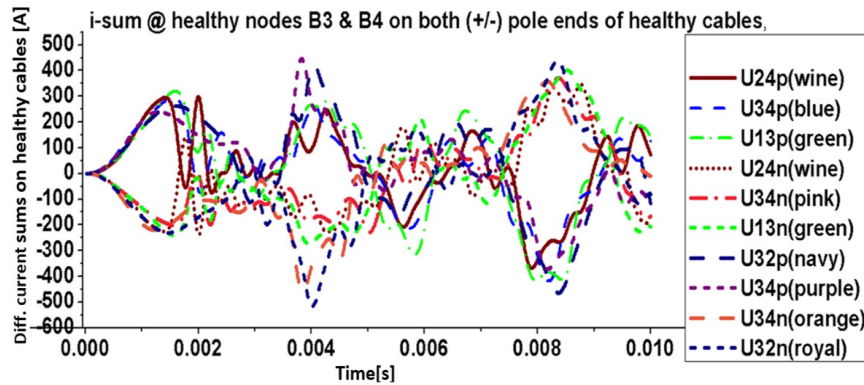


FIGURE 4.21: Differential current sums on the healthy cables for a solid P2P fault at 1ms b/w S_1 at 10km and S_2 at 40 km in the cable L_{12} .

In terms of the current derivative or the rate of change of current, τ_w ms is a short time (a minimum sample) window selected.

$$= di_{sm}(t_0)/dt - di_{sm+1}(t_0 - \tau_w)/dt \quad (4.17)$$

Threshold level /fault detection is based on the associated SFCL quenching criteria and maximum currents on both the faulty and the healthy cables during the fault event. Both thresholds ($+I_{dTH}$ & $-I_{dTH}$) are set large enough so that the unwanted noise, potential sensor or communication errors, and incorrect tripping of healthy lines are avoided.

4.3.3 Results of Accurate Faulty Line and Faulty Segment Determination

In Fig. 4.20, a faulty line L_{12} (red-solid curve) with 300 km length, was accurately discriminated among the healthy ones for a solid P2P fault incepted at 1 ms between S_1 (B_1) at 10 km and S_2 at 40 km to the fault in the cable L_{12} by measuring the differential current sums on each cable connected to nodes B_1 to B_4 in the meshed 4-terminal grid (Fig. 3.1). The other cable lengths were cable L_{13} of 120 km, L_{32} of 300 km, L_{34} of 180 km, and L_{24} of 90 km respectively. Current measuring units were distributed as seven on L_{12} with 50 km separation b/w each adjacent pair. Five on L_{13} , eleven on L_{32} , seven on L_{34} and four on L_{24} with 30km distance b/w each adjacent pair. Table 4.2 lists the values and for a solid P2P fault at 1 km to B_1 , highest peak (25 kA) of the current sum is seen Fig. 4.21, shows the differential current sums on the healthy cables. Fig. 4.21, shows the differential current sums on the healthy cables (both positive and negative pole ends) measured at healthy nodes B3 and B4 for the P2P fault scenario of Fig.4.20.

In Fig. 4.22, a faulty segment (red-solid curve) of the cable L_{12} (180 km long) was accurately discriminated for a solid P2P fault at 1ms b/w S_1 at 1 km and S_2 at 29 km to the fault by measuring a series of differential currents on the positive pole of the cable L_{12} . Seven sensors were distributed on the cable L_{12} with 30 km separation b/w each adjacent pair. Lengths of the other healthy cables were taken as L_{12} of 120 km, L_{32}/L_{14} of 300 km, L_{34} of 180 km and L_{24} of 90 km in the meshed 4-terminal grid. Current measuring units on these cables were distributed as seven on L_{12} , five on L_{13} , eleven on L_{14}/L_{32} , seven on L_{34} and four on L_{24} with 30km distance b/w each adjacent pair. As shown ' I_{diff1} ' derived from the faulted pair S_1 and S_2 quickly and sharply rises to much higher value and the adjacent sensor pair values are extremely low.

In order to detect the high impedance fault, R_f was increased from 0.01Ω to 500Ω for a P2P fault in the cable L_{12} (180km) with B_1 (S_1) at 1 km to 10 km to this fault. Variation of distributed (multipoint) series differential current profile with the increasing fault resistances showing corresponding haar-2 WC magnitudes and

damping effect for P2P fault in the cable L12(180 km long) in the four-terminal grid with B1 at 1 km -10 km to the fault location is shown in Fig. 4.8 and Fig. 4.23. Both the fault current and the WC magnitudes decrease with the increasing fault resistances and fault distances due their damping effect. With the differential current profile, it is seen that initially it is difficult or impossible to discriminate the faulty segment or line using larger fault resistances due to their damping effect without protection. The WC remained constant up to 4-5 Ω . Beyond this value it kept on reducing. However, its value remained well above the threshold level and WCs of healthy line currents. Therefore, DWT discriminated the faulted line even with large fault resistances and with protection.

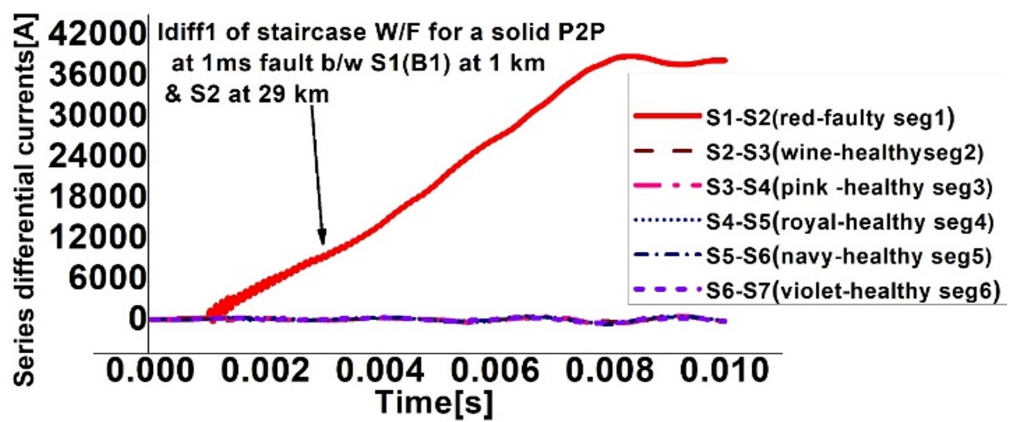


FIGURE 4.22: A Faulty segment (red-solid curve showing a clear TW effect in zoomed DC fault current like a staircase W/F) of L_{12} discriminated for a solid P2P fault at 1 km to S_1 (B_1) by measuring a series of differential currents on it without protection.

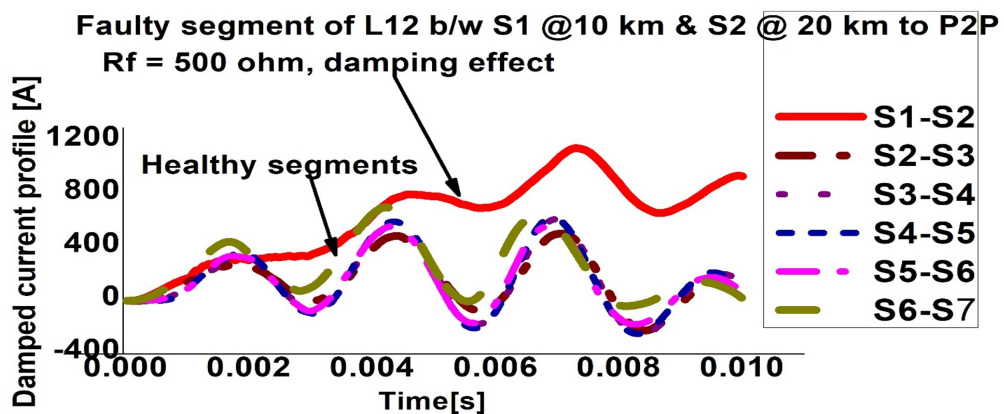


FIGURE 4.23: Damped profile of series differential currents for $R_f = 500 \Omega$ without protection.

TABLE 4.2: Maximum current sums at DC buses with different distances to a P2P fault

D_f from B_1	1km	10km	150km	198km
$i_{sumL12(+)} @B1(\text{faulty})$	25 kA	22 kA	13.1 kA	10.6 kA
	7.7 ms	8.24 ms	9.3 ms	10 ms
$i_{sumL32(+)} @B2(\text{healthy})$	684 A	674 A	487 A	1500 A
	2 ms	1.1 ms	2.71 ms	2.26ms
$i_{sumL13(+)} @B1(\text{healthy})$	1 kA	435 A	389 A	400 A
	1.3 ms	1.6 ms	1.71 ms	1.57 ms
$i_{sumL13(+)} @B3(\text{healthy})$	856 A	861 A	1 kA	1 kA
	6.5 ms	1.51 ms	4.4 ms	4.26 ms
$i_{sumL32(+)} @B3(\text{healthy})$	717 A	718 A	794 A	659 A
	1.8 ms	2.01 ms	2.3 ms	1.9 ms

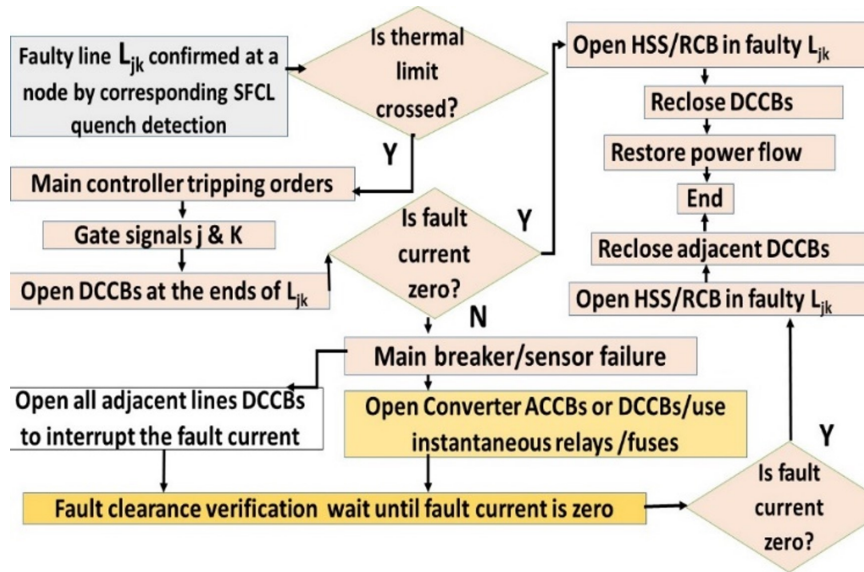


FIGURE 4.24: Fully selective methodology to isolate only the faulted line with backup plans in an MTDC grid.

4.4 DC Fault Current Interruption and Isolation of the Faulty Line

After the faulty line/segment determination and the fault detection, the main controller uses current information and sends appropriate switching commands to

initiate the gating signals and trip the corresponding HDCCBs to isolate only the faulty line from the system, while resuming normal operation of the healthy grid zones after a little power flow adjustment.

Thus, seamlessness of the scheme is achieved by reducing the impact of DC side faults on the AC grids or vice versa, such that any type of DC system is connected to any type of the AC grid.

Fig. 4.24 illustrates the flowchart for fully selective isolation of only the faulty line from the system. Since, only the R-SFCLs installed on the faulty line will quench and limit the fault current. Thus, a communication-based fault discrimination algorithm, confirms the faulty line among multiple lines at a fault related node, depending on the quench detection of the associated R-SFCL.

In equation 4.14, the controller monitors the difference of two currents in the faulty line L_{jk} . As soon as the difference exceeds a preset, and large threshold level and the faulted line L_{jk} is confirmed based on the quench detection of the associated R-SFCL, the controller sends tripping orders to the concerned HDCCBs at both ends of L_{jk} to interrupt the fault current and isolate only it, while resuming normal power flow in the healthy grid zones. Thus, a HDCCB opens to interrupt the fault current only when the associated R-SFCL quenches.

An R-SFCL helps to selectively isolate a faulty line, eliminates the chances of false tripping/trigging, reduces the electrical stress on the other FCU components, and helps to quickly perform a backup option if required. For a faulty line both the HDCCBs are opened, while for a healthy line only one HDCCB is tripped if necessary. Thus, the time constraint is made less strict in HVDC systems.

If in equation 4.11 among the differential current sums U_{12} , U_{13} and U_{14} , both U_{12} and U_{14} have a positive sign (ascending behavior), and the sign of sum U_{13} is negative (descending behavior) or zero. Then among the current sums U_{12} and U_{14} , the HDCCB that exhibits the highest magnitude of the sum is opened, while the other HDCCBs at B_1 remain closed. The HDCCB through which the current sum does not surpass either of (+/-) thresholds, remains closed.

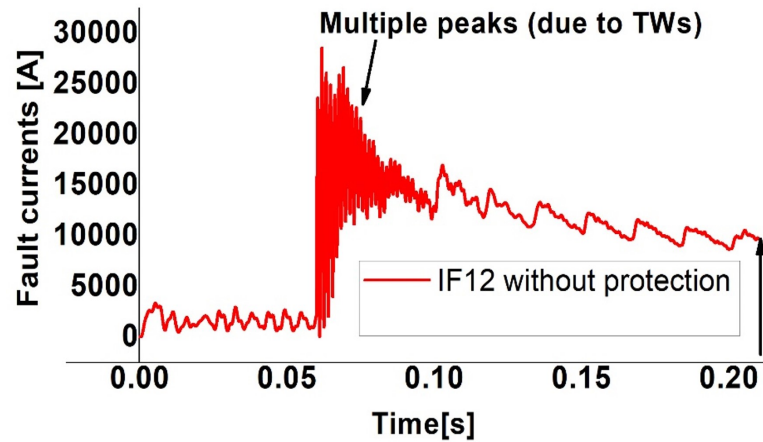


FIGURE 4.25: Huge DC fault current with multiple peaks without protection.

Fig. 4.25, shows a huge fault current with multiple peaks due to the TW effects for a solid P2P fault ($R_f = 0 \Omega$) incepted at 60 ms in the cable L12 and at a distance of 10 km to the source converter MMC_1 without protection. At the start of stage 2 of this solid P2P fault, the DC voltage drops to zero level when the capacitors are fully discharged. A sudden (abrupt) overcurrent puts the diodes at a high risk. Larger the overcurrent magnitude, shorter the critical time, and hence, the station and the cable connected to it are at highest risk. It is seen that the peak fault overcurrent is nearly 28 kA. The fault provoked travelling current surges or transients' travel along the cable in both directions away from the fault point. As the TW reaches to converter stations/sensors, it is reflected/refracted. Thus, the reflected wave at the converter station travels back to the fault point.

This phenomenon of reflections of the travelling current surges at the terminals and at the fault point continues causing multiple peaks in the fault current pattern till they attenuate to zero. Further, a clear stepwise increase in the fault current pattern is seen when zoomed in particularly, when the distance to fault D_f is 1 km to 11 km from the source station/detecting sensor. Now after significantly limiting this overcurrent with effective FCLs, fast isolation is not required.

Maximum of the HDCCB current depends on series reactor, DC capacitor, distance to the fault D_f , fault resistance R_f and power of the adjacent AC source.

Additionally, during testing it is seen that smaller the fault resistance or smaller the DC capacitance, larger is the overcurrent magnitude. On the other hand, larger

DC capacitors of $100\ \mu\text{F}$ - $200\ \mu\text{F}$ increase system inertia. However, they also improve voltage stability in the grid (suppress over-voltages while increase minimum terminal voltages). Capacitor size may only marginally affect HDCCB voltage. Therefore, four DC-node capacitors of $10\ \mu\text{F}$ - $50\ \mu\text{F}$ were added to accelerate SFCL quenching.

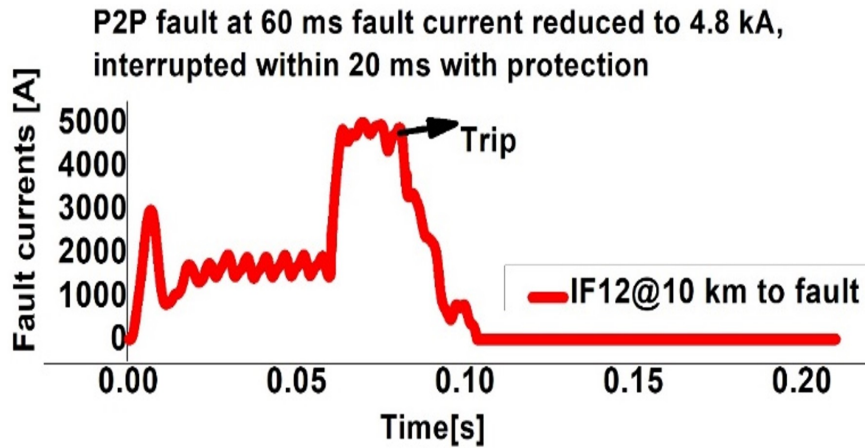


FIGURE 4.26: DC Fault current effectively limited to 4.8 kA, interrupted and isolated within a short time with protection.

In Fig. 4.26, the huge fault current of Fig. 4.25, is effectively reduced to 4.8 kA with protection and is interrupted within 20 ms. Now taking I_{quench} of $3 \times 2\text{kA} = 6\text{kA}$, it can be seen that the criteria of fault current limiting is satisfied as $2\text{kA} < 4.8\text{kA} < 6\text{kA}$.

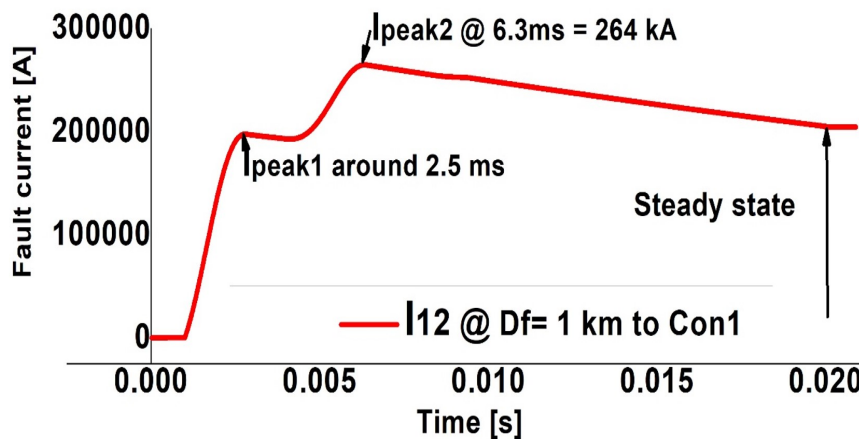


FIGURE 4.27: Huge P2P fault current with strong AC sources (800 kV).

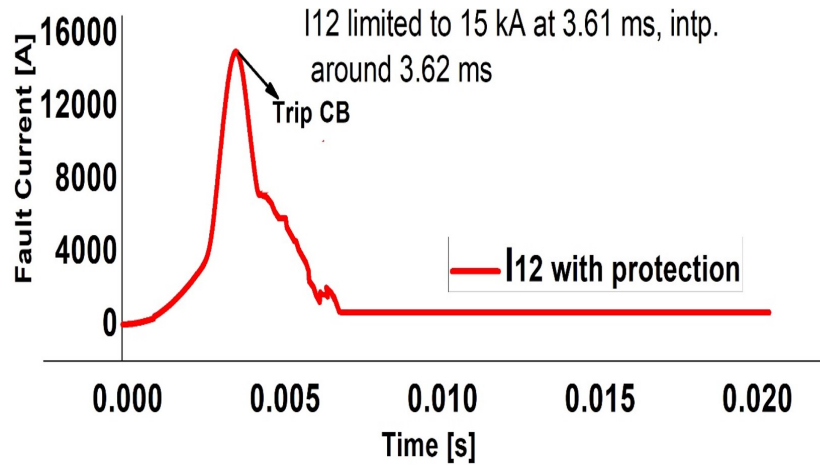


FIGURE 4.28: Fault is isolated at around 5.2 ms with protection.

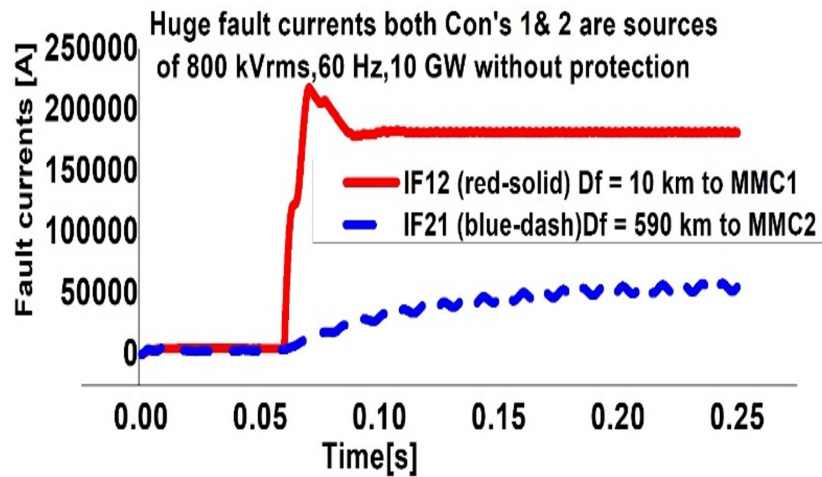


FIGURE 4.29: Influence of different distances to a solid P2P fault on DC fault current transients showing the damped transient (blue dash).

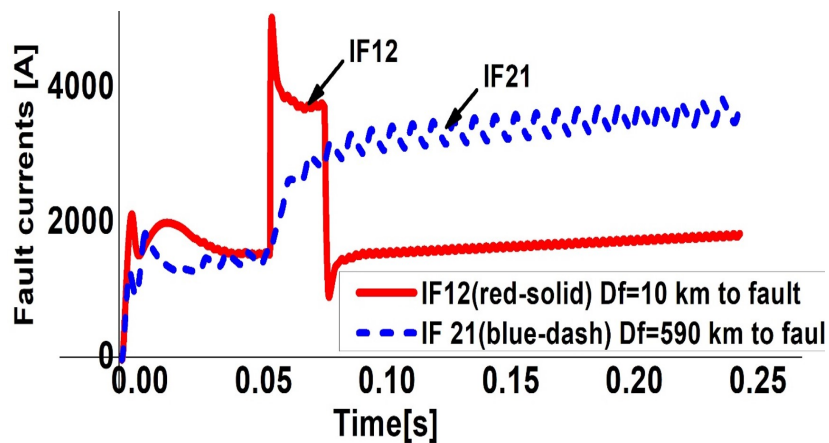


FIGURE 4.30: DC fault currents with protection.

4.4.1 DC Fault Current Interruption and Isolation Results

Fig. 4.27, shows the timely development of a huge fault current through the $HDCCB_1$ for a solid P2P fault in the cable L_{12} at 1 ms and at 1 km to the source node B_1 . Both the terminals 1 and 2 were very strong AC power sources of 800 kV with the nominal power/ frequency of 10 GVA/60 Hz in a 2-level bipolar 3-terminal grid. There are two peaks visible clearly, one at 2.5 ms and the other at 6.3 ms. During the first 2.5 ms, fault current pattern is determined by the DC capacitor discharges and the current surges (Stage 1). In Stage 3, the AC contribution keeps on increasing and recharges the DC capacitor (capacitors) until the peak arrives. After this discharging into the fault takes place, and the maximum $HDCCB_1$ current I_{peak2} is arrived at 6.3 ms. Gradually the DC capacitor contribution decreases until the steady-state at around 20 ms arrives. The DC capacitor is still charged and discharged in the steady-state, but without any contribution to the fault current.

In 4.28 with protection, at around 3.62 ms, $HDCCB_1$ and $HDCCB_2$ are tripped to interrupt the DC fault current and isolate the faulty cable L_{12} at around 5.2 ms. The time elapsed b/w the fault trigger at 1 ms and the CB tripping at 3.62 ms is 2.62 ms. In order to limit the fault current within the acceptable levels, it should be interrupted in less than 20 ms [91]. Theoretically a DC protection scheme with the total fault clearance time of up to 5.1 ms is regarded as a fast scheme. Hence, the proposed scheme with $t_{total} = 5.12 \sim 5.28$ ms can be deemed as a fast scheme respectively.

Let us represent the AC/DC source converter by a constant DC voltage V_{dc} and suppose the series R-SFCL in FCU is replaced by an inductive-type SFCL in future. After the DC fault, if I_o is the maximum HDCCB breaking current and t_f is the fault trigger time then:

$$V_{dc} = V_{L-SFCL} + V_{HDCCB} = L_{dc} di/dt \quad (4.18)$$

$$I_o = di/dt(t_f) = V_{dc}/L_{dc}(t_f) \quad (4.19)$$

Then total energy dissipated across the HDCCB is given as:

$$E_{total} = \frac{1}{2}L_{SFCL}(I_{max})^2 + E_{dc-source} \quad (4.20)$$

The P2P fault was evaluated in terms of its location within the grid, distance from the measuring unit or source station, and the fault resistance R_f . The influence of these factors on the fault induced current and voltage transients was studied in depth using Mat-Lab results.

Distance to the fault D_f on a TL from the detecting sensor/station is one of the key factors used to estimate the fault location in a TL in this research thesis. As the TL length increases, its resistance also increases therefore, attenuating the current magnitudes of the EM waves. Hence, the closer the fault is to a source station/detecting sensor/measuring unit, the higher the frequency change and DC fault current/derivative magnitude gets making the critical time much shorter. However, as the distance to fault increases the fault current/derivative magnitude is decreased (damping occurs in the fault current transients). This is already explained in chapter 3.

Fig. 4.29 shows the influence of varied fault distances of a solid P2P fault on the DC fault current transients without protection. The intensity of the fault current depends on the power production generated from the source converters. In a VSC- MTDC grid, the DC voltage is fixed and the power flow depends on the DC current direction. DC cable short circuit faults with different distances to the terminals and detecting sensors (measuring units) ranging from 1 km to 600 km with different fault trigger times were simulated in the cable L12 to determine the worst-case fault scenario. Different lengths of L12 from 200 km to 800 km were taken.

In Fig. 4.29, both the converters MMC1 and MMC2 were very strong AC power sources of 800 kV AC voltage and nominal power /frequency of 10GVA/60Hz in a 2-level bipolar 3-terminal meshed VSC- MTDC grid. The red-solid curve is the magnitude of the fault current for a solid P2P fault at 10 km to the source

converter MMC1 and the blue-dash curve is the fault current when this fault is at 590 km to MMC2. It is seen that as the distance of the fault increases from the station damping occurs in the fault current derivatives/transients. In Fig. 4.30, the huge fault currents are effectively limited with protection.

4.5 Fault Location in an MTDC Grid

Fault location requires data obtained during the fault detection to be processed offline, therefore, high speed is no longer of the top priority. However, in order to facilitate the repairing work of the permanent faults after isolating the faulty line from the system, exact fault location with the data obtained from the fault detection within the fault clearance period is very essential. Fig. 4.31, shows the flowchart to locate the fault in a TL. The current derivative data or WC data obtained during the fault detection is used with TW methods to determine the wave-front (surge) arrival time and locate the fault in a TL. Factors like TL length, sampling time, and largest time delay estimate the buffer size.

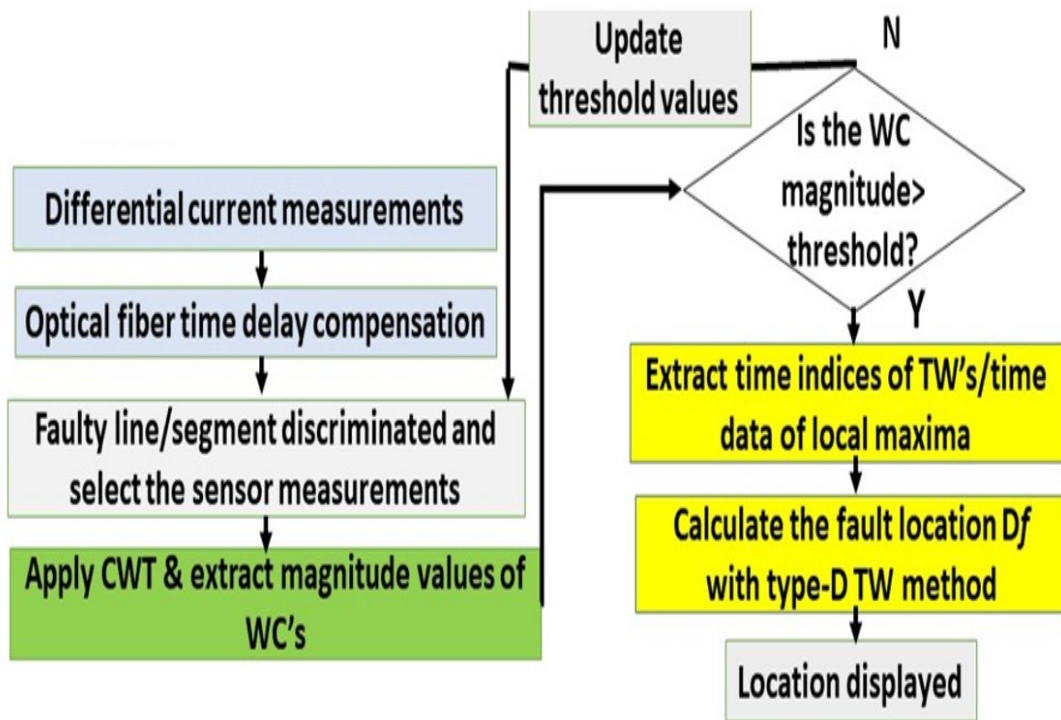


FIGURE 4.31: Flowchart for the fault location in a Transmission line.

The sensor data obtained during the fault detection is processed offline by using the CWT with either ‘Haar’ or ‘db’ MWs to locate the fault in a TL. Distance of a monitoring station/ sensor to the fault location ‘ D_f ’ in a TL, is one of the key factors affecting to the rate of rise of the DC fault current derivative and DC voltage transients and hence, is an important parameter to locate the fault in a TL as already discussed in Chapter 3.

DC fault provoked current TWs travel along the cable with reflections and refractions, causing step-wise increase in the development of the fault current like a staircase w/f. Information like time for the wave to travel from the fault point to a converter station/detecting sensor and the damping variable αn ($n=1,2,\dots$) accounting for the attenuation are useful in locating the fault in a TL. In this research thesis both Type A and Type D methods are utilized to fulfill the task of fault location with a certain degree of accuracy.

To locate the fault in the cable L_{12} (180 km long) using the current derivative data, first seven sensors were distributed on it with 30 km separation between each adjacent pair. A solid P2P fault was triggered at 0.5 ms in the cable L_{12} (180 km) b/w S_1 at 10 km and S_2 at 20 km to the fault for a simulation time of 1.5 ms. A short time window of information selected was 0.767 ms ($t_1 = 0.669$ ms and $t_2 = 0.767$ ms) with an estimated distance of 9.702 km. For a P2P fault at 0.2 ms b/w S_1 and S_2 with simulation time of 5 ms and a minimum window of 0.6 ms ($t_1 = 0.3$ ms and $t_2 = 0.6$ ms), the estimated distance was 29.7 km.

Then the cable L12 of 200 km length was tested for a solid P2P fault at 10 km to B_1 . A minimum window of information selected was 0.1866 ms ($t_1 = 0.0867$ ms and $t_2 = 0.1866$ ms) with an estimated distance of 9.8901 km using Type-A TW-based fault location method. Then Type-D TW-based method was tested and table 4.3 lists some of the results.

According to Type-A method:

$$D_f = (t_2 - t_1) \cdot v / 2 = t_{mea} = (t_2 - t_1) = 2D_f / v \quad (4.21)$$

Where

$$v = c/\sqrt{\varepsilon_r} = c/n = 1/\sqrt{LC} = 3 \times 10^5 (km/s) / \sqrt{2.3} = 198 km/ms$$

Where t_1 and t_2 are the arrival times of first two TWs to reach to a terminal (monitoring station/sensor) and 'n' is the refractive index of optical fiber = 1.4682. If $D_f = 50$ km to B_1 on the cable L_{12} which is 300 km long, then the total distance covered is 100 km such that $t_{mea} = 0.5$ ms. Total delay as in [54] is:

$$t_{total} = t_{CB} + t_{mea} + t_{process} \quad (4.22)$$

If $t_{process} = 1$ ms, $t_{mea} = 0.5$ ms and $t_{CB} = 2$ ms, then $t_{total} = 3.5$ ms. As shown in Fig. 4.27, $t_{CB} = 3.62$ ms, $t_{total} = 5.12$ ms, therefore, again the proposed scheme can be deemed as a fast scheme. According to the Type-D TW-based fault location method.

$$D_f = L_{seq} - \tau(t_{s1} - t_{s2})xv/2 = L - (T_j - T_k)xv/2 \quad (4.23)$$

TABLE 4.3: Type-A and Type-D fault location methods for a solid P2P fault

Distance D_f (type A)	10 km	30 km	100 km
Estimated distances(km)	9.8901	29.7	98.97
Absolute Error (km)	0.1099	0.3	1.03
Distance D_f (type D)	10 km	30 km	100 km
Estimated distances(km)	9.976	30.88	100
Absolute Error (km)	0.024	-0.88	0

4.6 Auxiliary Protection Methods (Simple Backup Plans)

Reliability of the proposed protection scheme is improved as the primary communication - based fault discrimination/ location algorithms and the independent DWT are aided with other efficient sub-protection methods and mature backup

plans. Expensive backup plans are avoided and simple, mature backup plans like overcurrent relays, neighboring HDCCBs/sensors/FCLs, and ACCBs are used. Even if all the protection methods fail from the DC side, the ACCBs trip and disconnect the fault.

Also, by limiting the DC fault current significantly, the performance of ACCBs is improved and there is no need of fast isolation. Additionally, using ACCBs with non-fault blocking half bridge converters as the backup options, there is no need of FCUs at converter terminals. As already observed in the simulation results that long distances cause damping in the fault provoked current transients (amplitude distortion/attenuation of EM waves). Therefore, failure of communication dependent differential protection is potential. Selectivity and fault discriminative property of differential protection is also reduced with high impedance faults and after installing the protection devices. Additionally, although the DWT detects the wave front in a relatively short time and distinguishes a faulty line from the healthy ones even with high impedance faults and after installing protection devices. However, due to the high sampling rate, large data processing /storage, and damped transients, even some times the WT can fail to detect a remote station close-up fault.

As seen in the simulation results the worst-case P2P fault scenario is 1 km to 3 km from a source station (remote source station). Thus, in such cases if both the WT and the current differential protection fail, instantaneous overcurrent relays (fuses) can be operated as a simple backup to clear these extremely close up faults. Importantly also, for cable protection in practice, the relay threshold can always be coordinated to the maximum cable current capacity.

In a VSC-based MTDC grid the diodes and cables are highly vulnerable components during the DC cable short circuit fault. Therefore, even if the HDCCBs fail at the line ends, overcurrent relays at the nodes (buses) can be operated to disconnect the station, thus avoiding damage to the converters and cables as early as possible. Further, passive (selective) RSFCL quench criteria, partially discriminative property of the current derivative polarity method with short time window

are the other sub-protection schemes used with differential protection and DWT to improve their overall performance.

Thus, the sub-protection methods and backup plans include:

- Instantaneous overcurrent relays for extremely close-up faults to the station nodes.
- Converter's AC side ACCBs.
- Neighboring sensors, HDCCBs and RSFCLs.
- Current derivative polarity method

4.6.1 Simple backup Plans with DCCBs Failure and Bus-bar Faults

The research work in this thesis avoids expensive back-up plans. In case of failure of the primary protection, the scheme ensures safety of the grid by simple and mature backup options. These include converter's ACCB, HDCCB in the FCU at the converter terminal, using all the neighboring FCUs and sensors and overcurrent relays. In case when the HDCCBs of a faulty line fail, the adjacent HDCCBs are tripped to interrupt the fault current using the relay at the faulty line. As soon as the fault current is interrupted, fast DC disconnectors/HSS's of the faulty line are tripped by the relay to isolate it. After opening the faulty line HSS, the relay on the faulty line recloses adjacent HDCCBs and the power flow is immediately restored after reconnecting the healthy components. If the RSFCL fails to quench on the faulty line, the adjacent RSFCLs in the neighboring line automatically quench to provide a backup and their associated HDCCBs open to interrupt the fault current. Some of the drawbacks of an RSFCL such as dissipation of a large amount of energy after quenching requires its cooling down which takes seconds and minutes. Hence it remains disconnected for some time before it is reconnected. In future an appropriately sized inductive saturated-iron core type SFCL or SFCL

using Yttrium barium copper oxide coated conductor can prove a good candidate for an MTDC grid respectively.

If all the protection methods fail from the DC side or if the RSFCLs and HDCCBs fail in a DC line, the ACCBs from the AC sides are used to clear the fault. Opening the converter's ACCB is a reliable option to eliminate the fault current contribution of the converter connected to the DC node having a failed SFCL/breaker. In this case additional components are not needed and after limiting the fault current significantly, fast isolation is not required. Importantly also, if the ACCBs with the non-fault blocking HB-VSC-MMCs are used as backup options to interrupt the fault current, then there is no need of FCUs at the converter terminals. Additionally, using the fault blocking (interrupting) FBMMCs, there is also no need of FCUs at the converter terminals.

4.6.2 Instantaneous Overcurrent Protection

In this research work, fast and independent DWT very practical for real time fault detection with applications of denoising, is used as the main detecting method [80–83]. However, sometimes even the WT fails to detect a remote station close-up fault because of the damped transients, complicated calculations, need of high sampling rate, and a large data storage or processing. Therefore, in situations when either the differential protection or the WT fail to detect an extremely close-up fault to a remote station, instantaneous overcurrent protection can be used as a final backup plan. During testing it is observed that the closer the P2P fault is to a station's node/measuring unit, the higher is the rate of change of the DC fault current (shorter the critical time). When the fault current is zoomed in, the TW effect in it for the fault distances of 1 km to 13 km to a source station's node/measuring unit is clearly observed. Since, practically only the converters or nodes connected to a faulted line or pole and those very close to the fault are affected. Therefore, instantaneous overcurrent relays are operated to clear these close-up faults quickly [58, 65]. In a VSC -based MTDC grid the diodes and cables are at a high risk during the DC cable P2P faults. Since oversizing the diodes makes

the cables more vulnerable. In such situations if the DCCBs fail, the overcurrent relay at a node (bus) can be operated to disconnect the VSC station. In this way, the damage to the converters and cables is avoided. Additionally, in a VSC-based HVDC system, the DC cables used are strong enough and oversizing the diodes to withstand the high cable currents with proper coordination of the overcurrent protection may not pose problems. Therefore, installation of the mechanical DC-CBs in series with the RSFCLs on the DC cables can also prove a feasible solution to clear the faults.

4.6.3 Current Derivative Direction Principles

In the previously proposed optical sensing schemes using the differential protection as a main fault discriminating algorithm, lack of reliability and synchronization of the telecommunication link for long distances (greater than 200 km) poses a major problem. Therefore, in order to reduce the communication errors in such cases a short time window can be set. By setting precise and large thresholds and selecting a time window of minimum number of samples, the current derivative polarity method can perform much better to locate the fault in an MTDC grid and even reduce the communication errors.

The current derivative direction method shows the fault directions (partial discrimination) and hence, assists the primary protection to selectively determine a faulty line. The basic concept to differentiate between the internal and external faults and identify the ‘selected DCCBs’ (to be opened) and ‘non-selected DCCBs’ (which remain closed), is based on the magnitude and sign of the DC fault current derivative after the fault start time respectively.

4.7 Summary

In this chapter, after theoretical analysis, an extensive set of fault scenarios are conducted in MATLAB simulations. The proposed scheme achieves all the general requirements of a feasible MTDC/HVDC protection scheme which are reliability, speed, robustness, seamlessness, selectivity, and sensitivity. All the important

aspects of the DC fault clearance time are presented comprehensively with an appropriate data, analysis and in-depth numerical simulations.

The scheme is deemed fast as the fault current is interrupted and the faulty line is isolated within a short time. The scheme is Selective as only the faulty part is isolated without shutting down the entire system. The scheme is reliable as it is aided with the efficient and mature backup plans. The scheme is sensitive and robust as it is capable of detecting any fault and is able to discriminate the DC side faults from other disturbances using the digitalized DWT. The scheme is seamless as it keeps the healthy parts in secure operations after the fault. Based on the preliminary conclusions, flaws of previously proposed schemes, and the results obtained in this research work, a comprehensive protection scheme is proposed for a meshed VSC-MTDC grid as below:

4.7.1 Faulty line Determination/Discrimination:

In the previously proposed optical sensor schemes, telecommunication based differential protection utilizing the measurements derived from multi-point series distributed optical sensors (optical fiber links) is successful only in determining a faulty segment with low impedance faults. The fault location is determined using the data obtained during the fault detection. MTDC grid requires quick real time fault detection which is not possible with the CWT. Using current derivative data with short time window for detecting the arrival times of the fault provoked TWs is a better method for fault location but in ideal situations.

Thus, taking both the source and load terminals and the fact that an MTDC grid feeds the fault from all directions, the basis used in the proposed scheme is the differential protection based on optical sensor networks combined with the current derivative sign principles. Differential current measurements are performed in three ways: 1) multipoint differential current series measurements as in previous optical schemes. 2) differential current sum measurements at every node (both the fault related and non-related). 3) current difference measurements between the two

ends of the DC link or difference b/w the magnitude of the faulty part current and the healthy part during a fault taking both the source and load terminals.

Importantly also, measurement of the differential current sums at every node, not only discriminated a faulty line, but also its faulty segment. Therefore, this method of measurement is faster than the series method of optical schemes. Since the algorithm relies on the optical sensor communication link b/w the two-line ends, therefore, continuous data transfer with bidirectional communication only during the fault events, can greatly relax the speed need for long distance power transmission along with backup plans.

Additionally, measuring differential current sums at every node, along with Type-D TW-based method, requires a smaller number of equidistantly distributed optical sensors (usually one sensor installed around the transition joint).

Importantly also during MATLAB tests, it is found that the current differential protection algorithm is unable to determine the faulty segment/line with large impedance (greater than 400 ohm) P2P faults due to damped transients. This is proved by comparing the damped profile of series differential currents in Fig. 4.23 and Figures 4.7 to 4.8. In Fig. 4.23 with series differential current measurements, it is impossible to discriminate a faulty segment (red-solid curve) from the healthy ones initially, due to the damping effect of large fault resistance, even without protection. Thus, the previous literature about discriminating high resistance faults using series differential current measurements in optical schemes is not satisfactory. Further, with protection devices (after installing FCUs and inductors) the situation becomes difficult again, because the current magnitude is limited and the current sum magnitudes become smaller. Thus, discriminating a faulty line from the healthy ones becomes difficult or needs updated threshold levels.

However, in Fig. 4.7 with the DWT in the proposed scheme, indeed the WC magnitude reduced greatly with protection and using R_f of 500 Ω . But even then, the WC magnitude of the faulty line current remained well above the WCs of the healthy cable currents and the threshold level, hence, clearly discriminating a faulty segment/line.

Thus, it is concluded that the selectivity and reliability of the differential protection is reduced in high impedance faults, and long-distance power transmission. Hence, in our proposed scheme the differential protection based on optical sensor links is aided with other efficient and independent auxiliary methods as follows:

- Since, only the R-SFCLs located on the faulty line will quench and limit the fault current. Thus, the communication-based differential protection/ fault discrimination algorithm, confirms the faulty line among multiple lines at a fault related node, depending on the quench detection of the associated R-SFCL. The controller monitors the difference of two currents in the faulty line. As soon as the difference exceeds a precise and large threshold level and the faulted line is confirmed based on the quench criteria of the associated R-SFCL, the controller sends tripping orders to the concerned HDCCBs at both the ends of the faulty line to interrupt the fault current, and isolate only it, while resuming normal power flow in the healthy grid zones. Therefore, a HDCCB opens to interrupt the fault current only when the associated R-SFCL quenches. In this way in our proposed scheme the selectivity of the differential protection in discriminating a faulty line is improved. Therefore, a HDCCB opens to interrupt the fault current only when the associated R-SFCL quenches. In this way in our proposed scheme the selectivity of the differential protection in discriminating a faulty line is improved
- It is aided with independent DWT for the fault detection, discrimination of high impedance faults, and denoising. Additionally, drawbacks of FCL installation like slowing down the system dynamics or transient response and resetting thresholds are mitigated with the efficient detecting schemes like DWT
- Current derivative data with short time window (minimum sample window) method despite being sensitive to noise and other disturbances indicates the fault directions as shown in simulations. Thus, this method being partially discriminative can improve the selectivity of the scheme.
- Instantaneous overcurrent protection is used as a backup plan for extremely close-up faults to the stations

4.7.2 Real time Detection of the Fault with DWT (Sensitive and Robust Scheme)

Among the important aspects of the DC fault clearance time, utmost requisite is the quick fault detection (detection of the surge arrival time or wavefront). CWT as in previous optical schemes is not suitable for quick real time fault detection in a non-stationary random signal with multiple peaks, as it consumes both time and memory space. CWT is more accurate in off-line fault location for which high speed is not required, except in the case of permanent short circuit faults. Since the fault provoked TW (surge) arrival time or wave-front detection requires Time-frequency analysis (which frequency at what time) in real time. Therefore, in the proposed scheme a unified flow chart is presented using independent digitalized DWT as the main fault detecting method to practically detect the wave-front arrival time in real time non-stationary signals with multiple peaks.

The DWT detects the fault by comparing the corresponding WC to a pre-set threshold, based on the local DC current measurements and is communication independent. DWT is locally applied to every node in the meshed MTDC grid. Thus, each terminal independently identifies its faulty line with the simple local DC current measurements in a relatively short time.

During fault detection, influence of the key parameters such as fault distance D_f , fault location in the grid, and fault resistance all are simulated with appropriate data and analysis. No doubt installation of the FCLs and HDCCBs slows down the transient response causing lower magnitudes of the WCs. However, with the DWT, faulty and healthy lines are easily distinguished (guaranteed selectivity). The mother wavelets used in the scheme are Haar wavelet and the Daubenchies wavelet.

However, with the DWT, faulty and healthy lines are easily distinguished (guaranteed selectivity). The mother wavelets used in the scheme are Haar wavelet and the Daubenchies wavelet. Thus, the scheme is robust, as it is able to discriminate the DC side faults from the AC side faults, noises, load changes, and the other external disturbances. Fast fault detection, accurate faulty line determination,

significant DC fault current limiting, and quick faulty line isolation guarantee its robustness.

In a VSC-HVDC system, the voltage signals cannot distinguish the faulty line from the healthy line when the fault occurs close to a station/ node. The DC voltage drops abruptly to zero /close to zero for very close P2P faults at distances of 1 km-13 km to station nodes/detecting sensors and the TW surge is not clearly visible at such distances. For close up faults the TW effect is shown as a stepwise increase in the DC current, while the DC voltage transients do not exhibit such effects. Thus, only the DC current is taken as the target signal for the fault detection and location in the MTDC system in this research thesis. Further, as D_f increased beyond 15 km to 20 km V_{dc} also increases above zero level, thus indicating closeness b/w the fault point (location) and detecting sensor/station. Therefore, DC link voltage transients may give an estimation of the fault location in a TL but are not perfect signals for fault detection.

Although the DWT detects fault in a relatively short time, however, as observed in some results sometimes even the WT can be unsuccessful to detect a remote station closeup fault because of the damped transients, time delay caused by filters, complicated calculations, and need of high sampling rate. Therefore, other sub-protection methods as below are used to enhance the performance of the DWT.

- RSFCL quench detection, large enough thresholds based on the diode and cable sizes, HDCCB properties and the other issues
- Instantaneous overcurrent relays for extremely closeup faults to the station nodes (worst case fault scenarios of 1 km to 3 km to a remote station)
- Current derivative polarity method to indicate the direction of the fault

4.7.3 Effective limiting of the DC fault current and Fault Coordination

In section 4.2.1 to practically verify the current limiting effects of the soothing inductors as proposed in the previous literature including optical schemes, DC fault current was limited to around 3.387 kA, however at the expense of large

sized and extra inductors (by inserting 200 mH inductors, 4/ each DC cable and 2/each converter in a meshed 4-terminal grid). Drawbacks of large sized and extra FCLs/inductors are already discussed.

A key design requirement of a feasible and secure MTDC protection scheme is the total fault clearance time of a few milliseconds including (fault detection, interruption, isolation and even location). Thus, speed of operation is taken as the main focus in this research work. Absence of frequency, lack of high rating DCCBs, negligible impedance /reactance, and the absence of naturally zero current points (inability of the DC current to change its polarity). Additionally, various time delays associated with the fault provoked TWs like fault propagation delay from the fault point to the detecting sensor/monitoring station, fault detection or threshold detection delay, fault current interruption and isolation delays from the concerned CBs action to the total isolation of the faulty part. All these major constraints in the HVDC systems demand a dedicated mechanism to interrupt the fault current and isolate the faulty line.

Since with the existing technologies and unavailability of a satisfactory DCCB for the HVDC systems, it is impossible to complete the fault clearance time with a few milliseconds. Thus, alternate solution is to extend the operating time using appropriate fault current limiters to gain extra /additional time especially for the fault detection and isolation. Since the proposed HDCCB is a prototype, has a limited fault current interrupting capability, and is expensive. Thus, in our research work a HDCCB is used with effective and appropriate FCLs to extend the operating time when protecting long transmission lines, as it cannot withstand very high fault currents.

Since the proposed HDCCB is a prototype, has a limited fault current interrupting capability, and is expensive. Thus, in our research work a HDCCB is used with effective and appropriate FCLs to extend the operating time when protecting long transmission lines, as it cannot withstand very high fault currents. In the previous optical sensor schemes, there is no brief description about how to achieve the fault coordination during the fault conditions in a meshed MTDC grid. However, in

our proposed scheme all the critically important aspects such as FCL installation, relay/sensor settings, and the DCCB selection have been discussed rigorously.

Both communication dependent and independent methods for the fault identification, detection, and location are coordinated with bidirectional HDCCBs, small and less inductors of 15~70 mH, R-SFCLs, half bridge VSC- MMCs, ACCBs, and the other passive components to compromise with the cost and size of the network. Utilizing the potential benefits of both the inductors and R-SFCLs, the DC fault current is significantly reduced to or below the breakable levels of a HDCCB.

In order to design a proper size and placement of the inductors and RSFCLs, multi-run simulations were conducted based on the important parameters like contributions from the weak, medium strong, and very strong AC sources to the DC fault current, rated AC and DC voltages, rated power, peak currents on the healthy and faulty cables, current ratio, precise thresholds, and the current limiting effects of the inductors and RSFCLs.

During testing following observations were noted and based on the conclusions drawn, appropriately sized FCLs were inserted in the network.

- RSFCLs effectively limited the DC cable short circuit current when installed on the DC cables. Thus, it was concluded that if the current breaking capability for the HDCCB at the converter output is increased up to the maximum fault current contribution from one converter, then the R-SFCLs (2/converter) placed at the converter output could be omitted.
- Since an arm overcurrent criterion is used to block the IGBTs of a VSC, which means that the Rectifier (source) IGBTs will block earlier than those of an Inverter. This helped to avoid extra inductors.
- Total contributions with timely development to the DC fault current for the P2P and P2G faults were studied in depth and contribution at every instant was noted. Based upon the above findings both active and passive limiting scheme was proposed as:
- RSFCLs were installed only on the DC cables (2/pole)

- Properly sized series inductors of 10~70 mH (1/pole or 2/converter) were added at the DC output of only source (AC/DC) converter stations to allow continuous operation of the grid without converter blocking during and after the fault. These inductors limited the AC side contribution to the fault current.
- Thus, utilizing the potential benefits of both the inductors and the R-SFCLs, the DC fault current was significantly reduced to below 1.7 kA. (while breaking capability of a HDCCB is assumed as 9-12 kA).

4.7.4 Fully Selective Isolation of only the Faulty Line (Fast, Novel and Seamless scheme)

In theory an HVDC protection scheme is fast if it selectively clears the fault within 5.1ms. According to [100-101], the protection system should operate in less than 10 ms to protect the system with reliability. The proposed scheme is able to effectively isolate the fault within the critical time limit along with instantaneous overcurrent backup protection. The scheme operates the concerned DCCBs before the critical time limit and protects the system from severe damages of the fault current. The total DC fault clearance time achieved is 5.12 ms to 5.2 ms, which proves its novelty and hence, the scheme is deemed a fast scheme. The scheme is a fully selective scheme, as only the faulted line is isolated from the system, without shutting down the entire system. Its selectivity is guaranteed by precise (large) threshold settings using the RSFCL quenching criteria, the DWT, and the differential protection. The scheme is also seamless as only the RSFCLs installed on the faulted line quench and the line is isolated by tripping the concerned CB. The remaining healthy grid zones continue operating safely after the fault with little power adjustments. Thus, any type of the DC system can be connected to any type of the AC grid.

Several parameters including on-state losses, interruption time, maximum withstanding current, and voltage capability are tested and then used to characterize the performance of a HDCCB. Considering the characteristics of an ideal CB, the requirements of a general CB in practical applications are as follows:

- A practical CB should have low voltage drop and low conducting losses in normal operation (ideally zero on-state losses)
- A CB should interrupt the fault current quickly without abnormal voltage spikes/transients (Ideally a CB is able to interrupt any current of any magnitude / polarity)
- A CB when open (off), should act as a perfect insulator and should be able to withstand the transient voltages
- A CB should be mechanically and thermally strong enough to withstand the rated current and the fault current

Many HVDC-CB concepts are available in the existing literature so far, however all have a similar structure, consisting of a commutation branch to drive the current to zero, a switching component for voltage withstand, and an absorption path to dissipate the energy.

In this research work with active and passive FCLs, interruption time of a CB is given more concentration. Thus, a proactive bidirectional hybrid HVDC breaker (HDCCB) is used as an interrupting and isolating device. With the HDCCB a breaking time of 2 ms is achievable and thus, it is suitable to use it for a clearance time of 5.1 ms to 5.2 ms.

- Analysis of the critical time limit under various fault conditions, diode sizing, contributions from weak, medium strong, and very strong AC sources to the DC fault current, rated line currents, and the fault discriminating/detecting algorithms. All these factors are used to analyze the speed need of the scheme.
- Different rated line currents / normal diode currents (maximum sizes) are considered like 2 kA, 3.9 kA, 4 kA, etc. According to the existing literature the fault has to be isolated at the instant when the current through the freewheeling diodes exceeds 2 p.u. With significant limiting effects of the active/ passive FCLs in the scheme diode current was seen within the above values throughout the simulation period. Further, influence of the key factors like distance to the fault, fault location in the grid, and fault impedance on

the fault provoked current and voltage transients is deeply studied with the simulation results. Based on all these studies backup plans are also introduced. It is concluded that

- The Differential protection being fast in discriminating coordinates well with small sized inductors and the proactive HDCCB (2ms)
- RSFCLs when installed on DC side of the converters effectively limited the fault current. Current limiting effect of the RSFCL was kept between the rated line current and its quenching current.
- If a bidirectional HDCCB is used with a proper combination of active and passive FCLs, fault clearance time of a few milliseconds is achievable making time constraint less stringent in an MTDC grid.

Additionally, based on the quench detection of the associated R-SFCL, the controller sends tripping orders to the concerned HDCCBs at both the ends of the faulted line to interrupt the fault current, and isolate only it, while resuming normal power flow in the healthy grid zones. In the scheme a HDCCB opens to interrupt the fault current only when the associated R-SFCL quenches. Hence it is a fully selective scheme.

To withstand higher cable currents, the diodes have to be oversized. For a HDCCB with breaking time achievable within 2ms, the suitable converter diode sizes are 2 kA, 3.9 kA. Since, a VSC-MTDC network implements the damage resistant cross-linked polyethylene (XLPE) cables of high mechanical strength, which are mostly buried except in the case of deep oceans. Therefore, in these cables, the reason for the fault is mostly due to mechanical damage. These cables are strong enough to withstand high cable currents. Thus, in a VSC-HVDC system diode oversizing to withstand high cable currents may not pose much problems. With proper coordination of the overcurrent protection as a backup plan, even mechanical CBs can be installed on the DC cables in series with the FCLs to isolate the faulty line. Thus, in our research the clearance time is no longer highly strict and a mechanical DC breaker is also competent in fault isolation.

4.7.5 Relatively Accurate Fault Location

After isolating the faulty line from the system, it is very important to locate the fault accurately using the data obtained from the fault detection within the fault clearance time. Thus, off-line data processing of either current derivative data or current wavelet coefficients (obtained during the fault detection) is used to determine the wavefront arrival time. Current derivative method can prove more accurate with a short time window (minimum sample window) only in ideal conditions without noise, load changes or fluctuations. On the other hand, DWT is a robust scheme for the fault detection, because the wavelet coefficients (higher level) are least susceptible (more resistant) to noise and other disturbances. Lower-level coefficients can be susceptible to noise. Thus, the mother wavelet type and the detail coefficient level have to be selected with much care taking both noise and time resolution into consideration which consumes a lot of time. Therefore, in the proposed scheme current derivative data method was tested for the fault location with both Type A (single ended) and Type D (double ended) methods. The thresholds were precisely selected large enough much above the noise level and a short time window was selected. The arrival time of each wave was roughly estimated as the instant when the current derivative exceeds a pre-set large enough threshold level. It was also observed that Type D method gave more accurate results than Type A method.

Therefore, in the proposed scheme current derivative data method was tested for the fault location with both Type A (single ended) and Type D (double ended) methods. The thresholds were precisely selected large enough much above the noise level and a short time window was selected. The arrival time of each wave was roughly estimated as the instant when the current derivative exceeds a pre-set large enough threshold level. It was also observed that Type D method gave more accurate results than Type A method. Since differential protection based on the communication link (optical sensor link) is the primary algorithm so Type-D TW method for fault location is better than Type-A method.

TABLE 4.4: A Detailed Comparison with Previous Research Work

Technique & Ref #	Previous Schemes	Proposed Scheme
Optical Schemes [55],[76]	<p>1. Reliability for long distance power transmission not guaranteed due to potential telecommunication shut-down. Differential protection utilizing the optical sensor communication link is successful with cable lengths of up to 200 km. Because with these cable lengths, delay of 1 ms is ok. However, for very long distances failure of this link is potential.</p> <p>2. No comprehensive details on all the important aspects of the DC fault clearance time. No detailed flow charts. These schemes discriminate a faulty segment and are only focused to locate the fault.</p> <p>3. CWT is not suitable for real-time detection of wavefront arrival time [76].</p>	<p>1. Reliability and performance of communication-dependent differential protection and Type-D TW methods based on distributed optical sensor networks [76] for long-distance power transmission is enhanced and improved by aiding them with other sub-protection/independent techniques and simple backup plans. These auxiliary sub-schemes include current derivative polarity principles, DWT, instantaneous overcurrent relays, RSFCL quench criteria, ACCBs, other passive devices and backups.</p>

Technique & Ref #	Previous Schemes	Proposed Scheme
	<p>4.No comprehensive report on P2P and P2G faults is provided. No concept of critical time limit and DC cable current/overcurrent at this critical time is provided.</p>	<p>2.All the important aspects of the DC fault clearance time such as faulty line determination, wavefront detection fault current interruption, isolation, and the fault location, are deeply analyzed and</p>
	<p>5.Differential protection is unable to discriminate the faulty line/segment in case of high impedance faults like 400 Ω to 500 Ω with damped transients. There are no simulations for such high impedance faults.</p>	<p>are presented using appropriate data and extensive set of numerical simulations. Additionally, every aspect is explained with a detailed flow chart.</p>
	<p>a. Limited simulations. b. No description about source and load terminals. c.No in-depth simulations of the influence of varied P2P fault distances and fault impedances on the fault provoked DC voltage and current TWs with and without protection.</p>	<p>3. A unified and practical way of fault detection is proposed in real time using the DWT.</p>
	<p>6. No fault coordination discussed briefly or achieved comprehensively.</p>	<p>4. A comprehensive report on P2P and P2G faults is provided both theoretically and with simulations in depth. Three stages of the DC cable P2P fault response are briefly discussed.</p>

Technique & Ref #	Previous Schemes	Proposed Scheme
	<p>7. Fault current limited to 4 kA, however at the expense of extra and large sized inductors (150-200 mH). Drawbacks of large sized and extra inductors/FCLs ignored</p>	<p>5. DWT easily discriminates the faulty line in high impedance faults even with protection.</p> <p>6. Both communication dependent and independent methods of the fault discrimination, detection, and location are coordinated with bidirectional HDCCBs, small sized and less inductors of 15~70 mH, R-SFCLs, sensor/relay threshold settings, 3-level half bridge VSC-MMCs, ACCBs, and the other passive components/ backup plans to compromise with the cost and size of the network.</p> <p>7. Large and extra FCLs are avoided through successful fault coordination.</p>

Technique & Ref #	Previous Schemes	Proposed Scheme
		<p>The fault current is significantly reduced to much below 1.7 kA using proper (10-70) mH inductors only at the DC output of source converters (2/converter) and RSFCLs on the DC cables (2/pole).</p>
		<p>8. AC sources tested are medium, strong and very strong. The rated AC voltages tested are from 400 kV to 800 kV with frequencies of 50 Hz -60 Hz. Reasonably small inductors only at the DC output of sources of 10 mH -70 mH. are inserted.</p>
		<p>9. In the proposed scheme through proper coordination of overcurrent relays even mechanical DCCBs can be installed on the DC cables as the isolation tools. Thus, making the fault clearance time least strict in the MTDC grid.</p>

Technique & Ref #	Previous Schemes	Proposed Scheme
[32],[33]	ACCBs as the fault current interrupting devices	10. The scheme is capable of achieving all the general requirements of a feasible MTDC protection scheme such as high speed, robustness, selectivity, reliability, sensitivity, and seamlessness. ACCBs used as one of the final backup plan
[34]	FBFB-VSC-MMCs	Non-fault blocking half-bridge VSC-MMCs Fault location is off-line and is calculated with
[66]	Fault location using similarity of voltage signals	data of either current derivative or WC obtained during the fault detection.
[55],[56]	Single-ended method if used with extra and large sized inductors might fail for fault location.	Type-D TW method considered for fault location using current derivative data

Chapter 5

Conclusion and Future Work

A VSC-MMC-HVDC/MTDC technology with a key benefit of constant voltage polarity offers considerable benefits and infinite extensions to fulfil the basic requirements of the future Super-grid for long-distance and large-capacity electrical power transmission. However, extreme vulnerability of a VSC-HVDC system to the DC faults, particularly solid DC line/cable short circuit fault, demanding an extraordinary strict fault clearance time of a few msec. (5 msec or less) has remained a core technical challenge in both research and practice so far.

During this fault, even when all the IGBTs are blocked for self-protection, it is impossible to prevent the AC grid from feeding the fault via the freewheeling diodes which form an uncontrolled bridge rectifier. The problem is more severe in a meshed MTDC grid with multiple sources and feeders to feed the fault causing even collapse of the entire transmission system.

A major contribution of the research work presented in this thesis is that the reliability and/performance of communication dependent optical sensor schemes for long distance power transmission can be enhanced by aiding them with DWT, mature backup plans and other auxiliary (sub-protection) methods.

For this purpose, a meshed four-terminal HB-VSC-MMC-MTDC grid consisting of both sources and loads is modelled and verified with MATLAB results.

DC cable P2P and P2G fault are studied in-depth and appropriate simulation results. Since VSC's are extremely vulnerable to the DC cable short circuit fault hence, its three-stage fault response and the effects of TWs are deeply analysed. The conclusion is that a DCCB must be operated before the critical time limit of a few msec. (5 msec. or less) to protect the system from the damaging overcurrents of the DC cable/line short fault. The proposed scheme has comprehensively reported all the important aspects of the DC fault. The DC fault clearance time achieved is up to 5.2 msec. in a meshed VSC-MMC-MTDC grid. Through effective fault coordination the DC fault current is reduced much below 1.7 kA. Thus, the scheme achieves all the general requirements of a feasible MTDC protection scheme i.e., comprehensive, reliable, fast/robust, fully selective, novel, cost-effective, seamless, & scalable. The proposed scheme is not restricted only to a 4-terminal meshed VSC-MTDC, but describes a general design procedure for a meshed MTDC grid with any number of terminals. Experimental validation of the scheme can be verified using the simulation results. The scheme is applicable to medium and large scale meshed MTDC grids

5.1 Limitation and Future Work

The primary focus of this research thesis is to reach to a feasible, scalable, robust, and mature protection scheme for a large-scale meshed VSC-based MTDC grid. However, due to limited time, the scope is narrowed down to:

1. A Meshed four-terminal MTDC grid consisting of bipolar half-bridge VSC-MMCs.
2. Symmetrical bipolar pi-section DC cable configuration.
3. Study of the P2P faults of varied fault resistances from 0Ω to 500Ω and P2G faults.
4. MATLAB/Simulink results as the study method.
5. Current measuring units assumed as optical sensors.
6. No hardware implementation.

7. Each AC grid is modelled as an ideal voltage source.
8. HDCCB is modeled as an ideal switch.

Therefore, the future work includes:

1. Working on a more complicated mesh type VSC-based-MMC-MTDC grid, consisting of more than five terminals including configurations of full-bridge MMCs (FBMMCs).
2. Deep Study on the P2G faults, AC side faults, DC voltage control, power flow recovery/restoration, and the post-fault reboot.
3. Deep research on efficient backup plans, superconductivity, protection devices, and implementation of the DWT with other efficient algorithms to detect the hidden anomalies in a meshed HVDC grid.
4. Implementing the MATLAB software simulation results in practical laboratory hardware testing projects.
5. Studying the role of superconducting FCLs, DC/DC buck converters, and other effective FCLs in an MTDC grid.
6. Optimizing the sizes of freewheeling diodes, DC capacitors, inductors, and other FCLs. Improving the fault detecting/locating methods, fault isolation tools, AC grid models, and the relays.
7. Rigorous analysis and experiments on the effective backup plans and verification of the proposed algorithm on RTDS systems for an MTDC grid.
8. Implementation of the stationary wavelet transform (SWT) and its comparison with the DWT.

Bibliography

- [1] S. S. McPherson, *War of the Currents: Thomas Edison vs Nikola Tesla*, 1st ed. Twenty-First Century Books, 2012.
- [2] M. Leppäranta and K. Myrberg, *Physical oceanography of the Baltic Sea*, 1st ed. Springer Science & Business Media, 2009.
- [3] S. Cole, K. Karoui, T. K. Vrana, O. B. Fosso, J. Curis, A. M. Denis, and C. C. Liu, “A european supergrid: present state and future challenges,” 2011.
- [4] D. Ingemansson, J. Wheeler, N. MacLeod, F. Gallon, and O. Ruiton, “The south-west scheme: a new hvac and hvdc transmission system in sweden,” 2012.
- [5] R. Zeng, L. Xu, L. Yao, S. J. Finney, and Y. Wang, “Hybrid hvdc for integrating wind farms with special consideration on commutation failure,” *IEEE Transactions on Power Delivery*, vol. 31, no. 2, pp. 789–797, 2015.
- [6] W. Leterme, P. Tielens, S. De Boeck, and D. Van Hertem, “Overview of grounding and configuration options for meshed hvdc grids,” *IEEE Transactions on Power Delivery*, vol. 29, no. 6, pp. 2467–2475, 2014.
- [7] A. Raza, X. Dianguo, L. Yuchao, S. Xunwen, B. Williams, and C. Cecati, “Coordinated operation and control of vsc based multiterminal high voltage dc transmission systems,” *IEEE Transactions on Sustainable Energy*, vol. 7, no. 1, pp. 364–373, 2015.

-
- [8] G. Tang, Z. He, H. Pang, X. Huang, and X.-p. Zhang, “Basic topology and key devices of the five-terminal dc grid,” *CSEE Journal of Power and Energy Systems*, vol. 1, no. 2, pp. 22–35, 2015.
- [9] L. Zhen-dong, T. Yu-dong, Z. Zhe-yuan, W. Xiao-bo, F. Cai-jie, L. Li, H. Yan *et al.*, “The model and parameters based on the operation mode of a 500kv multi-terminal flexible dc power grid,” *International Journal of Power Engineering and Engineering Thermophysics*, vol. 1, no. 1, pp. 16–24, 2017.
- [10] A. J. Al-Nasser, “Enhancement of ac transient stability through multiterminal dc (mtdc) systems,” Ph.D. dissertation, King Fahd University of Petroleum and Minerals, 1995.
- [11] G. Li, “Analysis and protection of hvdc systems subject to ac and dc faults,” Ph.D. dissertation, Cardiff University, 2017.
- [12] B. K. Bose, *Power Electronics in Renewable Energy Systems and Smart Grid: Technology and Applications*, 1st ed. John Wiley & Sons, 2019.
- [13] G. Buigues, V. Valverde, A. Etxegarai, P. Eguía, and E. Torres, “Present and future multiterminal hvdc systems: current status and forthcoming developments,” in *Proc. Int. Conf. Renewable Energies Power Quality*, vol. 1, no. 15, 2017, pp. 83–88.
- [14] A. Moawwad, M. S. El Moursi, and W. Xiao, “A novel transient control strategy for vsc-hvdc connecting offshore wind power plant,” *IEEE Transactions on Sustainable Energy*, vol. 5, no. 4, pp. 1056–1069, 2014.
- [15] W. Wang, G. Wang, and M. Andersson, “Development in uhvdc multi-terminal and vsc dc grid,” in *International High Voltage Direct Current Conference (HVDC 2016)*, 2016, pp. 1–7.
- [16] S. Wang, C. Li, O. D. Adeuyi, G. Li, C. E. Ugalde-Loo, and J. Liang, “Coordination of mmcs with hybrid dc circuit breakers for hvdc grid protection,” *IEEE Transactions on Power Delivery*, vol. 34, no. 1, pp. 11–22, 2018.

-
- [17] Y. Li, H. Liu, X. Fan, and X. Tian, "Engineering practices for the integration of large-scale renewable energy vsc-hvdc systems," *Global Energy Interconnection*, vol. 3, no. 2, pp. 149–157, 2020.
- [18] H. Rao, Y. Zhou, S. Xu, X. Cai, W. Cao, Y. Xu, and C. Ren, "Key technologies of ultra-high voltage hybrid lcc-vsc mt dc systems," *CSEE Journal of Power and Energy Systems*, vol. 5, no. 3, pp. 365–373, 2019.
- [19] K. Meah and S. Ula, "Comparative evaluation of hvdc and hvac transmission systems," in *2007 IEEE Power Engineering Society General Meeting*. IEEE, 2007, pp. 1–5.
- [20] H. Dong, Z. Xu, P. Song, G. Tang, Q. Xu, and L. Sun, "Optimized power redistribution of offshore wind farms integrated vsc-mt dc transmissions after onshore converter outage," *IEEE Transactions on Industrial Electronics*, vol. 64, no. 11, pp. 8948–8958, 2016.
- [21] S. Mirsaeidi, X. Dong, and D. M. Said, "A fault current limiting approach for commutation failure prevention in lcc-hvdc transmission systems," *IEEE Transactions on Power Delivery*, vol. 34, no. 5, pp. 2018–2027, 2019.
- [22] G. Li, T. An, J. Liang, W. Liu, T. Joseph, J. Lu, M. Szechtman, B. R. Andersen, and Y. Lan, "Power reversal strategies for hybrid lcc/mmc hvdc systems," *CSEE Journal of Power and Energy Systems*, vol. 6, no. 1, pp. 203–212, 2020.
- [23] M. Daryabak, S. Filizadeh, J. Jatskevich, A. Davoudi, M. Saeedifard, V. Sood, J. Martinez, D. Aliprantis, J. Cano, and A. Mehrizi-Sani, "Modeling of lcc-hvdc systems using dynamic phasors," *IEEE Transactions on Power Delivery*, vol. 29, no. 4, pp. 1989–1998, 2014.
- [24] J. Pan, R. Nuqui, K. Srivastava, T. Jonsson, P. Holmberg, and Y.-J. Hafner, "Ac grid with embedded vsc-hvdc for secure and efficient power delivery," in *2008 IEEE Energy 2030 Conference*. IEEE, 2008, pp. 1–6.

- [25] M. Hajian, D. Jovcic, and B. Wu, "Evaluation of semiconductor based methods for fault isolation on high voltage dc grids," *IEEE Transactions on Smart Grid*, vol. 4, no. 2, pp. 1171–1179, 2013.
- [26] X. Han, W. Sima, M. Yang, L. Li, T. Yuan, and Y. Si, "Transient characteristics under ground and short-circuit faults in a ± 500 kv mmc-based hvdc system with hybrid dc circuit breakers," *IEEE Transactions on Power Delivery*, vol. 33, no. 3, pp. 1378–1387, 2018.
- [27] M. K. Bucher and C. M. Franck, "Fault current interruption in multiterminal hvdc networks," *IEEE Transactions on Power Delivery*, vol. 31, no. 1, pp. 87–95, 2015.
- [28] B. Xiang, Z. Liu, Y. Geng, and S. Yanabu, "Dc circuit breaker using superconductor for current limiting," *IEEE transactions on applied superconductivity*, vol. 25, no. 2, pp. 1–7, 2014.
- [29] W. Wang, M. Barnes, O. Marjanovic, and O. Cwikowski, "Impact of dc breaker systems on multiterminal vsc-hvdc stability," *IEEE Transactions on Power Delivery*, vol. 31, no. 2, pp. 769–779, 2015.
- [30] K. Sano and M. Takasaki, "A surgeless solid-state dc circuit breaker for voltage-source-converter-based hvdc systems," *IEEE Transactions on Industry Applications*, vol. 50, no. 4, pp. 2690–2699, 2013.
- [31] R. Dantas, J. Liang, C. E. Ugalde-Loo, A. Adamczyk, C. Barker, and R. Whitehouse, "Progressive fault isolation and grid restoration strategy for mtdc networks," *IEEE Transactions on Power Delivery*, vol. 33, no. 2, pp. 909–918, 2017.
- [32] L. Tang and B.-T. Ooi, "Locating and isolating dc faults in multi-terminal dc systems," *IEEE transactions on power delivery*, vol. 22, no. 3, pp. 1877–1884, 2007.
- [33] D. Tzelepis, A. O. Rousis, A. Dyśko, C. Booth, and G. Strbac, "A new fault-ride-through strategy for mtdc networks incorporating wind farms and

- modular multi-level converters,” *International Journal of Electrical Power & Energy Systems*, vol. 92, pp. 104–113, 2017.
- [34] C. Petino, M. Heidemann, D. Eichhoff, M. Stumpe, E. Spahic, and F. Schetler, “Application of multilevel full bridge converters in hvdc multiterminal systems,” *IET Power Electronics*, vol. 9, no. 2, pp. 297–304, 2016.
- [35] Q. Song, S. Xu, Y. Zhou, Y. Gim, Z. Li, and Z. Deng, “Active fault-clearing on long-distance overhead lines using a hybrid modular multilevel converter,” in *2019 IEEE 28th International Symposium on Industrial Electronics (ISIE)*. IEEE, 2019, pp. 2033–2038.
- [36] A. Raza, X. Dianguo, L. Yuchao, S. Xunwen, B. Williams, and C. Cecati, “Coordinated operation and control of vsc based multiterminal high voltage dc transmission systems,” *IEEE Transactions on Sustainable Energy*, vol. 7, no. 1, pp. 364–373, 2015.
- [37] E. Kontos, R. T. Pinto, S. Rodrigues, and P. Bauer, “Impact of hvdc transmission system topology on multiterminal dc network faults,” *IEEE Transactions on Power Delivery*, vol. 30, no. 2, pp. 844–852, 2014.
- [38] W. Wang, M. Barnes, O. Marjanovic, and O. Cwikowski, “Impact of dc breaker systems on multiterminal vsc-hvdc stability,” *IEEE Transactions on Power Delivery*, vol. 31, no. 2, pp. 769–779, 2015.
- [39] J. Yang, J. E. Fletcher, and J. O’Reilly, “Short-circuit and ground fault analyses and location in vsc-based dc network cables,” *IEEE transactions on Industrial Electronics*, vol. 59, no. 10, pp. 3827–3837, 2011.
- [40] W. Ahmed and P. Manohar, “Application of superconducting fault current limiter and chopper controlled resistor for protection of vsc-hvdc system,” *Power Research*, vol. 15, no. 1, pp. 25–38, 2019.
- [41] H. Radmanesh, S. H. Fathi, G. Gharehpetian, and A. Heidary, “Bridge-type solid-state fault current limiter based on ac/dc reactor,” *IEEE Transactions on Power Delivery*, vol. 31, no. 1, pp. 200–209, 2015.

- [42] T. Q. Fonséca, R. Ribeiro, T. d. O. A. Rocha, F. B. Costa, and J. M. Guerrero, "Voltage grid supporting by using variable structure adaptive virtual impedance for lcl-vsc dg converters," *IEEE Transactions on Industrial Electronics*, 2019.
- [43] U. A. Khan, J.-G. Lee, F. Amir, and B.-W. Lee, "A novel model of hvdc hybrid-type superconducting circuit breaker and its performance analysis for limiting and breaking dc fault currents," *IEEE Transactions on Applied Superconductivity*, vol. 25, no. 6, pp. 1–9, 2015.
- [44] Y. Ma, G. Zou, S. Song, J. Guo, and Z. Gao, "Novel fault current-limiting scheme for mmc-based flexible hvdc system," *The Journal of Engineering*, vol. 2019, no. 16, pp. 2233–2238, 2019.
- [45] Q. Qiu, L. Xiao, J. Zhang, Z. Zhang, N. Song, L. Jing, W. Zha, X. Du, Y. Teng, Z. Zhou *et al.*, "Design and test of 40-kv/2-ka dc superconducting fault current limiter," *IEEE Transactions on Applied Superconductivity*, vol. 30, no. 6, pp. 1–5, 2020.
- [46] L. Zhang, J. Shi, Z. Wang, Y. Tang, Z. Yang, L. Ren, S. Yan, and Y. Liao, "Application of a novel superconducting fault current limiter in a vsc-hvdc system," *IEEE Transactions on applied Superconductivity*, vol. 27, no. 4, pp. 1–6, 2017.
- [47] R. Strumpler, J. Skindhøj, J. Glatz-Reichenbach, J. Kuhlefeldt, and F. Perdoncin, "Novel medium voltage fault current limiter based on polymer ptc resistors," *IEEE transactions on power delivery*, vol. 14, no. 2, pp. 425–430, 1999.
- [48] H. Wu, X. Li, M. Zhang, D. Stade, and H. Schau, "Analysis of a liquid metal current limiter," *IEEE Transactions on Components and Packaging Technologies*, vol. 32, no. 3, pp. 572–577, 2009.
- [49] Y. Li, "A dc-dc power converter study for high voltage direct current (hvdc) grid: Model and control of the dc-dc modular multilevel converter (m2dc)," Ph.D. dissertation, 2019.

- [50] M. E. Baran and N. R. Mahajan, "Overcurrent protection on voltage-source-converter-based multiterminal dc distribution systems," *IEEE Transactions on Power Delivery*, vol. 22, pp. 406–412, 2007.
- [51] F. Deng and Z. Chen, "Design of protective inductors for hvdc transmission line within dc grid offshore wind farms," *IEEE Transactions on Power Delivery*, vol. 28, no. 1, pp. 75–83, 2012.
- [52] H. Li, "Impact of variable dc reactors in voltage-source converter based multiterminal high-voltage dc transmission systems," *The Journal of Engineering*, vol. 2019, no. 16, pp. 1816–1819, 2019.
- [53] W. Leterme, J. Beerten, and D. Van Hertem, "Nonunit protection of hvdc grids with inductive dc cable termination," *IEEE Transactions on Power Delivery*, vol. 31, no. 2, pp. 820–828, 2015.
- [54] D. Tzelepis, A. Dyśko, G. Fusiek, J. Nelson, P. Niewczas, D. Vozikis, P. Orr, N. Gordon, and C. D. Booth, "Single-ended differential protection in mtdc networks using optical sensors," *IEEE Transactions on Power Delivery*, vol. 32, no. 3, pp. 1605–1615, 2016.
- [55] H. Livani and C. Y. Evrenosoglu, "A single-ended fault location method for segmented hvdc transmission line," *Electric Power Systems Research*, vol. 107, pp. 190–198, 2014.
- [56] Y. Chen, S. Li, J. Sheng, Z. Jin, Z. Hong, and J. Gu, "Experimental and numerical study of co-ordination of resistive-type superconductor fault current limiter and relay protection," *Journal of superconductivity and novel magnetism*, vol. 26, no. 11, pp. 3225–3230, 2013.
- [57] S.-H. Lim, H.-S. Choi, D.-C. Chung, Y.-H. Jeong, Y.-H. Han, T.-H. Sung, and B.-S. Han, "Fault current limiting characteristics of resistive type sfcl using a transformer," *IEEE transactions on applied superconductivity*, vol. 15, no. 2, pp. 2055–2058, 2005.

-
- [58] Y. Song, J. Sun, M. Saeedifard, S. Ji, L. Zhu, and A. S. Meliopoulos, "Optimum selection of circuit breaker parameters based on analytical calculation of overcurrent and overvoltage in multiterminal hvdc grids," *IEEE Transactions on Industrial Electronics*, vol. 67, no. 5, pp. 4133–4143, 2019.
- [59] R. Li, L. Xu, and L. Yao, "Dc fault detection and location in meshed multiterminal hvdc systems based on dc reactor voltage change rate," *IEEE Transactions on Power Delivery*, vol. 32, no. 3, pp. 1516–1526, 2016.
- [60] A. Meghwani, S. Srivastava, and S. Chakrabarti, "A non-unit protection scheme for dc microgrid based on local measurements," *IEEE Transactions on Power Delivery*, vol. 32, no. 1, pp. 172–181, 2016.
- [61] S. P. Azad and D. Van Hertem, "A fast local bus current-based primary relaying algorithm for hvdc grids," *IEEE Transactions on Power Delivery*, vol. 32, no. 1, pp. 193–202, 2016.
- [62] J. Liu, N. Tai, and C. Fan, "Transient-voltage-based protection scheme for dc line faults in the multiterminal vsc-hvdc system," *IEEE Transactions on Power Delivery*, vol. 32, no. 3, pp. 1483–1494, 2016.
- [63] O. K. Nanayakkara, A. D. Rajapakse, and R. Wachal, "Location of dc line faults in conventional hvdc systems with segments of cables and overhead lines using terminal measurements," *IEEE transactions on power delivery*, vol. 27, no. 1, pp. 279–288, 2012.
- [64] J. Beerten, O. Gomis-Bellmunt, X. Guillaud, J. Rimez, A. van der Meer, and D. Van Hertem, "Modeling and control of hvdc grids: A key challenge for the future power system," in *2014 Power Systems Computation Conference*. IEEE, 2014, pp. 1–21.
- [65] M. Farshad and J. Sadeh, "A novel fault-location method for hvdc transmission lines based on similarity measure of voltage signals," *IEEE transactions on power delivery*, vol. 28, no. 4, pp. 2483–2490, 2013.

-
- [66] S. D. Fletcher, P. J. Norman, K. Fong, S. J. Galloway, and G. M. Burt, "High-speed differential protection for smart dc distribution systems," *IEEE Transactions on Smart Grid*, vol. 5, no. 5, pp. 2610–2617, 2014.
- [67] K. Pathirana, A. Rajapakse, O. Nanayakkara, and R. Wachal, "Detecting fault generated surges in dc line of vsc hvdc schemes for travelling wave based fault location," in *2012 CIGRÉ Canada Conference*, 2012.
- [68] J.-D. Park and J. Candelaria, "Fault detection and isolation in low-voltage dc-bus microgrid system," *IEEE transactions on power delivery*, vol. 28, no. 2, pp. 779–787, 2013.
- [69] S. D. Fletcher, P. J. Norman, K. Fong, S. J. Galloway, and G. M. Burt, "High-speed differential protection for smart dc distribution systems," *IEEE Transactions on Smart Grid*, vol. 5, no. 5, pp. 2610–2617, 2014.
- [70] S. Azizi, M. Sanaye-Pasand, M. Abedini, and A. Hasani, "A traveling-wave-based methodology for wide-area fault location in multiterminal dc systems," *IEEE Transactions on Power Delivery*, vol. 29, no. 6, pp. 2552–2560, 2014.
- [71] H. Livani and C. Y. Evrenosoglu, "A single-ended fault location method for segmented hvdc transmission line," *Electric Power Systems Research*, vol. 107, pp. 190–198, 2014.
- [72] M. Hajian, L. Zhang, and D. Jovcic, "Dc transmission grid with low-speed protection using mechanical dc circuit breakers," *IEEE Transactions on Power Delivery*, vol. 30, no. 3, pp. 1383–1391, 2014.
- [73] S. D. Fletcher, P. J. Norman, K. Fong, S. J. Galloway, and G. M. Burt, "High-speed differential protection for smart dc distribution systems," *IEEE Transactions on Smart Grid*, vol. 5, no. 5, pp. 2610–2617, 2014.
- [74] J. Sneath and A. D. Rajapakse, "Fault detection and interruption in an earthed hvdc grid using rocov and hybrid dc breakers," *IEEE Transactions on Power Delivery*, vol. 31, no. 3, pp. 973–981, 2014.

- [75] D. Tzelepis, G. Fusiek, A. Dyśko, P. Niewczas, C. Booth, and X. Dong, “Novel fault location in mtde grids with non-homogeneous transmission lines utilizing distributed current sensing technology,” *IEEE Transactions on Smart Grid*, vol. 9, no. 5, pp. 5432–5443, 2018.
- [76] R. Nasr, O. Falou, A. Shahin, E. Hysi, L. A. Wirtzfeld, E. S. Berndl, and M. C. Kolios, “Mean scatterer spacing estimation using cepstrum-based continuous wavelet transform,” *IEEE Transactions on Ultrasonics, Ferroelectrics, and Frequency Control*, vol. 67, no. 6, pp. 1118–1126, 2020.
- [77] T. K. Vrana, Y. Yang, D. Jovicic, S. Denetière, J. Jardini, and H. Saad, “The cigre b4 dc grid test system,” *Electra*, vol. 270, no. 1, pp. 10–19, 2013.
- [78] F. V. Lopes, K. M. Dantas, K. M. Silva, and F. B. Costa, “Accurate two-terminal transmission line fault location using traveling waves,” *IEEE Transactions on Power Delivery*, vol. 33, no. 2, pp. 873–880, 2017.
- [79] L. Tang, X. Dong, S. Luo, S. Shi, and B. Wang, “A new differential protection of transmission line based on equivalent travelling wave,” *IEEE Transactions on Power Delivery*, vol. 32, no. 3, pp. 1359–1369, 2016.
- [80] V. Maier, S. G. Pavel, B. CD *et al.*, “Correct application of the discrete fourier transform in harmonics,” *Advances in Electrical and Computer Engineering*, vol. 8, no. 1, pp. 26–30, 2008.
- [81] K.-Y. Su and W.-L. Lee, “Fourier transform infrared spectroscopy as a cancer screening and diagnostic tool: A review and prospects,” *Cancers*, vol. 12, no. 1, p. 115, 2020.
- [82] H. Chen, Z. Liu, L. Zhu, C. Tanougast, and W. Blondel, “Asymmetric color cryptosystem using chaotic ushiki map and equal modulus decomposition in fractional fourier transform domains,” *Optics and Lasers in Engineering*, vol. 112, pp. 7–15, 2019.
- [83] P. J. Sparto, M. Parnianpour, E. A. Barria, and J. M. Jagadeesh, “Wavelet and short-time fourier transform analysis of electromyography for detection of

- back muscle fatigue,” *IEEE Transactions on rehabilitation engineering*, vol. 8, no. 3, pp. 433–436, 2000.
- [84] J. Chen, C. Zhang, J. Zuo, Y. Wu, and Z. Li, “Urban talent demand analysis based on deep learning and wavelet threshold denoising,” in *International Conference on Frontier Computing*. Springer, 2019, pp. 1305–1315.
- [85] C. Zhou and X. Chen, “Predicting energy consumption: A multiple decomposition-ensemble approach,” *Energy*, vol. 189, p. 116045, 2019.
- [86] M. J. Shensa, “The discrete wavelet transform: wedding the a trous and mallat algorithms,” *IEEE Transactions on signal processing*, vol. 40, no. 10, pp. 2464–2482, 1992.
- [87] J. E. Fowler, “The redundant discrete wavelet transform and additive noise,” *IEEE Signal Processing Letters*, vol. 12, no. 9, pp. 629–632, 2005.
- [88] M. R. Ali and D. Baleanu, “Haar wavelets scheme for solving the unsteady gas flow in four-dimensional,” *Thermal Science*, no. 00, pp. 292–292, 2019.
- [89] S. A. Niaki, H. K. Karegar, and M. G. Monfared, “A novel fault detection method for vsc-hvdc transmission system of offshore wind farm,” *International Journal of Electrical Power & Energy Systems*, vol. 73, pp. 475–483, 2015.
- [90] O. K. Nanayakkara, A. D. Rajapakse, and R. Wachal, “Traveling-wave-based line fault location in star-connected multiterminal hvdc systems,” *IEEE transactions on power delivery*, vol. 27, no. 4, pp. 2286–2294, 2012.
- [91] N. Belda and R. Smeets, “Test circuits for hvdc circuit breakers,” *IEEE Transactions on Power Delivery*, vol. 32, no. 1, pp. 285–293, 2016.
- [92] M. K. Bucher and C. M. Franck, “Fault current interruption in multiterminal hvdc networks,” *IEEE Transactions on Power Delivery*, vol. 31, no. 1, pp. 87–95, 2015.

-
- [93] C. Franck, R. Smeets, and M. A. 34, “Technical requirements and specifications of state-of-the-art hvdc switching equipment,” *CIGRE WG A3/B4. 34, Report No. 683*, 2017.
- [94] J. Hafner, “Proactive hybrid hvdc breakers—a key innovation for reliable hvdc grids,” in *Proc. CIGRE Bologna Symposium*, 2011, pp. 1–8.
- [95] D. Jovicic, G. Tang, and H. Pang, “Adopting circuit breakers for high-voltage dc networks: Appropriating the vast advantages of dc transmission grids,” *IEEE Power and Energy Magazine*, vol. 17, no. 3, pp. 82–93, 2019.
- [96] G. Stamatiou, *Analysis of VSC-based HVDC systems*, 1st ed. Chalmers Tekniska Hogskola (Sweden), 2016.
- [97] W. Leterme, I. Jahn, P. Ruffing, K. Sharifabadi, and D. Van Hertem, “Designing for high-voltage dc grid protection: Fault clearing strategies and protection algorithms,” *IEEE Power and Energy Magazine*, vol. 17, no. 3, pp. 73–81, 2019.

Appendix A

Appendix

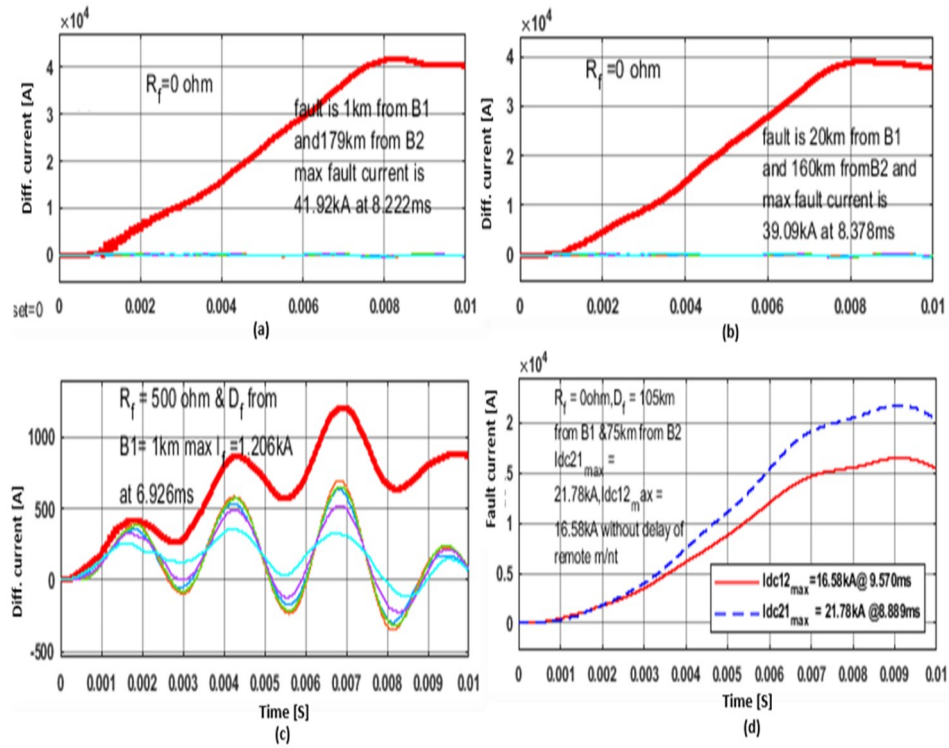


FIGURE A.1: Results for an internal P2P fault in the cable L_{12} (180 km long) at 1ms. (a) Series differential current profile on L_{12} for a solid P2P fault in it at 1 km to the sending node B_1 and 179 km from the receiving node B_2 discriminating the faulty segment of the cable L_{12} (red solid curve) with highest differential current of 41.92 kA derived from the faulted sensor pair. (b) Series differential current profile for a solid P2P fault at 20 km to B_1 and 160 km from B_2 discriminating the faulty segment of L_{12} (red solid curve) with highest differential current of 39.09 kA at 8.378 ms). (c) Damped series differential current profile for a high impedance P2P fault in the cable L_{12} with $R_f = 500$ Ω and at 1 km to B_1 . (d) DC fault currents I_{12} and I_{21} for a solid P2P fault in the cable L_{12} at 1 ms and at a distance of 105 km from B_1 (red solid curve) and 75 km from B_2 (blue dash curve) without delay between the two currents and without protection.

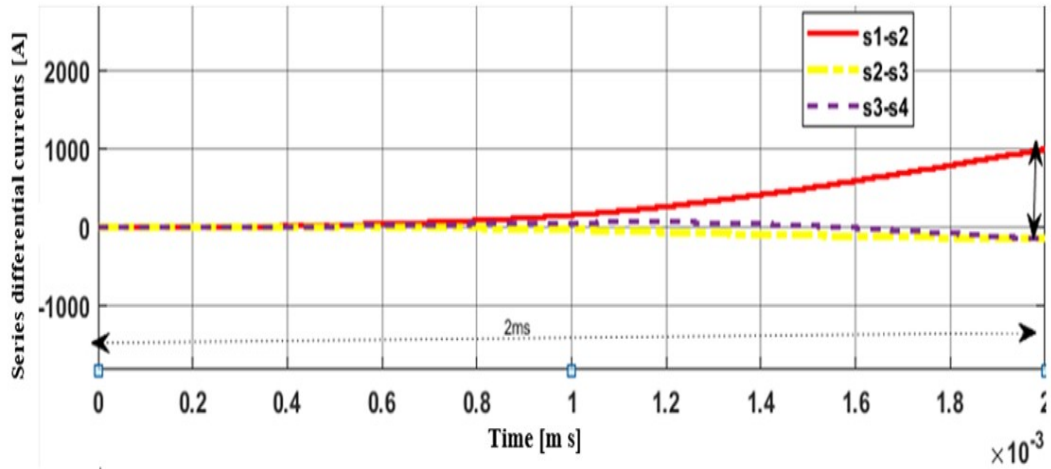


FIGURE A.2: Internal P2P fault in DC line L12 shows zoomed area of initial 2ms that clearly distinguishes the faulted segment between S1 & S2 from non-faulted segments.

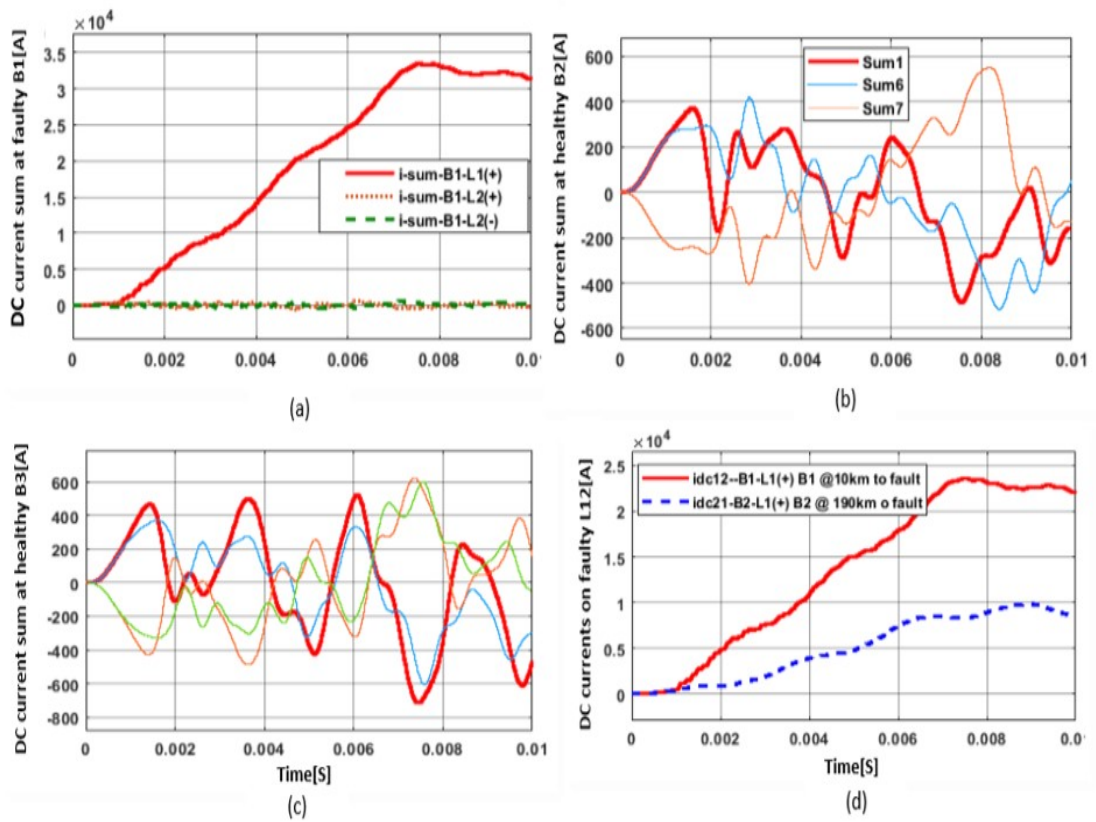


FIGURE A.3: Solid internal P2P fault at 1 ms in the cable L_{12} (L_1) between S_1 and S_2 . Differential current sums measured at B_1 with selective discrimination of the faulty line L_{12} or its segment (red solid curve). (b) and (c) Differential current sums on both (+/-) poles of the healthy cables. (d) Delayed DC fault currents I_{12} and I_{21} for a solid P2P fault in the cable L_{12} at 1 ms and at a distance of 10 km from B_1 and 190 km from B_2 without protection.

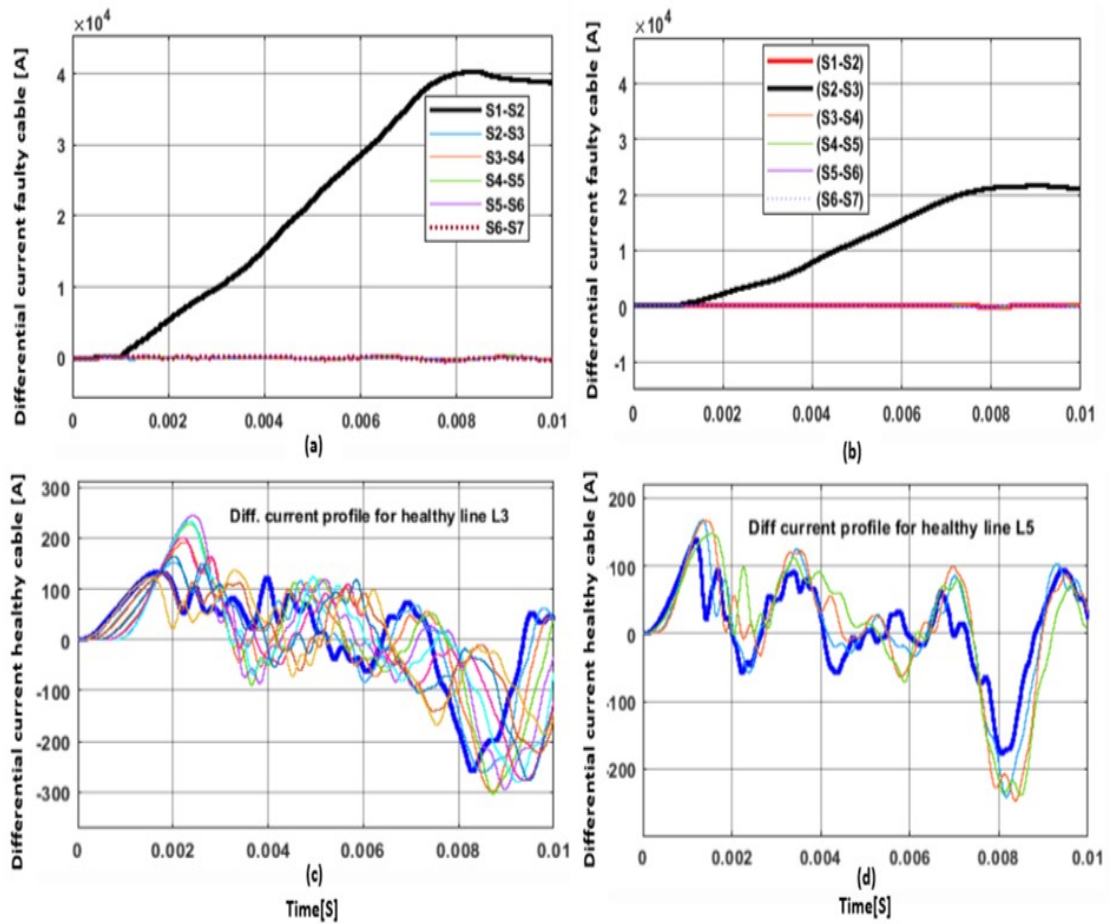


FIGURE A.4: Solid internal P2P fault at 1 ms in the cable L_{12} (180km) with equidistant sensor pairs. (a) Selective discrimination of the faulty segment of L_{12} between S_1 and S_2 (black solid curve). (b) Selective discrimination of the faulty segment between S_2 and S_3 (black solid curve) by measuring series of differential currents on the cable L_{12} . (c) and (d) Series differential current profiles on the healthy cables without protection.

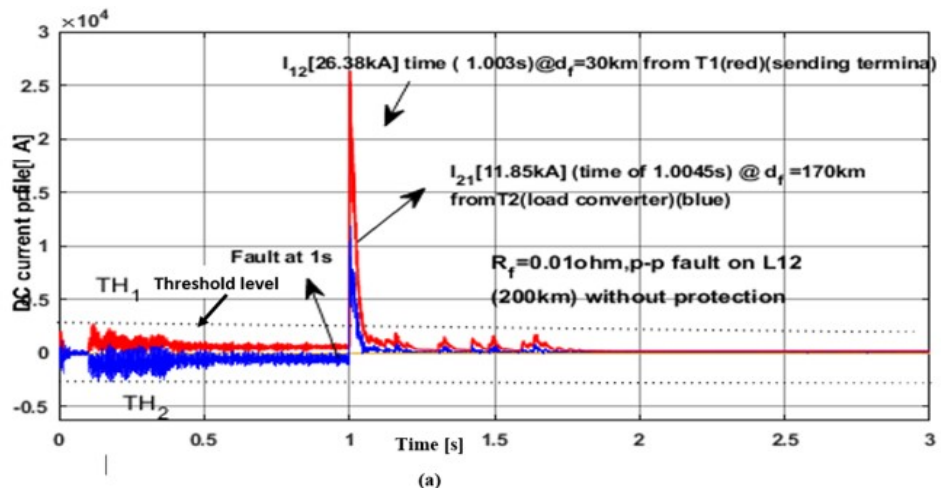


FIGURE A.5: Influence of different distances to a solid P2P fault.

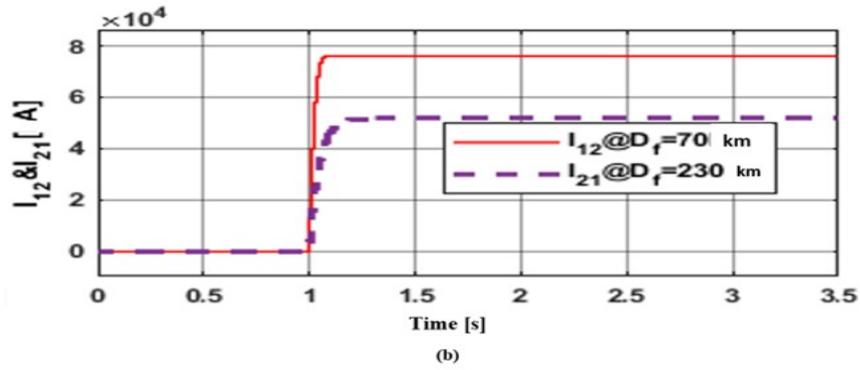


FIGURE A.6: Influence of different distances to a solid P2P fault at 1s in the cable L_{12} on DC fault current transients without protection.

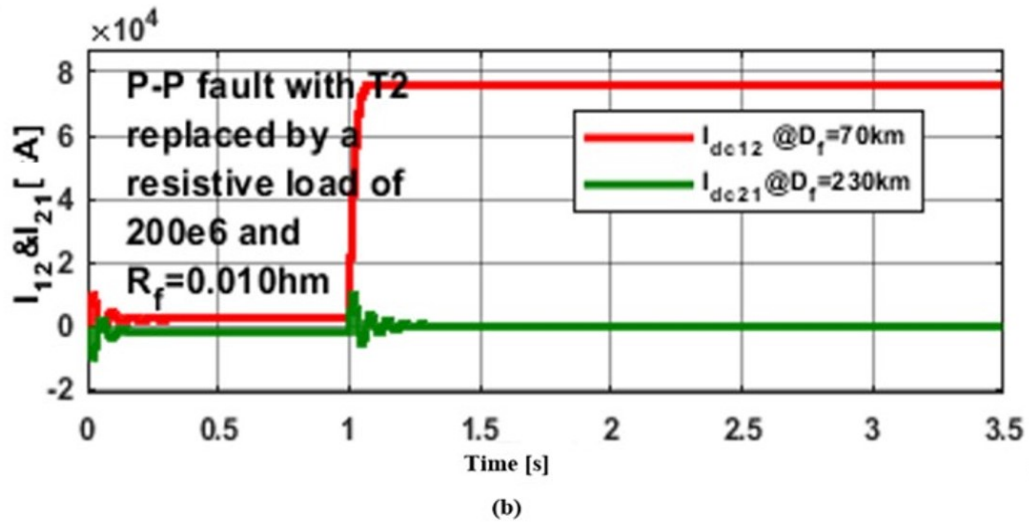
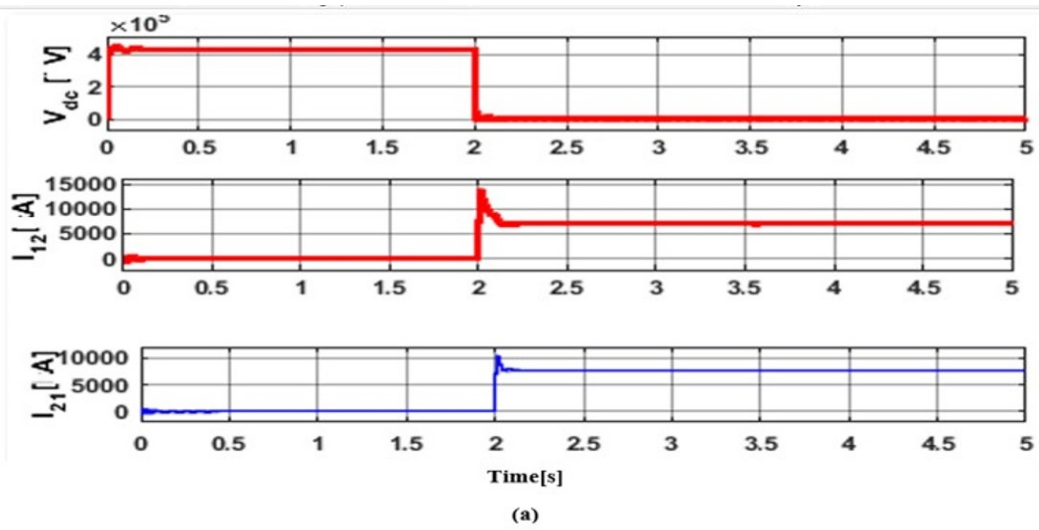


FIGURE A.7: (a) Influence of different distances to a solid P2P fault in the cable L_{12} at 2s on DC fault current transients and DC Voltage. DC voltage and DC fault current for the P2P fault at 3 km to source (red solid curves). (b) Influence of different distances to a solid P2P fault in the cable L_{12} at 1s with terminal 2 replaced by a load resistance of 200 MΩ.

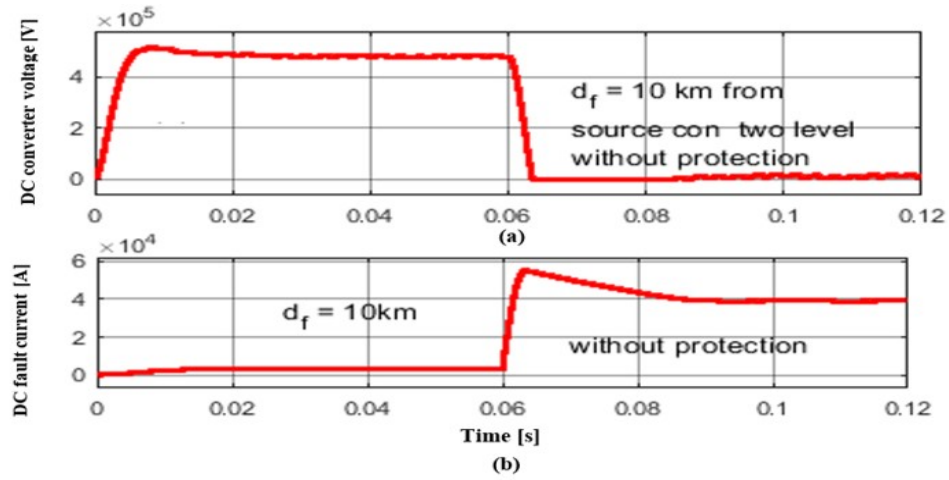


FIGURE A.8: P2P fault in the cable L_{12} at 60 ms and at 10km to the source. (a) HVDC link voltage. (b) HVDC link fault current without protection.

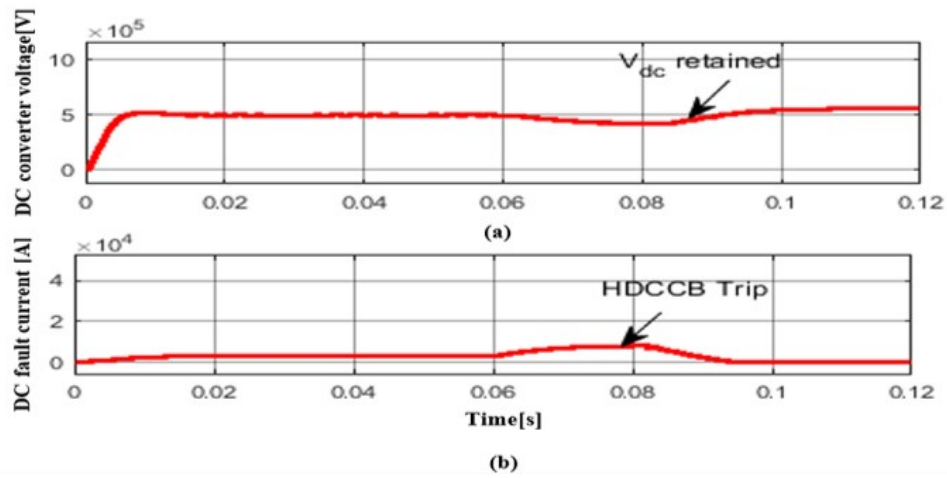


FIGURE A.9: P2P fault in the cable L_{12} at 60 ms and at 10 km to the source. (a) HVDC link voltage. (b) HVDC link fault current with protection.

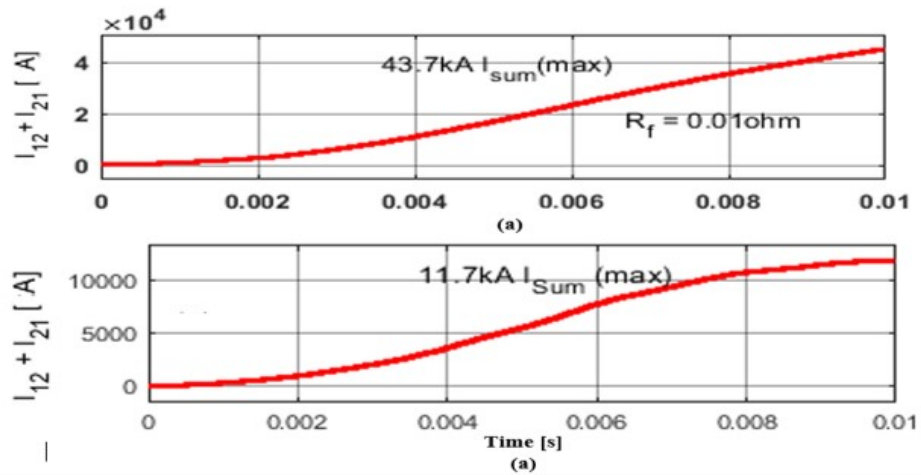


FIGURE A.10: Solid P2P fault at 1ms. (a) Huge sum of the two fault currents without FCLs. (b) Effective suppression of the sum of fault currents with active and passive FCLs.

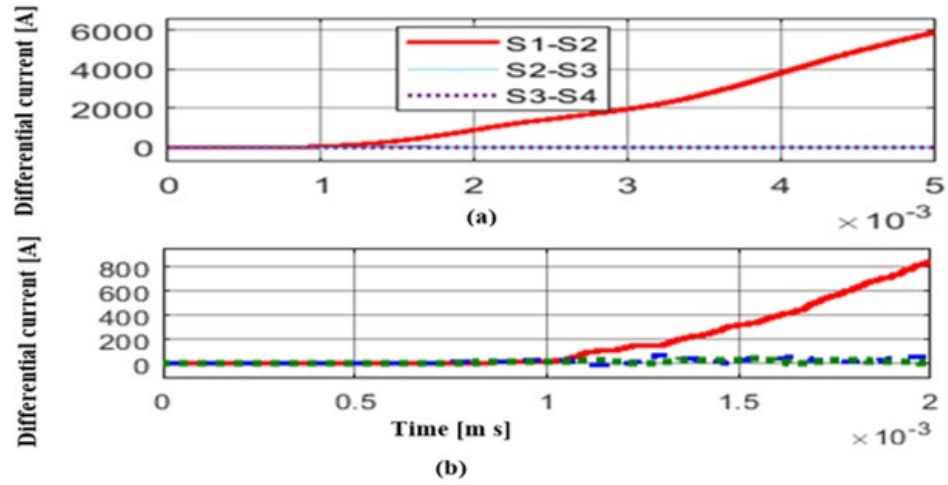


FIGURE A.11: Effective active and passive fault current limitation with protection for a P2P fault at 1 ms both (a) and (b).

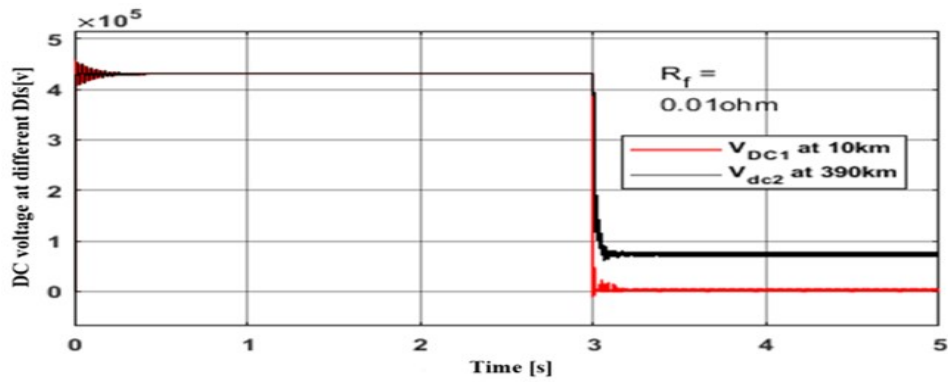


FIGURE A.12: Influence of different distances to a P2P fault on HVDC link voltage transients for a solid P2P fault at 3s.

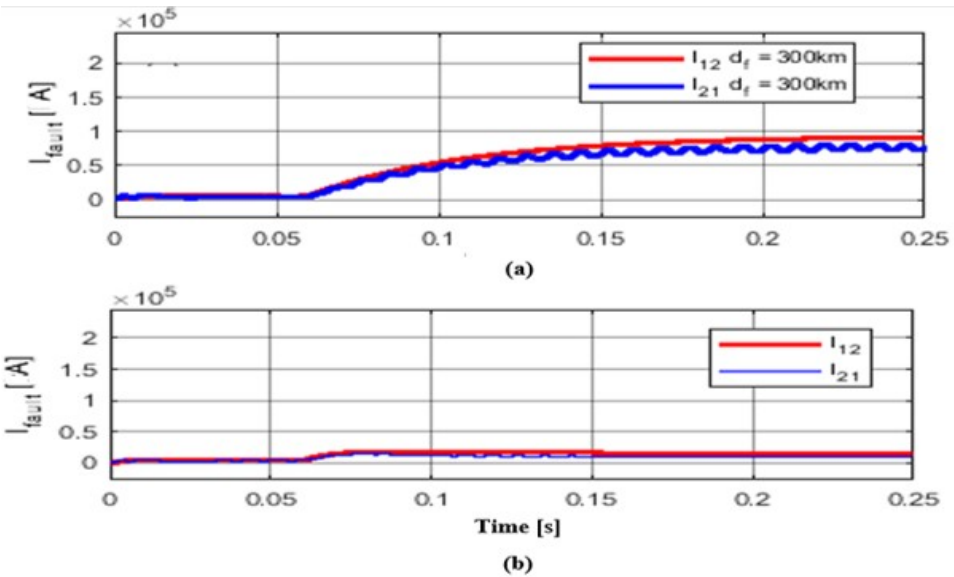


FIGURE A.13: Solid P2P fault at 60 ms in the cable L_{12} . (a) Fault currents without protection. (b) Fault currents significantly reduced to much lower value with active/passive FCLs with protection.